Understanding Temporal Changes of Glacial Dynamics with Numerical Modeling: A Case Study of Upernavik Isstrøm, Greenland

MA, Ho Yin

A Thesis Submitted in Partial Fulfillment

of the Requirements for the Degree of

Master of Philosophy

in

Earth and Atmospheric Sciences

The Chinese University of Hong Kong

September 2016

Thesis Assessment Committee

Professor WONG, Teng-Fong (Chair)

Professor LIU, Lin (Thesis Supervisor)

Professor YANG, Hongfeng (Committee Member)

Abstract of Thesis titled:

Understanding Temporal Changes of Glacial Dynamics with Numerical Modeling: A Case Study of Upernavik Isstrøm, Greenland

Submitted by **MA, Ho Yin**

for the Degree of **Master of Philosophy in Earth and Atmospheric Sciences**

at The Chinese University of Hong Kong in **September 2016**.

Glaciers, moving 'ice rivers', are known to vary their dynamic behaviors across a wide range of spatial and temporal scales. Changes in glacier dynamics in Greenland in recent decades have caused significant ice loss, contributing to global sea level rise. Nonetheless, many key processes in glacier dynamics remain poorly understood or quantified. Satellite observations revealed that one of the outlet glaciers in Upernavik Isstrøm in western Greenland sped up abruptly from about 4 kilometres/year to 6 kilometres/year during July 2010. Motivated by these observations, this study aims to investigate the potential factors and mechanisms that control temporal variations in outlet glacier dynamics through numerical modeling. Using the Community Ice Sheet Model (CISM), we designed and conducted a series of numerical simulations with high spatial (100 metres) and temporal (1 day) resolutions. The numerical experiments have been performed with varying ice temperatures and surface mass balance rates, as well as user-defined large-scale calving events. We found that increasing ice temperatures can lead to higher glacial velocities with greater fluctuations in magnitude. A more negative

surface mass balance rate leads to slower velocity. This contradicts a common hypothesis that melting can promote glacial speed-up. This is because the consequential hydrological response after surface melting is not included in the model. Thus, more negative surface mass in CISM only leads to a thinning of glaciers but not an enhancement of basal sliding. More importantly, our simulation results suggest that large-scale calving could lead to a jump in velocity and the magnitude of this velocity increment is related to the size of ice calved away. However, it cannot be determined if the corresponding speed-up is a rapid or gradual process as the calving was not triggered by a physical process. The next version of CISM equipped with physical-based calving could be of greater use in solving the problem.

論文摘要

冰川（又稱冰河）的動力特性在空間及時間上有所變化。近數十年，格陵蘭冰川運動轉變加劇融冰，以致全球平均海平面上升，但現時對很多重要影響冰川動力的因素均了解不深。衛星遙感觀測顯示，二零一零年七月間，格陵蘭西部烏佩納凡克地區其中一條冰川的流速，由每年四公里急劇加速至每年六公里。由此觀測結果推動，本項目旨在利用數值模型以探索可導致短期冰川運動變化的潛在因素。利用冰川數值模型 「CISM」，我們進行了一系列高空間（一百米）、高時間（一天）解析度的地區性模擬，以研究不同冰川溫度、表面質量平衡、以及大型冰山崩解活動對冰川流速的影響。模擬顯示，當冰層温度愈高，冰川速度、和速度變化均較高。 同時模擬結果亦顯示，更強的冰川表面融化未有導致更高的速度，與常識相反，這因為模型未有考慮冰川對融化導致的水文變化和其於底部滑行之作用。更重要的結果為模擬顯示，大型冰山崩解可引致冰川速度大幅提升，而加速的幅度與崩離冰山的大小有關。然而，因模擬中加入的冰山崩解現象非模型中所包含的物理過程之結果，此結果未能反映冰山崩解所致的加速屬於突變或緩慢過程。下一版本的「CISM」將配備基於實際的冰川崩解物理，有望作為更佳的模型以解決上述問題。

Acknowledgement

I wish to express my deepest gratitude to my advisor, Professor Lin Liu for his endless support and guidance, without which this thesis would not be completed. During the past two years, he has led me into the world of cryosphere geophysics and has provided me with unique and valuable opportunities including the chance to participate in the field study in Svalbard which helped me develop my skills and character as a researcher. He encouraged me to think critically when it comes to my research and to always discover my academic interests. He is a kind supervisor who is always ready to offer assistance when needed, ever patient with my progress and supportive with my decisions and time arrangements.

I would like to thank the CISM developer and user community, especially Dr. Matthew Hoffman, Dr. Stephen Price, Dr. William Lipscomb and Dr. Wentao Ma, for their kind assistance on operating the CISM during the early stages of using the model. I am also grateful for the many insights obtained from experienced and knowledgeable scientists during the 2015 AGU Fall Meeting on researching with numerical modeling. I also wish to express special gratitude to my thesis assessment committee for evaluating and providing useful comments on my work.

Finally, I want to thank my parents and Aunt Ping for their endless support with my education over the years; my wife Leafynn for her love, courage and confidence in me; my daughter Lauren, whose birth has brought great joy to my family and provided me the determination to continue with the path of academic research; and my parents-in-law for broadening my thoughts on future development.

Table of Contents

Chapter

Appendix

List of Figures

Figure

List of Tables

Table

Chapter 1

Introduction

1.1 Research Background

1.1.1 Increasing Ice Loss in Greenland Outlet Glaciers

Glaciers are massive ice bodies supported by bedrock, formed from accumulation and freezing of precipitation in cold regions, and moving at its own weight. By playing roles in affecting global water cycle and storing fresh water on land, future changes in glaciers draw the attention of scientists and the public alike. They are among the fastest-moving objects in the solid Earth systems. For instance, the Jakobshavn Glacier, the fastest moving glacier in Greenland, moved at a speed of over 17 kilometres per year in summer 2012 (Joughin et al., 2014).

Among all types of glaciers, tidewater glaciers are of particular interest because land ice is contributed into the ocean. Similar to ice shelves, with the terminus in the ocean, tidewater glaciers directly contribute ice into the ocean through calving fronts. The lost ice from tidewater glaciers eventually contributes to global sea level rise (Church et al., 2013; Nick et al., 2013; Enderlin et al., 2014). Especially under

increasingly warm climate, tidewater glaciers around the globe have been losing ice and the extent has been observed to be increasing (Khan et al., 2014; Gardner et al., 2013; Rignot et al., 2008; Vaughan et al., 2013). Therefore, it is of great significance to understand the dynamics of tidewater glaciers and how they change and interact with the other Earth systems in a warming climate.

There are a few observables to characterize the variations of tidewater glaciers, including thinning of glacial thickness, retreat of glacier front and change in flowing speed. All of these changes are related to the stability of bedrock supporting, surface mass balance, ice loss to ocean at calving front and the subsequent ice transport (Cuffey and Paterson, 2010). In recent decades, observations suggest that tidewater glaciers in Greenland and Antarctica have not only shown a trend of an increasing speed, but also been retreating (Howat et al., 2008; Moon et al., 2008; Rignot et al., 2011) and thinning (Howat et al., 2007; Pritchard et al., 2009; Rignot et al., 2010; Bevan et al., 2015). These are signs of enhanced ice mass loss. However, how different mechanisms lead to ice loss in a warming climate remain poorly understood. Therefore, understanding the short-term or transient variations in tidewater glaciers becomes more important. As compared with long-term variations, which often refer to changes over decades or centuries, short-term variations refer to differences during days or weeks.

1.1.2 Glaciological Changes of Upernavik Isstrøm

Upernavik Isstrøm outlet glaciers drain a vast amount of Greenland land ice westward into the ocean. Khan et al. (2013) analyzed ice volume changes in Upernvaik Isstrøm during 1985 to 2010 and estimated that the accelerated mass loss trend began in 2005, which was found to associate with a 5-kilometre retreat of calving front. Since that, from 2005 to 2010, the total ice mass loss induced from melting and dynamic factor in Upernvaik Isstrøm catchment basin was approximated to be 10.5 and 43.0 gigatonnes respectively.

In addition to that, our Radar Interferometry and Global Positioning System (GPS) observations suggested that one of the outlet glaciers in Upernavik Isstrøm, western Greenland, sped up abruptly from about 4.6 km/year to 6 km/year during July 2010 (see Figure 1.1). On the other hand, other glaciers in the region showed stable velocities. It is also observed that at the calving front position of Glacier 1 of Upernavik Isstrøm has retreated by 1 kilometre from June to September 2010, whereas no anomalous terminus position change was noticed in that period (see Figure 1.2). Since two phenomena occurred at a consistent timing, it is of interest to investigate the relation between these two events and to investigate other potential factors leading to a velocity jump.

(a) (b)

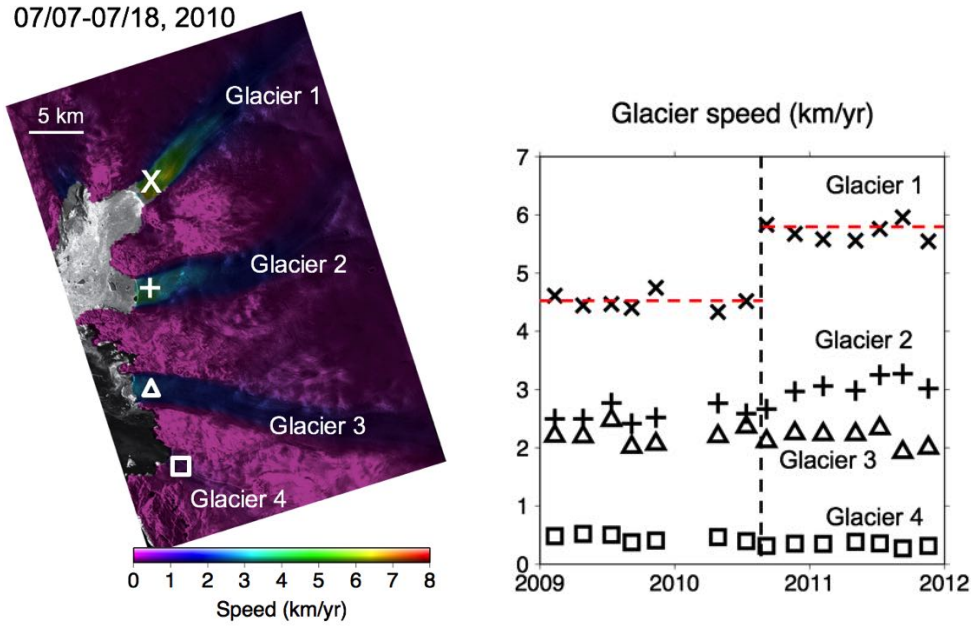

Figure 1.1 : InSAR derived speed of Upernavik glaciers (a) during 07-18 July 2010; and (b) trend from 2009 – 2012, showing only Glacier 1 exhibits sudden acceleration in 2010 summer.

(a) (b)

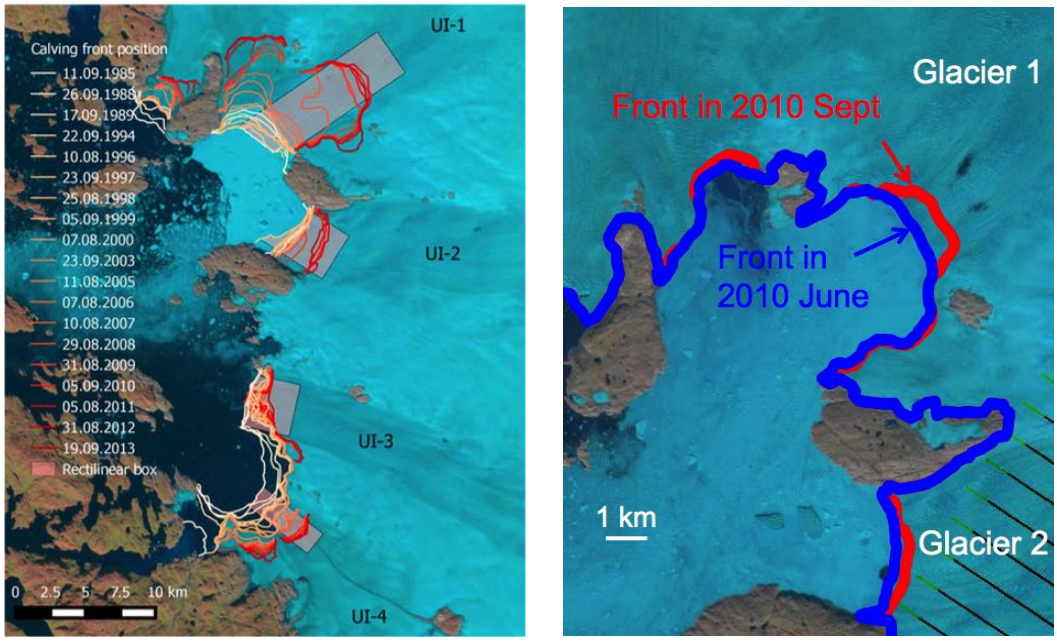

Figure 1.2 : Calving front position changes (a) of Upernavik Isstrøm outlet glaciers from 1985 to 2013 (adopted from Larsen et al., 2016), and (b) of Glacier 1 of Upernavik Isstrøm from June to September 2010 (produced by L. Liu).

1.2 Research Objectives

The purpose of this research is to investigate the potential factors leading to short-term (in a time scale of days) speed variation of a tidewater glacier with numerical modeling as a tool. By studying the short-term speed variation, it would be helpful to further understand the possible glacier dynamics mechanisms which could very possibly improve our current ice sheet system models, considering that the current large-scale ice models are yet to be able to provide realistic simulations to these changes from climatic forcing (Vieli and Nick, 2011).

Secondly, concerns of glaciers reacting extensively to the forcing of the atmosphere and the ocean. In recent years there have been some studies supporting a melt-driven glacial dynamics change, like Holland et al. (2008); Nielsen et al. (2013). To understand the sensitivity of glacier dynamics to these factors, it is necessary to have more frequent observations.

Lastly, one of the ultimate goals of glacial dynamics study is to provide a reasonable and physically based projection of long-term evolution of glacier mass balance and dynamics. Accordingly, it is important to observe short-term changes in glaciers since it allows a reduction in errors and uncertainties in the projections and improves our understanding of the fundamental dynamics of glaciers. Recent studies often use coarse inter-annual or seasonal glacial mass balance data to estimate long-term glacier contribution of ice into ocean to project future sea level rise (Rignot et al., 2011; Nick et al., 2013). The method introduces large uncertainties, both in estimating glacier mass loss and deriving potential sea level rise. By having a higher temporal solution observation on glaciers, resolving short-term variation of certain characteristics, for example, surface speed, of a glacier stream is possible thus resulting in a more reliable quantification of seasonal and inter-annual glacial mass balance.

1.3 Fundamentals of Glacier Dynamics

The movement of glaciers is primarily dictated by ice deformation, sliding relative to bedrock and also physical changes of the bedrock. In the context of short-term controls of tidewater glacier dynamics, interaction between glacier and atmosphere, glacier and bedrock and glacier and ocean are also possible criteria. They affect ice dynamics by way of melting ice into water, feedback from drainage of water content, and changing the

stability of the structure. Fundamentals in glacier dynamics are extensively introduced in Chapter 2. This subsection aims to introduce the basic concepts and key aspects that are investigated in this thesis study.

1.3.1 Surface Mass Balance

The surface of a glacier interacts with the atmosphere. Precipitation is the source of ice content in glaciers - snow and rainwater slowly become firm and eventually turn to ice upon freezing and compression. At the same time, the surface absorbs solar radiation and heat from the external environment, hence melting ice into water or even directly sublimating into a state of vapour, which could be generalized into the term ablation. The boundary between the accumulation zone and ablation zone is called equilibrium line, at which surface ice mass gain balances the ice mass loss.

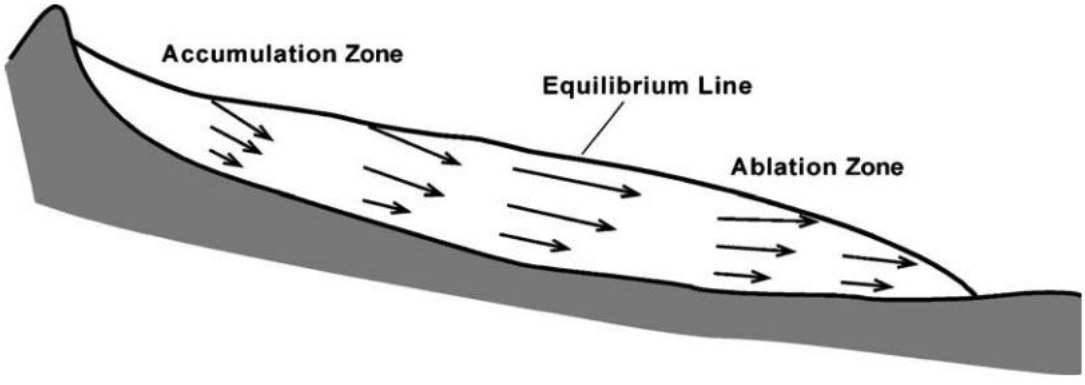

Figure 1.3 : Illustration of ice accumulation and ablation of ice at different zones of a glacier (adopted from Cuffey and Paterson, 2010).

The net balance between the sum of all processes of accumulation and ablation on the glacier surface is called surface mass balance (SMB). It does not take into account any mass change due to ice flow. Usually in high-elevation regions, temperature is relatively cooler thus inhibiting surface melting. If a region receives more accumulation than ablation, it will result in a net surface mass gain, or a positive SMB, and vice versa.

1.3.2 Vertical Drainage of Surface Meltwater

Surface meltwater could flow to different parts of the glacier if they are not stored in supraglacial lakes. The presence of cracks, called crevasses, on the ice surface allows meltwater to flow into subglacial ice and then refreeze. This process is called cryohydrological heating and it releases a large amount of heat into the inner body of the glacier (Lüthi et al., 2015). The additional dissipated heat increases local ice temperature, which could reduce ice viscosity and lead to an increased velocity. Sometimes the heat is sufficient to boost the local ice temperature to its pressure melting point, and melting could take place inside and water could drain further down. However, such a process yields great uncertainty in estimating glacial velocity due to the difficulty in identifying surface and internal crevasses across the glacial body (Schlegel et al., 2015).

Moulins are vertical channels of a few metres wide connecting glacier surface with the base. If a moulin is present nearby, large amounts of meltwater could be drained directly from the glacier surface to the base. It has a pronounced impact on the short-term water supply to the base and consequently will change glacial speed. The mechanism for that would be illustrated in the subglacial hydrology part of this text.

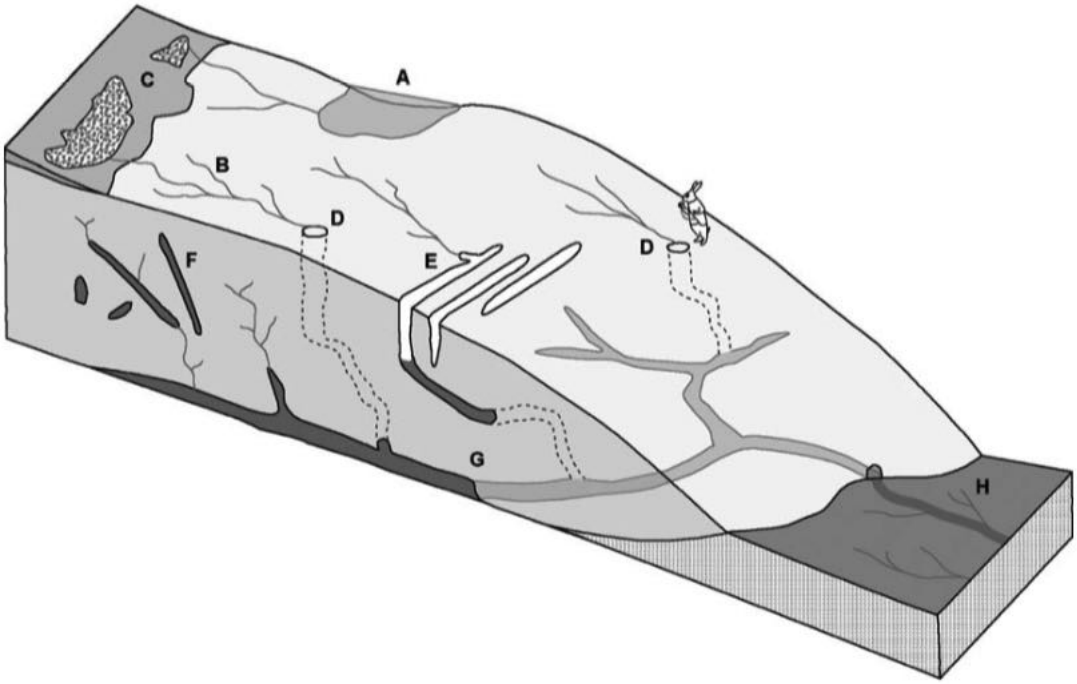

Figure 1.4 : Scheme diagram describing glacier hydrologic system on a glacier (A: Supraglacial lakes; B: Streams on surface; C: Swap zones near firn edge; D: Moulins; E: Surface crevasses; F: Water filled internal fractures; G: Subglacial tunnels, H: Foreland runoff) (adopted from Cuffery and Paterson, 2010).

1.3.3 Basal Melting

In addition to surface melting, ice can also melt in the glacier body from latent heating and strain heating, and at the bottom from geothermal heating. The base of ice sheet is subject to heat source from the interior of the Earth diffusing through the lithosphere (Davies and Davies, 2010). This contribution of heat is called geothermal heat flux which has a magnitude of around 5 mW/m^2 in western Greenland and slightly higher eastwards due to variations in lithosphere thickness (Petrunin et al., 2013). Across the depth in a glacier, weight accumulates and pressure increases. By the phase diagram, water is special because its melting point lowers as pressure increases (Van der Veen, 2013). The combination of geothermal heat flux and pressure melting effect implies ice could melt at depth. This serves as another source of basal water content apart from the direct contribution from the surface as mentioned in Chapter 1.2.3.

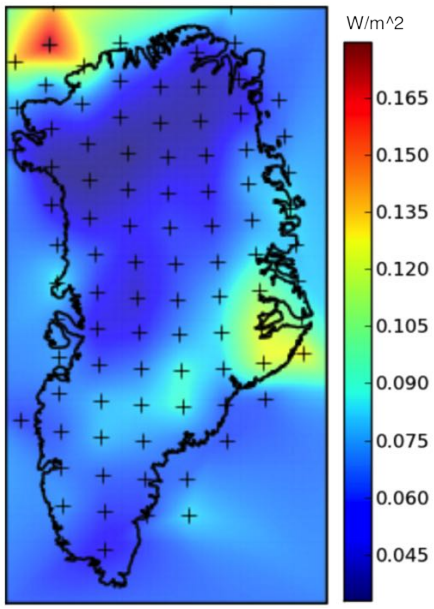

Figure 1.5 : Greenland basal heat flux map in 5kilometres resolution (Fox Maule et al., 2005).

1.3.4 Subglacial Hydrology

Zwally et al. (2002) proposed that a layer of basal melt water between the glacier and the bedrock could increase basal lubrication, which reduces the friction of glacier movement and thus enhances flow speed in general, a process known as the 'Zwally effect'. However, the varying geometry of the bedrock leads to a complex relationship between meltwater supply and basal slipping. Complicated networks that are present at the base of glaciers can be classified into two types of subglacial drainage systems: channels and cavities. Channels are generally divided into two types: Rothlisberger-channel (also called R-channels) are formed from ice melting and are in upward semi-lunar shapes (Röthlisberger,

1958); whereas Nye-channels (also called N-channels) exist in the bedrock and are in downward semi-lunar shapes (Nye, 1976). Channels allow the flowing of water; and their sizes are subjected to change by melting from frictional heat dissipation at the channel wall, and creep closure due to the weight of the overhead ice layer. Cavities are formed when ice slides over a bump on bedrock. When ice meets a protrusion ahead, there would be a jump in pressure at the region where it promotes pressure melting. This is one of the sources of water in cavities. Ice sliding over the bump would travel for a short distance before descending to the subglacial bedrock. This creates space in the cavities and such a phenomenon is called the bridging effect (Van der Veen, 2013).

(a) (b)

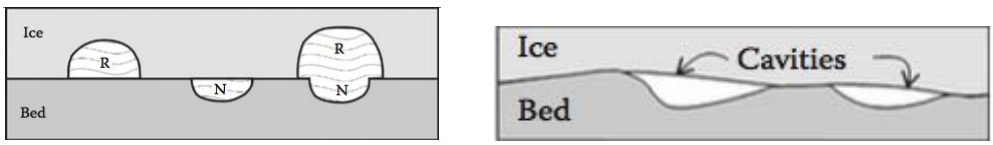

Figure 1.6 : Schematic diagram illustrating (a) R-channel, N-channel and (b) cavities as subglacial tunnels (adopted from van der Veen, 2013).

The differences in channels and cavities are not limited to their sizes and forming mechanisms but also in their responses to meltwater supply. The response to meltwater variation of channels and cavities can be derived from a simple first-order ordinary differential equation, which also depicts the evolution of R-channels and cavities, by relating the change in

cross-sectional area to wall melting, ice flux inside and the creep closure (Schoof, 2010). The derivation suggests that when water discharge is low in cavities, effective water pressure (the difference between ice burden and water pressure) decreases with it. In contrast, when there is a higher water discharge through channels, effective water pressure increases. As different conduit systems can transport water more efficiently at different water pressure, variation in meltwater supply alters effective water pressure and thus affects the efficiency of water drainage. Accelerated or decelerated in the rate of draining of meltwater as a result would change the water pressure acting on ice body, and therefore driving stress for glacial movement. For instance, in channels, higher water discharge will lead to lower water pressure and vice versa for cavities.

More interestingly, there is an interchangeable relationship between channels and cavities (Schoof, 2010). Mathematically, the equation possesses two equilibriums: the larger and smaller cross sections correspond to cavities and channels, respectively. Perturbation analysis of cavity size suggests that cavities are straightly stable whereas channels are unstable. When the size of cavities is perturbed slightly, either towards a smaller or a larger side, there is a tendency for it to evolve back to original size. However, for a channel, when the perturbation is towards the smaller side, it tends to further shrink to another stable equilibrium, which corresponds to the cavities; whereas when the perturbation is towards the larger side, it shows a tendency to grow. It is shown that there exists a

critical water discharge exceeding which, cavities will become channels, but the reverse process requires a much lower water discharge level.

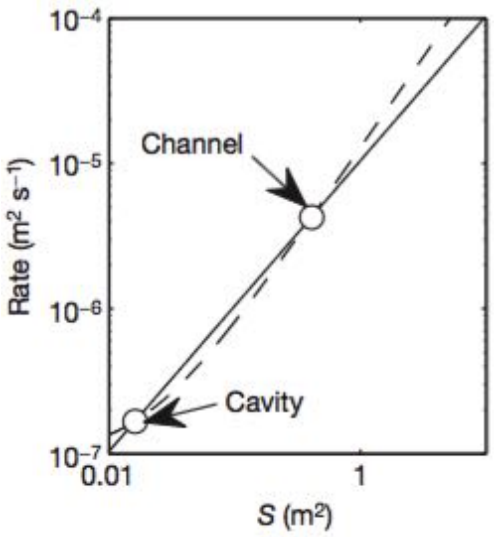

Figure 1.7 : Phase diagram of equation modeling subglacial channel changes, with the dashed line representing conduit opening rate, the solid line representing closure rate at different channel cross section size (*S*), illustrating that cavity is a stable equilibrium but not R-channels (adopted from Schoof, 2010).

Hence it could be seen that the relation between surface meltwater supply to sliding of glacier is not as simple as: more meltwater gives more lubrication and so encourages sliding. Instead, the extent of sliding is driven by variation in melt water supply and response of subglacial hydrology. Seasonally it has already been observed that there is a correlation between seasonal changes and patterns of glacier speed, possibly due to variations in surface meltwater supply (Sundal et al., 2011).

1.3.5 Grounding Line Stability

For tidewater glaciers, the grounding line is the margin at which tidewater is still being supported and beyond which ice becomes afloat on marine water. It has a significant role in the stability of the glacier. There was a hypothesis that marine ice discharge increases with local ice thickness, resulting in instability (Weertman, 1974). It suggested that for a marine ice sheet residing on an upward sloping bed, it is more likely to retain oceanic water which is warmer than ice. The ice loss by direct melting would be enhanced, resulting in retreat of the grounding line, and a larger portion of ice becomes afloat. In addition, ocean water at grounding line can further penetrate into the base of grounded ice, which reduces the friction between flowing ice and bedrock, promoting sliding.

Recent theoretic development provides mathematical formulation on the sensitivity of grounding line ice flux to local ice thickness, grounding line position and ice temperature (Schoof, 2007). It agrees with the conventional hypothesis that upward bedrock for grounding line would result in ice sheet instability. Because ice elevation is lower at the terminus side, enhanced melting of ice at the grounding line leads to a retreat and thus results in an increment of local ice thickness. As outflowing ice flux in grounding line is highly sensitive to ice, it implies that as grounding line retreats at this bedrock topography, outflow ice flux

also increases, causing a further retreat. This results in a positive feedback, i.e., an irreversible ice loss and retreat process.

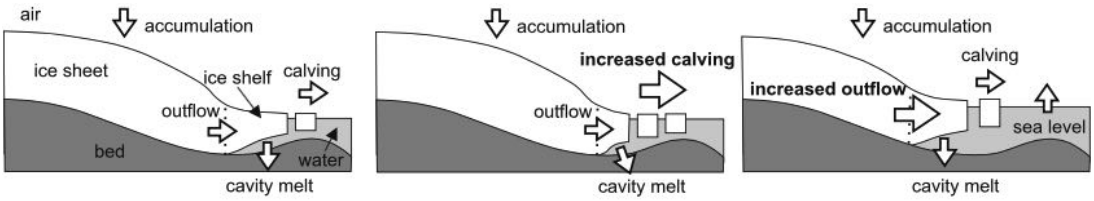

Figure 1.8 : Schematic diagram showing the positive feedback of enhanced ice loss on positive bedrock slope locating ice tongues (adopted from Schoof, 2007).

Groundling line stability also has a crucial role in the transient changes of glacial velocity because it controls stability of ice tongue, which resists the motion of grounded ice. Grounding line retreat implies some portion of ice originally grounded becomes floating. The stress distribution in the transition zone will change corresponding to vertical shear dominating into longitudinal stressing. This increases the instability of ice tongue which is supported by the buoyancy of oceans and prone to oceanic currents and eventually more ice would be calved away from the tongue. The longitudinal stress resistance of ice tongue to grounded ice inhibits the motion of glacier, thus soothes the velocity increase. Reduction of ice at ice tongue reduces the resistive stress and hence allows glacier ice to speed up. This effect is particularly strong in summer when the ocean water is warm enough to melt a large extent of floating ice.

1.3.6 Oceanic Melting and Ice Calving

Current trend of oceanic warming is also believed to lead to increased marine-terminating glacier speed (Radić and Hock, 2013). Since the specific heat capacity of ocean water is significantly greater than that of ice, warm ocean water has the potential to raise ice temperature in direct contact. Along the east coast of Greenland, warmer ocean water from the Atlantic subsides beneath cooler ocean water from the North Pole due to salinity difference (Murray et al., 2010). This suggests that the lower portion of floating ice tongue will be more likely to encounter melting. This condition favours grounding line retreat and increases the chance of ice calving.

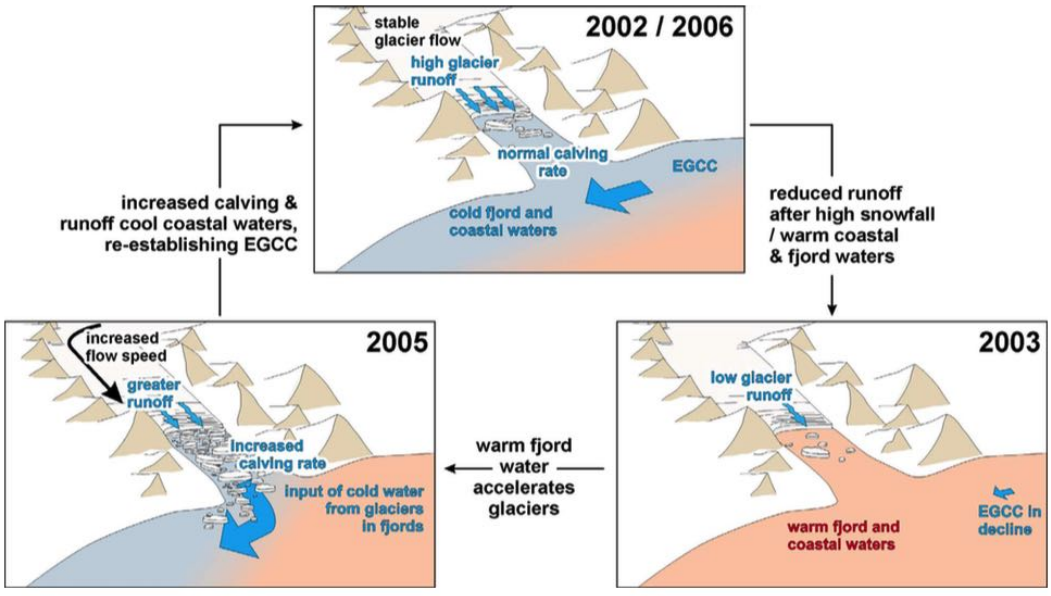

Figure 1.9 : Diagram describing the feedback between the strength of Eastern Greenland Costal Current (EGCC) and the dynamics of an outlet glacier (adopted from Murray et al., 2010).

Ice calving refers to loss of blocks of ice mass from outlet glaciers into the ocean. The size of calved ice could range from a small iceberg to an island-like chunk. The process and response of calving are short and thus massive calving is believed to be associated with glacier transient speed changes. Traditional views are that the loss of floating ice mass would lead to a reduction in internal resistive stress, which ultimately results in a speed-up. However, recent work provides an insight of alternative dynamical effect caused by calving events. Laboratory experimental results suggest that a temporary slowdown might occur as a reverse force would be applied to remaining floating ice from the calved ice when their size is comparable (Murray et al., 2015).

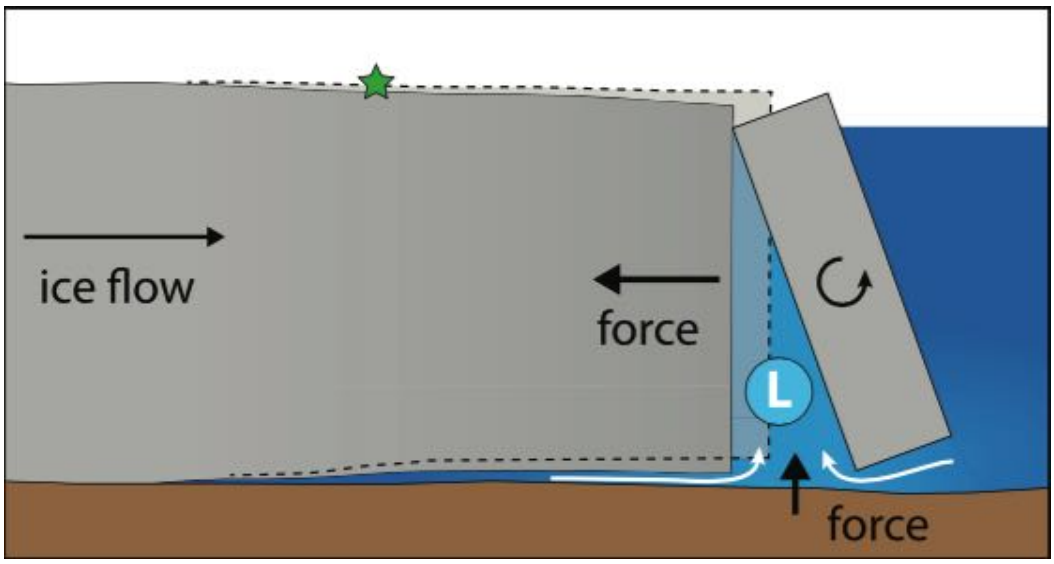

Figure 1.10 : Schematic diagram illustrating the opposing force exerting on outlet glacier main body as an extreme portion of ice calved out, which potentially lead to an instantaneous slowdown or reversed motion of glacier (adopted from Murray, 2015).

1.3.7 Terminus Conditions

The condition of ice mélange, which is a mixture of sea ice and icebergs, near the terminus of tidewater glacier has a role in altering the resistive stress of ice tongue to ground ice, thus affecting its speed. (Howat et al., 2008). Recent modeling works also suggest that ice mélange conditions sometimes play a more important role than submarine melting on terminus calving (Todd and Christoffersen, 2014). Ice mélange involves a complex process of interactions between land ice, sea ice, the atmosphere and the ocean (see Figure 1.11).

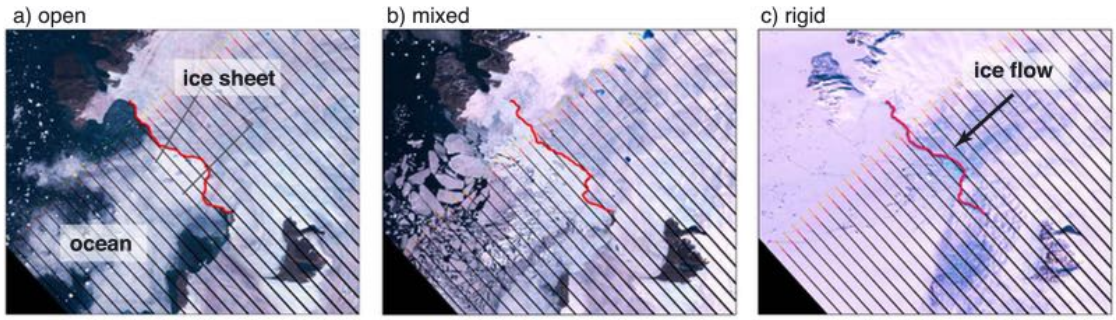

Figure 1.11 : LANDSAT image showing (a) open, (b) mixed, and (c) rigid ice mélange condition at the terminus of an outlet glacier (adopted from Moon et al., 2015).

There is a strong correlation between mélange conditions and the change in position of terminus (Moon et al., 2015). A high tendency of terminus advances is often associated with rigid ice mélange condition, which means that the sea cover around terminus is nearly completely covered by mélange. In contrast, an open ice mélange condition, where the environment is basically open water, is found to correlate with terminus retreats. It was suggested that an abundant amount of ice mélange limits the sea ice motion on ocean surface, which in turn suppresses calving at terminus (Joughin et al., 2008). This helps to preserve the resistive stress a terminus can yield on the motion of grounded ice.

Accumulating observational evidences suggest that terminus position changes could be a more important control on short-term ice velocity variation than subglacial hydrology. A combined effort of satellite imaging, SMB models and glacial hydrological models suggested that the base of Greenland Ice Sheet at low elevations are mainly wet; and meltwater supply from high elevations are increasing notable (Poinar et al., 2015). As covered previously, subglacial drainage varies upon variations in basal water content. Upon a water-filled basal condition, the effect of relative variation becomes less significant than the case of a dry or partially wet base, which suggests that speed variation from subglacial hydrology aspect would be outweighed by terminus changes.

1.4 Thesis Roadmap

This thesis begins by introducing the background and objectives of my research on studying transient speed variation of Greenland outlet glaciers by numerical modeling. Chapter 1 also provides qualitative insight on how various factors might contribute to dynamical changes of glacier motions. Chapter 2 presents the mathematical and numerical tools adopted in current ice sheet models. In Chapter 3, the capabilities of different models are compared and the reasons for choosing Community Ice Sheet Model (CISM) in this study are explained. The data sources and how the model is configured will be introduced in Chapter 4. Chapter 5 illustrates the modeling results and discusses the use of CISM to investigate different factors on transient speed variation. Conclusions are presented in Chapter 6.

Chapter 2

Ice Sheet Physics & Models

2.1 Physical Properties of Ice

It is common knowledge that the phase transition between ice and water occurs, at room pressure (1 atm), at 0 °C. However, unlike most other natural materials, the melting point of ice decreases as the exerted pressure increases. This could be reflected by the negatively sloped ice-water phase boundary in the phase diagram of water (Figure 2.1). Considering the containment of air bubble in ice, the local ice pressure melting point *T'* could be approximated by the empirical equation:

$$T' = T_0 - \beta P \qquad (1)$$

where $T_0 = 0.01$ °C is the triple point temperature of water,

$\beta = 9.8\times 10^{-8}$ K Pa^{-1},

P is the relative pressure to triple point pressure of water (0.006 atm).

For example, in a 1000-metres thick ice column, the melting point of ice at bottom is around -0.87 °C. This is an essential piece of information to be

taken account of in ice sheet thermomechanical model, as ice at different locations shall process different melting points.

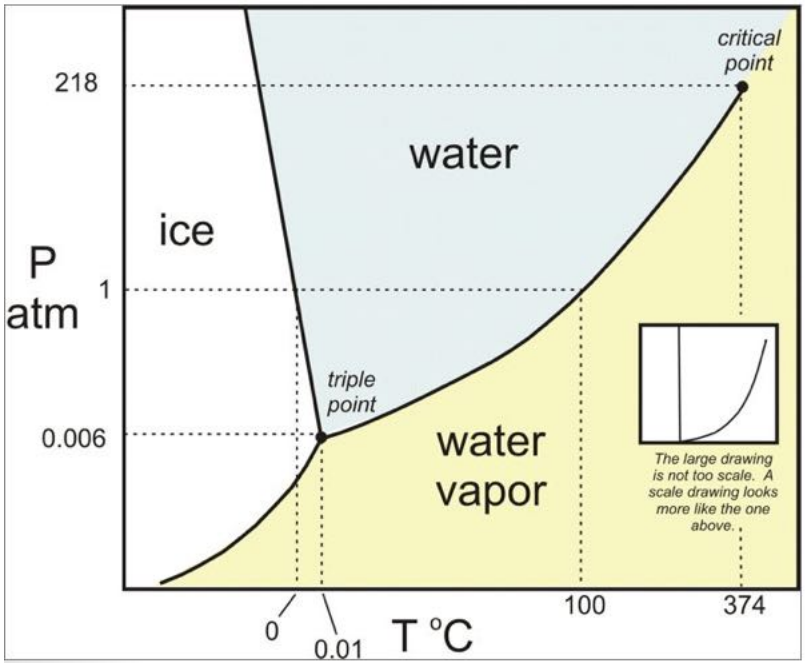

Figure 2.1: Phase diagram of water, with information of a triple point at which solid, liquid and vapour phases of water coexist.

Another significant property of ice, though trivial in nature, is that it has lower density than water. Again, most other substances have higher densities in solid state than liquid state. Transforming from snow, glacier ice has a typical density of 830 – 920 kg m^{-3}; whereas seawater generally has density of slightly higher than 1020 kg m^{-3}. The density difference creates a buoyancy force that allows ice to float on water surface.

Microscopically, these special physical properties of ice are associated with strong hydrogen-bonding between water molecules, arising from strong electronegativity at oxygen-hydrogen (O-H) covalent bond and the presence of lone pair electrons on oxygen atoms. The hydrogen bonds, together with the tetrahedral structure of water molecules (Figure 2.2 (a)), form hexagonal crystal structure (Figures 2.2 (b) & (c)) when water turns into ice. This structure is relatively stable, yet takes up more space compared with the randomly orientated water molecules in liquid form. Consequently, volume expands when water freezes into ice, which leads to a lower density of ice. Moreover, as greater pressure exerts on ice, some of the stable crystalline structures break down, which require fewer energy to further overcome the bonding, resulting in a lower melting point. The microscopic structure of ice polycrystalline in nature is made up of many impurities: for instance, air bubbles, dusts, salts, sands and rocks, which leads to different ice properties across the globe.

(a) (b)

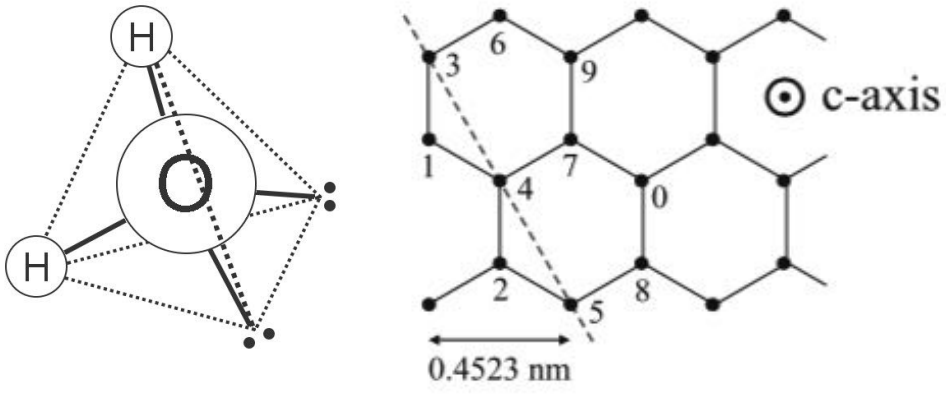

(c)

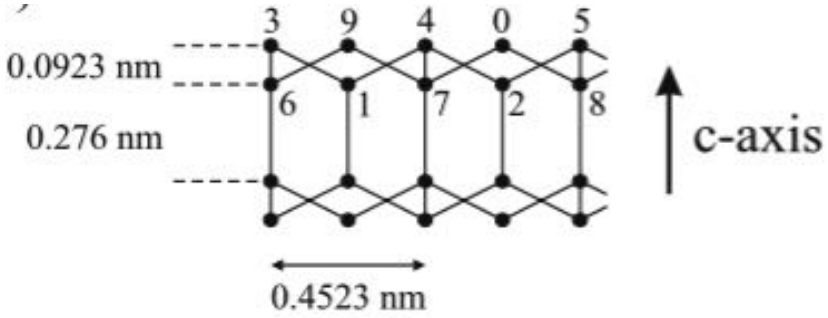

Figure 2.2 : (a) The tetrahedral structure of water molecule (solid dots represent lone electrons); (b) hexagonal structure in ice crystal viewed on basal plane (solid dots represent oxygen atoms in water molecules), *c*-axis is the direction perpendicular to the plane; (c) hexagonal structure in ice crystal viewed on plane of cross section of dotted line as shown in (b) (adopted from Greve and Blatter, 2009).

2.2 Ice Rheology

Ice, though has physical state as a solid, could behave as if it is a very viscous fluid under great stress. Such feature is important to understanding and modeling the flow in ice sheet as it involves tremendous gravitational driving stress arising from ice thickness of hundreds or thousands of metres, not to mention the stress variations due to other topographic factors. Hence, ice rheology is the fundamental of formulating mechanical models for ice flows.

2.2.1 Stress & Strain Analysis

Stress and strain are quantities used to describe force and deformation on a material element. Stress has unit of force per area while strain is a measure of displacement gradients. In ice dynamics, strain rate is used more often as it describes velocity gradients. In three dimensional space, stress $\boldsymbol{\sigma}$ and strain rate $\dot{\boldsymbol{\epsilon}}$ are represented using tensor notation as second order tensors, which could also be viewed as 3×3 matrices. In an ice sheet, the normal stresses experienced by ice parcels are compressive. A deviatoric stress tensor, $\boldsymbol{\tau}$, is defined by the combination of a stress tensor and mean normal stress tensor :

$$\boldsymbol{\tau} = \boldsymbol{\sigma} - P\boldsymbol{I} \tag{2}$$

where P denotes the mean normal stress, and $\boldsymbol{I}$ represents identity matrix. Deviatoric stress tensors, which account for stress deviation from isotropic state, are often used rather than full stress tensors in describing deformation of incompressible materials.

Tensor notations are used to describe stresses, strain and strain rate components. For example, σ_{ij} stands for stress on i-direction in j-plane (see Figure 2.3 for a graphic representation). σ_{ij} represents a normal stress if $i = j$, and a shear stress if $i \neq j$. It is interesting to note that in general the

stress tensor $\boldsymbol{\sigma}$ is symmetric, i.e. $\sigma_{ij} = \sigma_{ji}$ due to conservation of angular momentum.

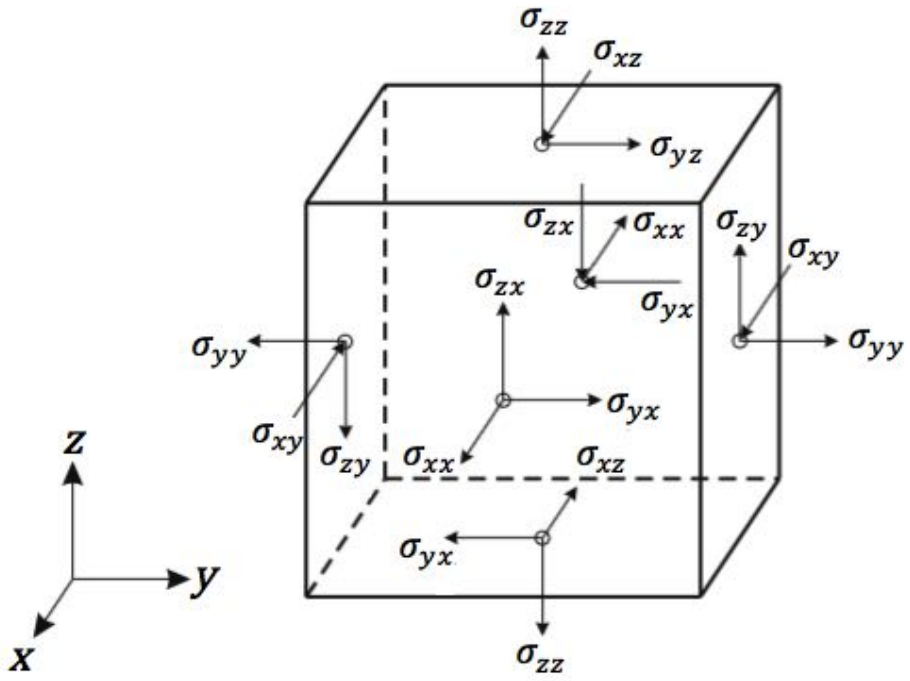

Figure 2.3 : Diagram representation of Cauchy stress tensor components on a cubic element (modified from Greve and Blatter, 2009).

The matrix form of Equation (2) is :

$$\begin{pmatrix} \tau_{xx} & \tau_{xy} & \tau_{xz} \\ \tau_{yx} & \tau_{yy} & \tau_{yz} \\ \tau_{zx} & \tau_{zy} & \tau_{zz} \end{pmatrix} = \begin{pmatrix} \sigma_{xx} & \sigma_{xy} & \sigma_{xz} \\ \sigma_{yx} & \sigma_{yy} & \sigma_{yz} \\ \sigma_{zx} & \sigma_{zy} & \sigma_{zz} \end{pmatrix} - \begin{pmatrix} P & 0 & 0 \\ 0 & P & 0 \\ 0 & 0 & P \end{pmatrix} \quad . \tag{3}$$

Also, as is defined as the mean normal stress,

$$P = \frac{1}{3}\left(\sigma_{xx} + \sigma_{yy} + \sigma_{zz}\right) \quad . \tag{4}$$

Equation (9) could be rewritten as :

$$\begin{pmatrix} \tau_{xx} & \tau_{xy} & \tau_{xz} \\ \tau_{yx} & \tau_{yy} & \tau_{yz} \\ \tau_{zx} & \tau_{zy} & \tau_{zz} \end{pmatrix} =$$

$$\begin{pmatrix} \frac{1}{3}(2\sigma_{xx} - \sigma_{yy} - \sigma_{zz}) & \sigma_{xy} & \sigma_{xz} \\ \sigma_{yx} & \frac{1}{3}(-\sigma_{xx} + 2\sigma_{yy} - \sigma_{zz}) & \sigma_{yz} \\ \sigma_{zx} & \sigma_{zy} & \frac{1}{3}(-\sigma_{xx} - \sigma_{yy} + 2\sigma_{zz}) \end{pmatrix}. \quad (5)$$

A strain rate component $\dot{\epsilon}_{ij}$ is defined as :

$$\dot{\epsilon}_{ij} = \frac{1}{2}\left(\frac{\partial u_i}{\partial x_j} + \frac{\partial u_j}{\partial x_i}\right) \quad (6)$$

where u_i, x_i ; u_j, x_j denote the velocity components and directions in i and j-direction respectively. It represents a normal strain if $i = j$, and a shear strain if $i \neq j$. Thus, the strain rate tensor $\dot{\boldsymbol{\epsilon}}$ in Equation (6) can be written in the following matrix form :

$$\dot{\boldsymbol{\epsilon}} = \begin{pmatrix} \dot{\epsilon_{xx}} & \dot{\epsilon_{xy}} & \dot{\epsilon_{xz}} \\ \dot{\epsilon_{yx}} & \dot{\epsilon_{yy}} & \dot{\epsilon_{yz}} \\ \dot{\epsilon_{zx}} & \dot{\epsilon_{zy}} & \dot{\epsilon_{zz}} \end{pmatrix}$$

$$= \begin{pmatrix} \frac{\partial u}{\partial x} & \frac{1}{2}\left(\frac{\partial u}{\partial y} + \frac{\partial v}{\partial x}\right) & \frac{1}{2}\left(\frac{\partial u}{\partial z} + \frac{\partial w}{\partial x}\right) \\ \frac{1}{2}\left(\frac{\partial v}{\partial x} + \frac{\partial u}{\partial y}\right) & \frac{\partial v}{\partial y} & \frac{1}{2}\left(\frac{\partial v}{\partial z} + \frac{\partial w}{\partial y}\right) \\ \frac{1}{2}\left(\frac{\partial w}{\partial x} + \frac{\partial u}{\partial z}\right) & \frac{1}{2}\left(\frac{\partial w}{\partial y} + \frac{\partial v}{\partial z}\right) & \frac{\partial w}{\partial z} \end{pmatrix} \quad (7)$$

where u,v,w are magnitude of velocities in x,y,z-directions respectively. It could be seen trivially that deviatoric and strain rate tensors are also symmetric.

The three invariants of stress, deviatoric stress and strain rates could be shown by finding the eigenvalues of respective matrix systems. The invariants of these tensors are quantities that are irrespective of orientation of coordinate systems. Take strain rate as an example, the first invariant $\dot{\epsilon_{I1}}$ is :

$$\dot{\epsilon_{I1}} = \dot{\epsilon_{xx}} + \dot{\epsilon_{yy}} + \dot{\epsilon_{zz}} \ . \tag{8}$$

The first invariant of strain rate tensor gives the fractional volume changing rate of a deforming ice. The second invariant $\dot{\epsilon_{I2}}$ is :

$$\dot{\epsilon_{I2}} = \frac{1}{2}\left[\dot{\epsilon}_{xx}^2 + \dot{\epsilon}_{yy}^2 + \dot{\epsilon}_{zz}^2 + 2\left(\dot{\epsilon}_{xy}^2 + \dot{\epsilon}_{xz}^2 + \dot{\epsilon}_{yx}^2\right)\right] \quad . \tag{9}$$

This quantity is the square of the effective strain rate. Lastly, the third invariant $\dot{\epsilon_{I3}}$ is the determinant of the strain rate matrix :

$$\dot{\epsilon_{I3}} = \det\left(\dot{\boldsymbol{\epsilon}}\right) \qquad . \tag{10}$$

2.2.2 Deformation of Ice

The hexagonal symmetry makes ice crystal one of the most anisotropic natural materials on the Earth. The deformation of polycrystalline ice occurs mainly along basal planes by dislocation glide (Budd and Jacka, 1989). This phenomenon is often observed near ice sheet peaks and where ice movement is slow. However, further downstream, ice is subject to more compression and shearing, eventually making the deformation less unidirectional favoured. In the development of classical ice dynamics theory, an isotropic creeping of ice was usually assumed.

"Glen's Law" (Glen, 1952; 1955) is the basics for modeling ice flow. It assumes that the creeping of ice is (1) isotropic throughout the flow, (2) independent of hydrostatic pressure, and (3) is incompressible. Rigorously speaking, the compressibility of ice, γ, which could be defined by :

$$\gamma = \frac{1}{\rho_i}\frac{\partial \rho_i}{\partial P} \tag{11}$$

is approximately 1.2×10^{-10} Pa^{-1} experimentally (Feistel and Wagner, 2006). Yet, the small value of γ suggests that ice is almost incompressible, making incompressibility a safe assumption. Glen's Law suggests that effective deviatoric stress τ_e, where

$$\tau_e = \sqrt{\frac{1}{2}\left[\tau_{xx}^2 + \tau_{yy}^2 + \tau_{zz}^2 + 2\left(\tau_{xy}^2 + \tau_{xz}^2 + \tau_{yz}^2\right)\right]},$$

and effective strain rate $\dot{\epsilon_e}$, where

$$\dot{\epsilon_e} = \sqrt{\frac{1}{2}\left[\dot{\epsilon}_{xx}^2 + \dot{\epsilon}_{yy}^2 + \dot{\epsilon}_{zz}^2 + 2\left(\dot{\epsilon}_{xy}^2 + \dot{\epsilon}_{xz}^2 + \dot{\epsilon}_{yz}^2\right)\right]},$$

are related in form of :

$$\dot{\epsilon_e} = A\tau_e^n \tag{12}$$

where A is a parameter called Glen's flow factor; and

n is a parameter called Glen's exponent.

Based on laboratory experiments and field work, it is eventually reached to a conclusion that $n = 3$ is a suitable choice for isotropic ice (Nye, 1953;

Weertman, 1973; Martin and Sanderson, 1980) and this value has been widely adopted until today.

The flow parameter A was found to be temperature dependent from early experimental stage (See Figure 2.4). Based on the Arrhenius Law, the flow parameter A is assumed to follow such a relation:

$$A = A_0 \exp\left(-\frac{Q}{RT'}\right) \tag{13}$$

where A_0 is the material dependent prefactor constant;

R = 8.31 J mol^{-1} K^{-1} is the universal gas constant;

T' is the pressure melting point as outlined in Equation (1); and

$Q = \begin{cases} 60 \text{ KJ mol}^{-1}, & \text{if } T' < 263.15 \text{ K} \\ 139 \text{ KJ mol}^{-1}, & \text{if } T' > 263.15 \text{ K} \end{cases}$ is the creep activation energy.

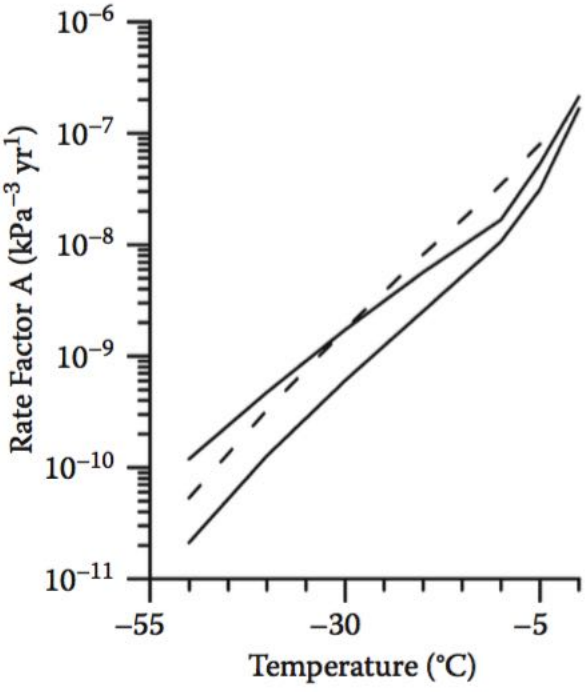

Figure 2.4 : Dependence of flow factor A on ice temperature. Dashed line represents experimental data by Hooke, 1981; solid lines represent upper and lower bound suggested by Peterson and Budd (1982) (adopted from van der Veen, 2013).

When higher than -10 °C, local melting occurs at ice crystal boundaries microscopically. This phenomenon results in a requirement of additional energy to activate the ice creeping and therefore different values of Q has to be used for ice temperature below and above -10 °C. At present, no experimental evidence seems to suggest the necessity of a more complex flow factor - ice temperature relation, compared with the Arrhenius Law as in Equation (13) (Cuffery and Paterson, 2010).

2.2.3 Constitutive Relation

The flow of ice, macroscopically, could be described using concepts from continuum mechanics. Formulating ice dynamics in this way reflects ice deformation under stress but avoids consideration of the microscopic changes. Continuum mechanics requires assumptions of conservations of mass, energy and momentum and the incompressibility of a material.

Constitutive relation of ice for incompressible viscous fluid is an equation relating the deviatoric stress tensor with strain rate tensor in an

ice element with a coefficient responding to viscosity. In the context of ice dynamics, the constitutive law is:

$$\boldsymbol{\sigma} = 2\mu\dot{\boldsymbol{\epsilon}} \tag{14}$$

where μ is the ice viscosity. Following Glen's Law (Equation 12) and the constitutive relation (Equation 14), ice viscosity can be expressed as:

$$\mu = B/\, 2\dot{\epsilon}_e^{\frac{1}{n}-1} \tag{15}$$

where $B = A^{-1/n}$ is the ice hardness.

Similar to the flow parameter *A,* ice hardness *B* and thus ice viscosity μ are temperature dependent. It can be shown that the ice viscosity has an inverse power relation with effective stress using Equation (15) (see Figure 2.5). However, unlike other incompressible Newtonian fluids, the flow of polycrystalline ice is non-linear and therefore the viscosity is not a constant.

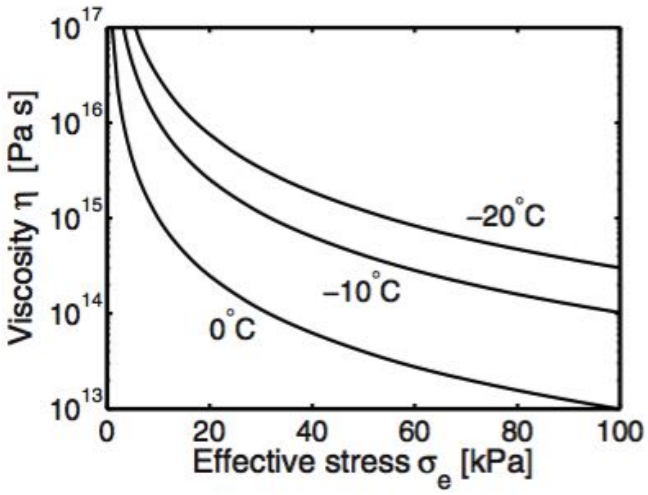

Figure 2.5 : Ice viscosity against effective stress with exponent n = 3 at different ice temperatures (adopted from Greve and Blatter, 2009).

2.3 Mechanical Models

Mechanical models describe and simulate ice motions by momentum/stress balances. Flow of glacier ice is considered as Stokes flow. Although a complete set of Navier-Stokes Equation takes full consideration of internal and external forces, the formulation and computation process are rather complex, especially when they are applied to large-scale ice sheet problems. To reduce model complexity while without neglecting the essential components, different simplifications have been made depending on the spatial/temporal scales. Hindmarsh (2004) and Schoof and Hewitt (2013) provide good references for rigorous mathematical derivations and numerical analysis of different mechanical

models. In the following discussion, all the mechanical models involved assume a stress-free ice surface condition, i.e.,

$$\boldsymbol{\sigma} \cdot \hat{\boldsymbol{n}} = 0 \tag{16}$$

where $\hat{\boldsymbol{n}}$ is the unit vector normal and outward to the surface.

2.3.1 Full Stokes (FS) Model

The three-dimensional flow in ice sheet can be described by Stokes Equation (Stokes, 1845). Certain assumptions could be made to simplify the sets of equation: (1) ice is incompressible; (2) acceleration of ice is negligible; (3) Coriolis effect from rotating motion of the earth is negligible; and (4) turbulence in ice is not considered. The last three assumptions could be verified valid from the scale analysis by Greve and Blatter (2009). Eventually, the vector formulation of Full Stokes model of ice sheet flow is formed as :

$$\begin{cases} \nabla \cdot \boldsymbol{\tau} + \rho \boldsymbol{g} = \mathbf{0} \\ \dfrac{d\rho}{dt} = 0 \end{cases} \tag{17}$$

where ρ is the density of ice, and

$\boldsymbol{g}$ is the effective gravity vector, after neglecting the Coriolis force.

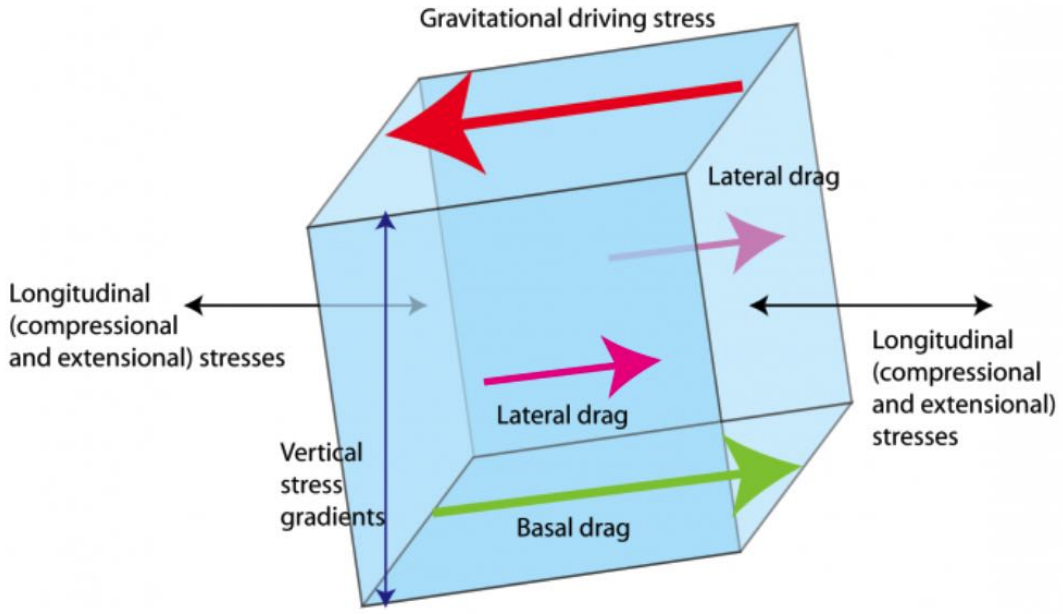

Figure 2.6 : Stress balance considered in Full Stokes model (adopted from www.AntarcticGlacier.org).

If scalar formulation is desired, one can apply the definition of deviatoric stress (Equation 2) into the constitutive law (Equation 14) and substitute into Equation (17), which would yield Equations (18 – 21). It would then be seen that the FS model is a set of nonlinear equations with 4 unknown variables (*u, v, w,* and *P*) and therefore it would be computationally very expensive.

$$\frac{\partial}{\partial x}\left(2\mu\,\frac{\partial u}{\partial x}\right)+\frac{\partial}{\partial y}\left(\mu\,\frac{\partial u}{\partial y}+\mu\,\frac{\partial v}{\partial x}\right)+\frac{\partial}{\partial z}\left(\mu\frac{\partial u}{\partial z}+\mu\frac{\partial w}{\partial x}\right)=\frac{\partial P}{\partial x}\quad ; \qquad (18)$$

$$\frac{\partial}{\partial x}\left(\mu\,\frac{\partial u}{\partial y}+\mu\,\frac{\partial v}{\partial x}\right)+\frac{\partial}{\partial y}\left(2\mu\,\frac{\partial v}{\partial y}\right)+\frac{\partial}{\partial z}\left(\mu\frac{\partial v}{\partial y}+\mu\frac{\partial w}{\partial y}\right)=\frac{\partial P}{\partial y}\quad ; \qquad (19)$$

$$\frac{\partial}{\partial x}\left(\mu\frac{\partial u}{\partial z}+\mu\frac{\partial w}{\partial x}\right)+\frac{\partial}{\partial y}\left(\mu\frac{\partial v}{\partial z}+\mu\frac{\partial w}{\partial y}\right)+\frac{\partial}{\partial x}\left(2\mu\frac{\partial w}{\partial z}\right)=\frac{\partial P}{\partial z}+\rho g \quad ; \qquad (20)$$

$$\frac{\partial u}{\partial x}+\frac{\partial v}{\partial y}+\frac{\partial w}{\partial z}=0 \quad . \qquad (21)$$

2.3.2 Blatter-Pattyn (BP) Higher Order Approximation

BP Higher Order Approximation (Blatter, 1995; Pattyn, 2003) is a three-dimensional mechanical model simplified from the FS model by assuming: (1), horizontal gradients of vertical velocities are negligible compared with vertical gradients of horizontal velocities, i.e. letting

$$\frac{\partial w}{\partial x}=\frac{\partial w}{\partial y}=0 \quad ; \qquad (22)$$

and (2) bridging effect (van der Veen and Whillians, 1989), referring to situations where ice is not supported from underneath as flowing across cavities, is negligible. At these occasions, the vertical shearing stresses are transferred to neighbouring ice that are grounded to bed, making them negligible in z-direction. Hence Equation (20) could be further reduced to :

$$\frac{\partial}{\partial z}\left(2\mu\frac{\partial w}{\partial z}\right)=\frac{\partial P}{\partial z}+\rho g \quad . \qquad (23)$$

From Equation (23), integrating both sides vertically gives the expression of ice pressure P :

$$P(z) = \rho g(s - z) + 2\mu \frac{\partial w}{\partial z} + P_{atm} \quad . \tag{24}$$

where s is the surface elevation of ice column; and

P_{atm} is the atmospheric pressure.

Equation (24), together with Equation (21) could then be substituted into Equation (18) and (19) after differentiation to yield the BP higher order model :

$$\frac{\partial}{\partial x}\left(4\mu\frac{\partial u}{\partial x} + 2\mu\frac{\partial v}{\partial y}\right) + \frac{\partial}{\partial y}\left(\mu\frac{\partial u}{\partial y} + \mu\frac{\partial v}{\partial x}\right) + \frac{\partial}{\partial z}\left(\mu\frac{\partial u}{\partial z}\right) = \rho g\frac{\partial s}{\partial x} \quad ; \tag{25}$$

$$\frac{\partial}{\partial x}\left(\mu\frac{\partial u}{\partial y} + \mu\frac{\partial v}{\partial x}\right) + \frac{\partial}{\partial y}\left(4\mu\frac{\partial v}{\partial y} + 2\mu\frac{\partial u}{\partial x}\right) + \frac{\partial}{\partial z}\left(\mu\frac{\partial v}{\partial z}\right) = \rho g\frac{\partial s}{\partial y} \quad , \tag{26}$$

which solves for horizontal velocities (*u,v)*. And *w* is solved by incompressibility as it is decoupled from the two equations above. The model is subjected to a stress-free upper surface and basal traction as boundary conditions.

BP higher order model is computationally much less heavy than FS model and still capable to perform three-dimensional simulation of ice sheet with high order of accuracy. However, FS model still has a major

advantage over BP in that it can simulate flows across grounding line where vertical velocity variation is not negligible.

2.3.3 Shallow Shelf Approximation (SSA)

Shallow Shelf Approximation was developed to apply to ice shelf flow problems (MacAyeal,1989). Later it was also found to perform reasonably well in ice streams at gentle bed topography and with weak lateral and basal shearing. SSA takes advantage of considering the driving stress in ice shelves are longitudinal dominating, and also the shallowness assumption (as the vertical length scale is much lower than horizontal length scale). These assumptions imply the flow in ice shelves can be considered constant with depth and thus vertical velocity gradient is negligible:

$$\frac{\partial u}{\partial z} = \frac{\partial v}{\partial z} = 0 \quad . \tag{27}$$

Depth averaging the equations yields SSA :

$$\frac{\partial}{\partial x}\left(4H\bar{\mu}\frac{\partial u}{\partial x} + 2H\bar{\mu}\frac{\partial v}{\partial y}\right) + \frac{\partial}{\partial y}\left(H\bar{\mu}\frac{\partial u}{\partial y} + H\bar{\mu}\frac{\partial v}{\partial x}\right) = \rho g H\frac{\partial s}{\partial x} \quad ; \tag{28}$$

$$\frac{\partial}{\partial x}\left(H\bar{\mu}\frac{\partial u}{\partial y} + H\bar{\mu}\frac{\partial v}{\partial x}\right) + \frac{\partial}{\partial y}\left(4H\bar{\mu}\frac{\partial u}{\partial x} + 2H\bar{\mu}\frac{\partial v}{\partial x}\right) = \rho g H\frac{\partial s}{\partial y} \quad , \tag{29}$$

where H is the thickness of ice column; and

$\bar{\mu}$ is the depth-averaged ice viscosity.

SSA is considered as a two-dimensional model because its governing equation solves for two unknowns (u,v). Even though vertical velocity w could be found as incompressibility assumption still holds, the magnitude is generally considered insignificant compared with horizontal velocities. The computational speed of SSA is much faster than BP on an ice shelve problem, as it has considered one dimension less.

2.3.4 Shallow Ice Approximation (SIA)

Shallow Ice Approximation (Hutter, 1983) is a very simplified model and yet considered as an important basis for future ice dynamics model development. SIA treats ice sheet as a shallow system and considers only the horizontal deviatoric stress components τ_{xz} and τ_{yz}. These components account for the vertical shearing characteristics at inland ice sheet flow. It also neglects the horizontal gradient of vertical velocity, which then yields the set of equations :

$$\frac{\partial}{\partial z}\left(\mu \frac{\partial u}{\partial z}\right) = \rho g \frac{\partial s}{\partial x} \quad ; \tag{30}$$

$$\frac{\partial}{\partial z}\left(\mu \frac{\partial v}{\partial z}\right) = \rho g \frac{\partial s}{\partial y} \quad , \tag{31}$$

in which u and v can be solved separately. Similar to SSA, SIA is also a two-dimensional model with high computational efficiency. It is often used in construction of ice sheet dynamics in a timescale of paleo-climate study

and applied on continental scale of ice sheet. However, SIA is unsuitable for short-term glacier dynamics study because it is oversimplified which does not consider the key stress components that alter ice flow.

2.4 Basal Traction and Sliding

At the base of ice sheet, basal traction exists to provide opposing stress to ice flow and generates frictional heating at the same time. Thus the formulation of basal traction serves as an important boundary condition for both momentum balance and thermomechanical models. It begins with the simple traction relation:

$$\boldsymbol{\tau_b} = -\alpha^2 \boldsymbol{u_b} \quad , \tag{32}$$

which suggests the basal traction $\boldsymbol{\tau_b}$ is linearly related to basal velocity $\boldsymbol{u_b}$ through a traction parameter α.

Based on Weertman friction law (Weertman, 1964), a modification work (Bindschadler, 1983) was constructed to include the dependence of friction on effective pressure, which is defined to be ice overburden minus water pressure at bed. It describes the basal friction as:

$$\boldsymbol{\tau_b} = \kappa^{-\frac{1}{p}} \boldsymbol{u_b}^{\frac{1}{p}} N^{\frac{q}{p}} \quad , \tag{33}$$

where κ is friction coefficient related to bed roughness and ice properties;

N is the effective pressure;

$p = 3$ and $q = 1$.

The modified Weetman friction law suggests that the basal traction is nonlinearly related to basal velocity and that it is affected by basal water depth.

Finally, a friction law considers at sub-grid scale which accounts for sliding of glacier ice over hard beds, allowing cavitation and bounded basal drag (Schoof, 2005) :

$$\boldsymbol{\tau_b} = C \left(\frac{\boldsymbol{u_b}}{\boldsymbol{u_b} + N^n \Lambda} \right)^{\frac{1}{n}} N \quad , \quad \text{with} \tag{34}$$

$$\Lambda = \frac{\lambda_{max}\, \chi}{m_{max}} \quad , \tag{35}$$

where C is a Coulomb friction coefficient;

χ is the sliding parameter without cavitation;

λ_{max} is the wavelength of dominant bedrock bumps; and

m_{max} is the maximum slope of dominant bedrock bumps.

Asymptotically, this model performs as a Coulomb friction law when effective pressure is low, and as a power law form against basal velocity in high effective pressure.

2.5 Thermo-mechanical Models

A thermo-mechanical model in ice temperature could be used to model the ice temperature, T. It considers an energy balance as:

$$\frac{\partial T}{\partial t} = \frac{k}{\rho c}\nabla^2 T - \boldsymbol{u}\cdot\nabla T + \frac{\Phi}{\rho c} \quad , \tag{36}$$

where k = 2.4 W m^{-1} K^{-1} is the thermal conductivity of ice;

c = 2.1 kJ kg^{-1} K^{-1} is the specific heat capacity of ice;

$\Phi = 4\mu\dot{\epsilon}_e^2$ is the internal heating rate; and

$\boldsymbol{u}$ is the local ice velocity.

The first term on the right hand of Equation (36) describes the heat diffusion, whereas the second term accounts for the change in temperature due to heat advection, and the last term considers internal heating due to viscous dissipation. In cases where the shallowness assumption holds, this thermomechanical equation could be further simplified to consider heat advection and diffusion only in the vertical direction instead of all three-dimensional space. An important criterion for T is that it must not exceed the local pressure melting point as phase transition occurs.

Pressure melting takes place when ice temperature T_{ice} exceeds pressure melting point T_{pmp} . Therefore as refreezing when water temperature T_{water} drops below T_{pmp}, the following relation could be used to find the basal ice mass change δM_b due to change in state :

$$\delta M_b = \frac{k}{\rho L}\frac{\partial}{\partial z}\left(T_{pmp} - T\right) \quad . \tag{37}$$

For instance, in case of basal melting k, ρ ,T in Equation (37) should be taken as thermal conductivity, density and temperature of ice respectively, whereas L = 0.334 MJ kg^{-1} is the specific latent heat of fusion of ice.

The thermomechanical model also takes surface ice temperature, and sometimes mean annual air temperature, as a boundary condition at upper surface. The base of grounded ice is subjected to both geothermal heat flux and frictional heating at ice-bedrock interface as ice flows through bedrock. Therefore, basal heat balance of grounded ice satisfies the following relation:

$$k\nabla T \cdot \hat{\boldsymbol{n}} = G - \boldsymbol{\tau_b} \cdot \boldsymbol{v_b} \quad , \tag{38}$$

where G = 0.05 W m^{-2} is the geothermal heat flux.

On the other hand, floating ice tongues and ice shelves do not subject to direct heating from interaction with bedrock; instead they exchange heat with seawater. Holland and Jenkins (1999) provided a parameterization on this problem :

$$k\nabla T \cdot \hat{\boldsymbol{n}} = -\rho_w c_M \gamma \left(T - T_f'\right) \quad , \tag{39}$$

where ρ_w = 1020 g m^{-3} is the density of seawater;

c_M = 3.97 kJ kg^{-1} K^{-1} is the specific heat capacity of mixed layer;

γ = 10^{-4} is the thermal exchange velocity; and

T_f' is the pressure dependent seawater freezing point (Equation 1).

However, this parameterization does not account for the phenomena that warm ocean water tends to melt tongue from the base and lead to dynamical thinning. The thermal coupling between ice and ocean remains a development area in many computer models. In most of current models, a no temperature change condition is imposed on floating ice.

2.6 Mass Transport Model

A mass transport model is based on mass balance on ice sheet and is used to simulate the evolution of ice thickness, H :

$$\frac{\partial H}{\partial t} = -\nabla \cdot (\boldsymbol{u}H) + \dot{M}_s - \dot{M}_b \quad , \quad (40)$$

where $\dot{M}_s$ is surface mass balance rate; and

$\dot{M}_b$ is basal mass balance rate.

The calculation of ice thickness depends on velocity field and is often updated each timestep after the stress balance calculations are completed. The numerical accuracy of ice thickness change and velocity field are mutually affected. Moreover, it also plays a role on the extent of isostatic adjustment (see Chapter 2.8.2) via altering bedrock elevation.

2.7 Iceberg Calving Model

Calving is a rapid ice loss process from a glacier terminus into ocean. When fractures penetrate through the ice tongue, calving occurs. Ice fractures, known as crevasses, can develop from the surface and at the bottom. Both crevasses could be enhanced by strain rate variations. In addition, propagation of fractures is favoured in exposure of water due to changes in effective pressure and release of latent heat of fusion. Surface crevasses could contain surface meltwater, and ocean water if the depth of crevasses is sufficient to reach sea level; whereas bottom crevasses constantly immerse in ocean water. Benn et al. (2007) derived a crevasse-penetration calving model (see Figure 2.7), assuming ice flow is in *x*-direction, to calculate fracture depths :

$$d_s = \frac{\tau_{xx}}{\rho g} + \frac{\rho_{ws}}{\rho}\, d_w \qquad ; \tag{41}$$

$$d_b = \frac{\rho}{\rho_{wb} - \rho}\left(\frac{\tau_{xx}}{\rho g} - H_{ab}\right) \qquad , \tag{42}$$

where d_s , d_b are depth of surface and bottom crevasses respectively;

ρ_{ws} , ρ_{wb} are water density at surface and bottom crevasses;

d_w is the depth of water in surface crevasses;

ρ is density of ice; and

H_{ab} represents the height above buoyancy:

$$H_{ab} = H - \frac{\rho_{wb}}{\rho} D \qquad , \tag{43}$$

where D is the depth of ice below sea level. Thus, calving occurs when the sum of d_s and d_b equals to local ice thickness, and the corresponding portion of ice detaches from tidewater glacier.

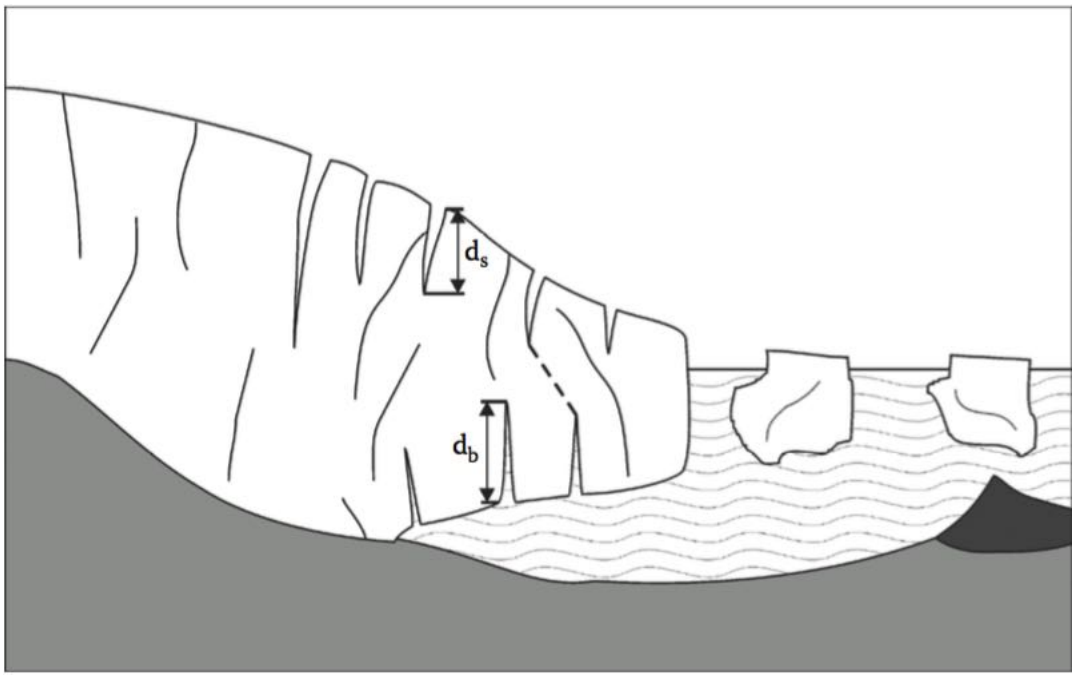

Figure 2.7 : Geometry used in crevasse-penetration calving model (adopted from Van der Veen, 2013).

2.8 Other Processes

2.8.1 Subglacial Hydrology

Channel systems at the bottom of glacier evolve and respond to variation of water supply, which can accelerate the ice stream by sliding due to effective pressure change. Schoof (2010) began the analysis by a simple equation to model the change of conduit size as :

$$\frac{dS}{dt} = c_1 Q\Psi + u_b h - c_2 N^n S \quad , \qquad (44)$$

where S is conduit cross section area;

Q is water discharge given in Darcy-Weisbach law (Clarke, 1996);

Ψ is the along conduit hydraulic gradient;

u_b is sliding velocity;

h is size of bed protrusion;

N is effective pressure;

n = 3 is Glen's factor; and

c_1 , c_2 are latent heat of fusion and ice viscosity related constants.

In equation (44), the first term on the right-hand side represents opening rate due to wall melting; the second term represents opening rate from ice sliding; while the last term represents roof creeping closure rate. This model not only gives insight on the criteria of interchanging of R-channels and cavities, but also provides a relation of effective pressure against water discharge at steady state :

$$N = \left(\frac{c_1 Q\Psi + u_b h}{c_2 c_3^{-\frac{1}{1.25}} Q^{\frac{1}{1.25}} \Psi^{-\frac{1}{2.5}}} \right)^{\frac{1}{n}} \quad . \qquad (45)$$

It suggests that N decreases with Q at low Q and vice versa (see Figure 2.8). Schoof's simulation implies that a short-term increment in water supply could induce a sudden glacial acceleration from fast sliding. This phenomenon could explain part of the speed-up in Greenland ice sheet when there is a spike in surface melting extent, which increases basal

water supply. For example, from winter to summer, or during peak summer. However, as a recent advancement, this new theory has not been included into many numerical ice sheet models.

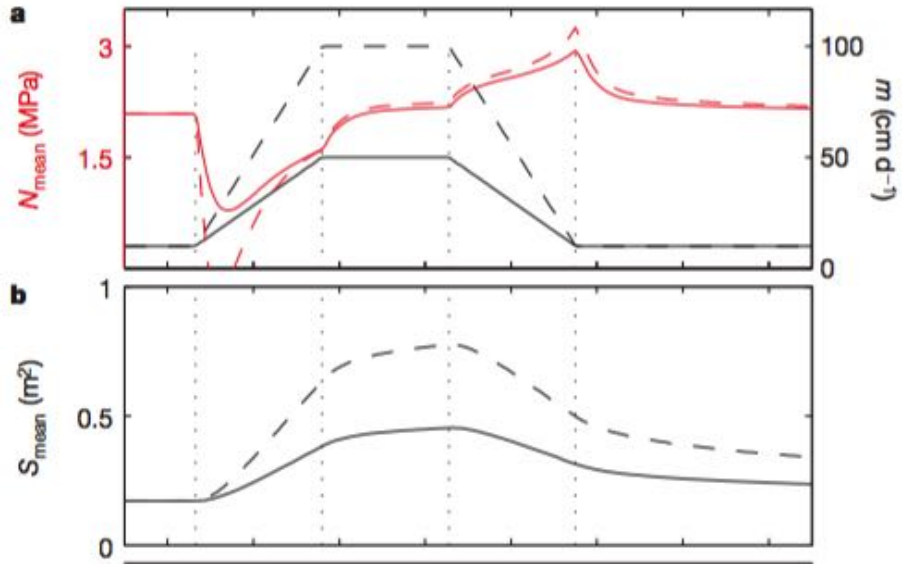

Figure 2.8 : Simulation on spatially uniform water supply, m, to (a) averaged effective pressure, N_{mean}; and (b) spatial mean conduit size, S_{mean}. Dotted line represents five times more water supply than solid line. (adopted from Schoof, 2010).

2.8.2 Glacial Isostatic Adjustment (GIA)

Isostatic adjustment refers to the bedrock displacement due to glacial mass changes . The viscoelastic behavior of the Earth allows it to readjust from the surface mass load changes with a considerable time delay. The deglaciation since the Last Glacial Maximum (LGM), around 21000 years ago leads to crustal uplift in a large region including

Greenland until today. As changes in bedrock elevation have big impact on marine ice sheet evolution, isostasy has to be taken into conservation in ice sheet modeling.

The vertical displacement response in glacial isostatic adjustment could be modeled by a viscoelastic lithosphere model (Lambeck and Nakiboglu, 1980), whereas the timescale could be controlled by an asthenosphere model. The vertical bed deformation, w, due to a cylindrical ice disc of radius R_A and thickness H, at a distance r away from center of mass loading, is given by :

$$w(r) = \frac{\rho_i H}{\rho_m}\left[1 + \frac{R_A}{L_r} Ker'\left(\frac{R_A}{L_r}\right) Ber\left(\frac{r}{L_r}\right) - \frac{R_A}{L_r} Kei'\left(\frac{R_A}{L_r}\right) Bei\left(\frac{r}{L_r}\right)\right] \quad (46)$$

for $r \leq R_A$; and

$$w(r) = \frac{\rho_i H}{\rho_m}\left[\frac{R_A}{L_r} Ber'\left(\frac{R_A}{L_r}\right) Ker\left(\frac{r}{L_r}\right) + \frac{R_A}{L_r} Bei'\left(\frac{R_A}{L_r}\right) Kei\left(\frac{r}{L_r}\right)\right] \quad (47)$$

for $r > R_A$,

where *Ber, Bei, Ker* and *Kei* are zeroth order Kelvin functions;

Ber', Bei', Ker' and *Kei'* are first derivatives of *Ber, Bei, Ker* and *Kei* functions respectively;

ρ_i , ρ_m are densities of ice and mantle respectively;

D is the flexural rigidity; and

$$L_r = \left(\frac{D}{\rho_m g}\right)^{\frac{1}{4}} \tag{48}$$

is the radius of relative stiffness.

Yet, the long response time of isostatic adjustment makes it not a particular concern in transient studies. Therefore, we can safely neglect any isostasy effect in this study. However, to understand past changes and future evolutions of ice sheets, particularly in large-scale, glacial isostatic adjustment becomes an essential component to accurately treat relative sea level, ice elevation, and bedrock topography (Gomez et al., 2010).

Chapter 3

Numerical Ice Sheet Models

Our understanding of processes in the dynamics of ice sheet, together with efforts of mathematical modeling and by making approximations or assumptions, eventually yields sets of equations. These physics-based equations could be used to describe behaviours or phenomena in an ice sheet system. In addition, numerical discretization made computation of the evolution of various quantities in ice sheet system possible by turning physical equations into computer codes.

Numerical ice sheet models simulate the flow of ice under a certain user defined ice sheet setting environment. They are important tools to understand the response of glaciers and ice sheets to external forcing. However, we should note that regardless of how sophisticated a model is, it only represents the current best understanding and application we could achieve, which is always insufficient to represent the true and complex nature accurately. Models are powerful tools for studying the nature, but we should not be too obsessed and over-interpret its outputs, as they are essentially a simplification to real world —— *"all models are wrong, but some are useful"* (Box and Draper, 1987).

To achieve specific features or strengths in a model, sometimes special numerical methods and parameterizations would be adopted, especially in areas where physical properties and mechanisms are complicating or not yet fully understood. It is worth noting that a numerical model involving complex phenomena is very sensitive to the choice of numerical scheme and technique of coding. These factors might affect the reliability and computational efficiency of a model. Hence, benchmark experiments are often carried out by comparing the model output with a particular case with analytic solutions (e.g. Halfar, 1983; Huybrechts et al., 1996; Pattyn et al., 2008) or real observations (e.g. MacAyeal et al., 1996).

3.1 Comparison Among Major Ice Sheet Models

Numerical ice sheet models have gained substantial development since The Fourth Inter-Governmental Panel on Climate Change Assessment Report (Solomon, 2007). The report suggested that the state of ice sheet models by then were unlikely to provide an accurate forecast for ice loss at polar ice sheets and thus unreliable for sea level rise projection. Models currently not only endeavour at improving numerical accuracy, stability and computational efficiency; but also attempt to include more comprehensive physics of ice sheet dynamics, from microscopic to large scale. There is an increasing number of ice sheet computer models for researchers worldwide to adopt. In the following

subsections, a summary on the capabilities, advantages and disadvantages of the four major open source models – Ice Sheet System Model (ISSM), Elmer/Ice, Parallel Ice Sheet Model (PISM) and Community Ice Sheet Model (CISM) – will be made.

Given the purpose of this research was to investigate short-term changes of outlet glaciers, the model of choice should be able to run at fine gridding (particular at ocean outlets) in order to well resolve the drainage basin and small timesteps. It should also take into account of iceberg calving and could simulate grounding line changes. Preferably, the model ought to have the feature of coupling to other earth system model, which would allow a future investigation on the impact of external forcing on transient ice dynamics.

3.1.1 Ice Sheet System Model (ISSM)

As the product of collaboration between Jet Propulsion Laboratory (JPL) and University of California at Irvine (UCI), Ice Sheet System Model (ISSM) is a thermo-mechanical finite element ice flow model featuring techniques of high spatial resolution, data assimilation and inclusion of higher order stresses (Larour et al., 2012). ISSM equips with all level of approximations to momentum balance equations, from the most complete FS model to BP higher order model, and also the two-dimensional SIA and SSA. Unlike the practice of many finite element modeling, which generates

regular meshes, ISSM uses Arbitrary Lagrangian-Eulerian (ALE), which produces an anisotropic mesh over the modeling domain (See Figure 3.1). Roughly, this could create a spatial resolution of 1 kilometre near the coast and up to 25 kilometres at inner continent, allowing the concentration of mesh elements at regions of fast ice flows without the need to increase mesh number globally. As a result, it reduces spending of computation effort on less significant regions. ISSM can also model grounding line migration (Seroussi et al., 2014) by using an adaptive grid method (Pattyn et al., 2012). Moreover, one strength of ISSM is that it could attempt to infer non-measurable quantities which significantly impacts the dynamics and behaviours of ice sheet from observed surface velocities. For instance, ISSM inverts for the basal friction for grounded ice (Larour et al., 2014). It could reduce a portion of uncertainly, arising from inability to obtain observation data of some parameter or inclusion of incomplete physics in the model, in modeling the ice sheet system. Efforts of users could thus be focused on tuning other parameters or investigating alternative environmental factors.

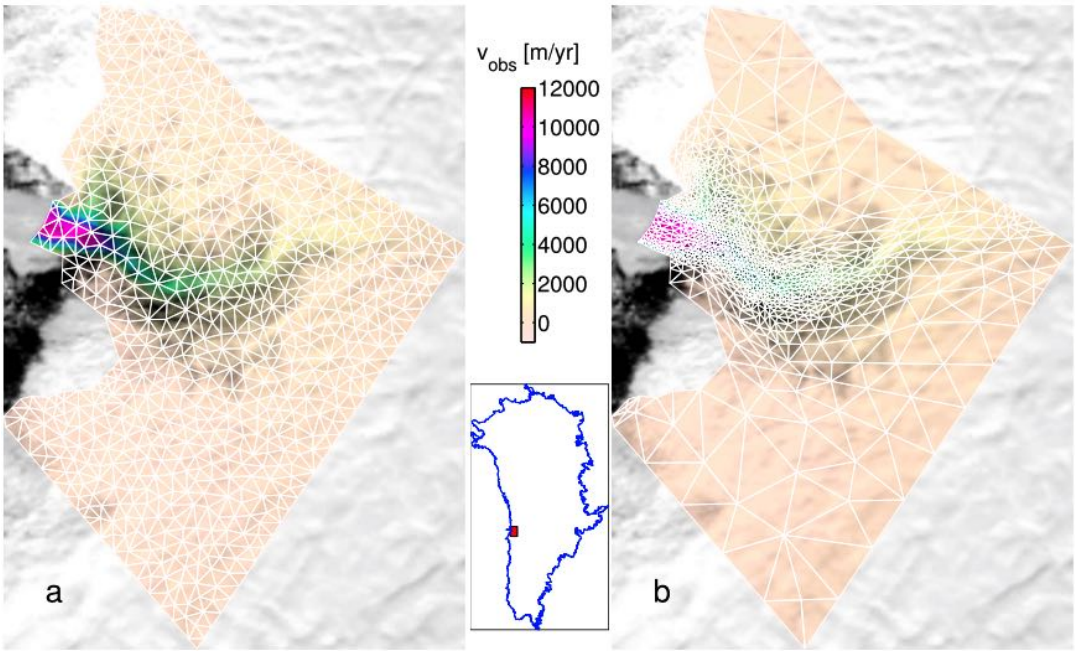

Figure 3.1 : Illustration of the difference between (a) regular mesh and (b) static adaptive anisotropic mesh over interpolated InSAR surface velocity map of Jakobshavn Isbrae using 1500 elements (adopted from Larour et al., 2012).

However, at the moment, only a fixed front position is allowed for ice-ocean boundary. Morlighem et al. 2016 presented a more sophisticated calving front evolution scheme applicable in a future release of ISSM, using Level Set Method (Osher et al., 1988). Though it allows a user-assigned surface mass balance as external forcing, coupling with climate models is not being designed. It is also not taking into account of basal hydrology.

3.1.2 Elmer/Ice

Elmer/Ice was developed based on a finite element multi-physics code named Elmer, by Center for Scientific Computing (CSC) at Finland (Gagliardini et al., 2013). It was originally designed to solve glaciological problems in local scale with high mechanical complexity and eventually becomes capable for larger scale ice sheet problems (Seddik et al., 2012). Elmer/Ice is comprised of complex physics on many aspects of marine ice sheet dynamics. From the fundamental prospective, it takes into account the process of snow-ice transition and is equipped with both isotropic and anisotropic ice rheology schemes dealing with the difference in ice crystal deformation behavior at various regions. It adopts Full Stokes model for computing momentum balances. Recently it also supports SSA and SIA, and uses Eulerian adaptive spacing to create meshes for finite element modeling. Similar to ISSM, Elmer/Ice also uses inversion methods to estimate several quantities in ice including basal friction and ice viscosity. One major advantage of Elmer/Ice on modeling tidewater glacier is that it implements physical models for calving, which is based on damage mechanics arising from glacier surface crevasses and oceanic buoyancy force (Krug et al., 2014). Figure 3.2 is a diagram illustrating this calving modeling method.

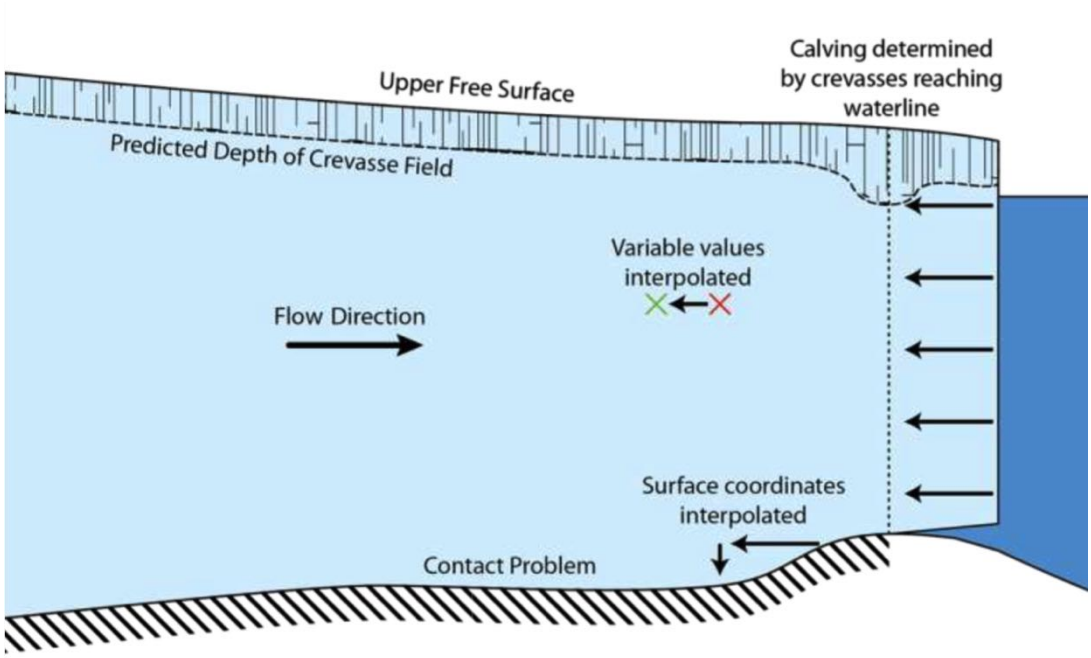

Figure 3.2 : A method overview of the damage mechanics based iceberg calving scheme in Elmer/Ice (produced by Todd and Zwinger).

Nevertheless, Elmer/Ice treats the grounding line as a contact problem instead of modeling its migration. Basal hydrology is not included. Also, improvement could be done in linking this model with external climate forcing.

3.1.3 Parallel Ice Sheet Model (PISM)

The main contributing groups of PISM include University of Alaska at Fairbanks (UAF) and Potsdam Institute for Climate Impact Research (PIK), Germany. It was firstly published online in 2006 and has been making modifications and improvements since then. The primary purpose

of PISM is to simulate long-term changes of Greenland and Antarctica Ice Sheets and their contribution to future sea level rise (Bindschadler et al., 2013). For the momentum balance part, it makes use a hybrid model formed from integration of SIA and SSA. The hybrid model analogizes the sliding area in ice streams to the buoyancy floating part of ice shelf in the hybrid model (Bueler and Brown, 2009), as illustrated in Figure 3.3. For instance, on the inner region of an ice sheet where ice is mostly frozen on bed and motion is mainly deformation based with little sliding, fully SIA would be used; whereas fully SSA would be adopted on ice tongues and ice shelves. For other transitional scenarios, the hybrid model varies the combination of the movement modeled by SIA and SSA through a proportion parameter. This method increases the accuracy in simulating ice movement in cases where it is mostly due to basal slipping and crossing the grounding line. In addition to typical thermomechanical model, PISM also has a polythermal energy conservation model based on enthalpy formulation (Aschwanden et al., 2012). The gridding of PISM is finite difference is adjustable by users. Its timestep is adaptive. Local basal water balance is available in PISM as basal meltwater model, which also controls over the bed strength. It is also capable of considering grounding line migration. PISM is designed to couple extensively with alternative ocean and atmosphere models. It is recently equipped with a strain rate dependent calving law at ocean margin (Winklemann et al., 2011), in addition to the initial fixed front setup.

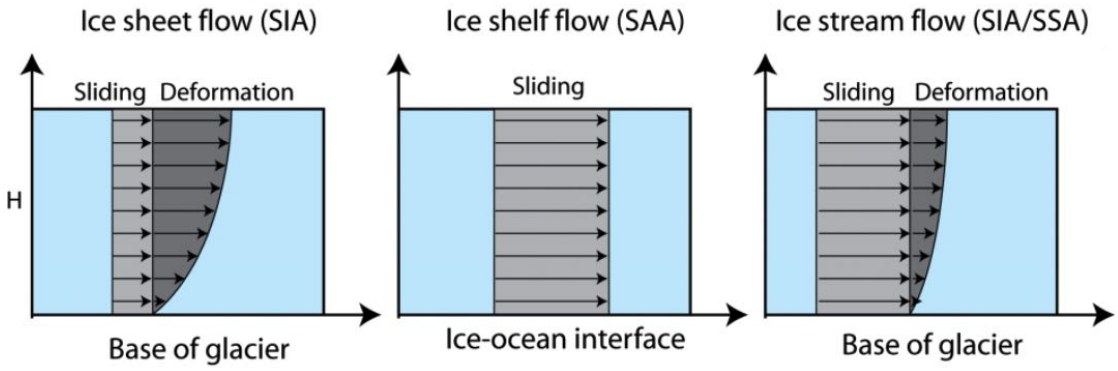

Figure 3.3 : Schematic diagrams showing the concept of hybrid model in PISM – – using SIA in region where motion is deformation dominating; using SSA in floating ice tongues or ice shelves; and a combination of both in grounded ice where sliding is significant (adopted from www.AntarcticGlaciers.org) .

3.1.4 Community Ice Sheet Model (CISM)

CISM is an updated version of Glimmer Ice Sheet Model (Rutt et al., 2009), released in late 2014. It is designed to be the land ice dynamic component in Community Earth System Model (CESM) (Lipscomb et al., 2013). CISM includes SIA, SSA, BP and L1L2 higher order models in its mechanical core. Similar to PISM, CISM also uses a user adjustable finite difference gridding. Moreover, it borrows ideas from meteorology (Holton and Hakim, 2012) to convert the vertical coordinate into a new scale to represent relative ice depth, from 0 (at surface) to 1 (at base). Figure 3.4 provides a conceptual picture on this coordinate system. The advantage of this method is that it facilitates construction of irregular vertical gridding, which can be finer at the bottom of ice where internal deformations are

mostly likely to take place. To improve the accuracy of thickness evolution and grounding line migration, CISM adopts an incremental remapping scheme (Lipscomb and Hunke, 2004), which is conservative, non-oscillatory, monotonicity-preserving and efficient for a large number of tracers (see Figure 3.5).

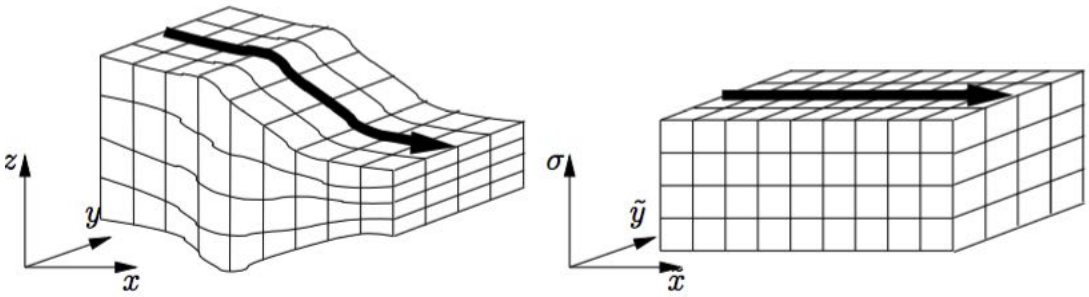

Figure 3.4 : CISM scales vertical gridding into unity, with $\sigma = 0$ represents ice surface; $\sigma = 1$ represents the base (adopted from CISM User Manual).

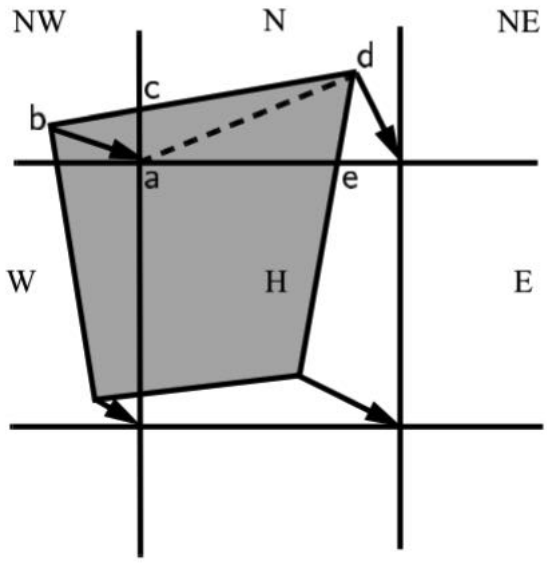

Figure 3.5 : Incremental Remapping Scheme remaps conserved quantities from shaded region to grid cell H, which then allows convenient computation of fluxes across cell edges (adopted from CISM User Manual).

CISM currently supports basal sliding inversely proportional to basal water thickness, Weertman and Coulomb friction laws. Apart from the standard thermomechanical model, an enthalpy model is under development. CISM equips with a calving function which reduces the frontal ice thickness by a fraction. A more physical damage mechanics based calving law is also under development.

3.2 CISM as Tool for Study

Consider the subject of study is a fast moving marine-terminating glacier stream, stress distribution is likely to be largely inhomogeneous across the domain. Neither SSA nor SIA is suitable to use for our research objective and having FS or BP higher order model as mechanical model is essential. Moreover, in addition to high temporal resolution, an ultra-high spatial resolution is needed to 1) resolve and represent ice flow in the narrow ice drainage basin well and 2) ensure a numerical stability. Also, it would be best if the model of choice is able to carry out numerical experiments of ice sheet with external forcing, or even couple to atmosphere and oceanic models, so the effects of air-ice and ice-ocean coupling, could as well be investigated.

Among the four open source models, PISM is unsuitable as it is targeted for the continental ice sheet scale simulations. The hybrid model constructed from Shallow Ice and Shallow Shelf Approximations in PISM cannot be applied as shallow approximation typically does not hold at fine scale fast moving glacier streams. It is necessary to adopt Full Stokes or other higher order momentum balance approximations. However, ISSM was also not chosen at the beginning of this study because it was not able to include the evolution of calving front position. This will pose a major missing piece in the modeling of tidewater glaciers, especially during summer time when frontal retreat is significant. Both Elmer/Ice and CISM are suitable models to make use of. Yet consider CISM would be able to couple to various other earth system models after being merged into the framework of CESM, which creates a great potential to study more diverse ice-ocean interaction problems in the future, it was chosen as the numerical modeling tool for this study.

	ISSM	**Elmer/Ice**	**PISM**	**CISM**
Mechanical Model	FS, BP, SSA, SIA	FS, SSA, SIA	SIA + SSA Hybrid	BP, SSA, SIA
Thermal Model	Energy Balance	Energy Balance	Energy, Enthalpy Balance	Energy Balance
Spatial Gridding	Adaptive Finite Element (Arbitrary Lagrangian-Eulerian)	Adaptive Finite Element (Eulerian)	Finite Difference	Finite Difference (Uneven Vertical Levels)
Time Stepping	Fixed	Fixed	Adaptive	Fixed
Basal Traction	Inversion of Observed Velocity	Inversion of Observed Velocity and Ice Viscosity	Parametri-zation of Hybrid Model	Columb , Weertman Friction Law
Hydrology Model	Nil	Nil	Local Basal Water Balance	Local Basal Water Balance
Grounding Line Migration	Yes (Adaptive Grid Size)	Yes (Contact Problem)	Yes (Hybrid Model)	Yes (Incremental Remapping)
Iceberg Calving Model	Nil (Fixed Front)	Damaged Mechanics Based	Strain Rate Dependent	Simple Parametri-zation
Coupling with other models	Nil	Nil	Yes	Yes (CESM)

Table 3.1 : Tabular summary of specialties and capabilities of Ice Sheet System Model (ISSM), Elmer/Ice, Parallel Ice Sheet Model (PISM) and Community Ice Sheet Model (CISM).

3.3 Numerical Testing with CISM on Ross Ice Shelf, Antarctica

Ross Ice Shelf, locating at western Antarctica, is the largest ice shelf currently on earth. Its thickness could reach 750 metres near the South Pole side. Ross Ice Shelf is one of the benchmark experiments that come with CISM. The purpose of this experiment is to simulate the flow of Ross Ice Shelf under idealized condition as outlined in MacAyael et al. (1996), with supplied data from Ross Ice Shelf Intercomparison Experiment. The resolution of modeling in this experiment is 6822 metres.

(a)

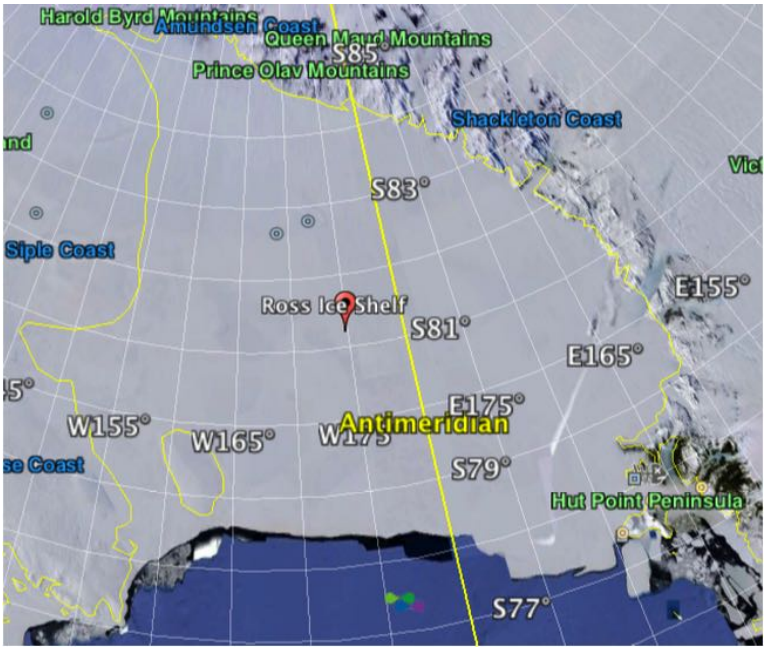

(b)

Figure 3.6 : Ross Ice Shelf from (a) Google Earth © (Imagery Date: 01/01/1999); and (b) Wikipedia © on Antarctica.

3.3.1 Uniform Flow Law with SSA

The benchmark experiment in CISM runs with SSA with a timestep of 1 year, for a model period of 1 year. It is an idealized condition by setting the flow factor A to be constant at 4.6×10^{-18} Pa^{-3} yr^{-1} over the domain of ice. The model output was then compared with velocity data for the Ross Ice Shelf (RIGGS) measurement (Thomas et al., 1984), which are shown below in Figures 3.7 (a) & (b).

(a)

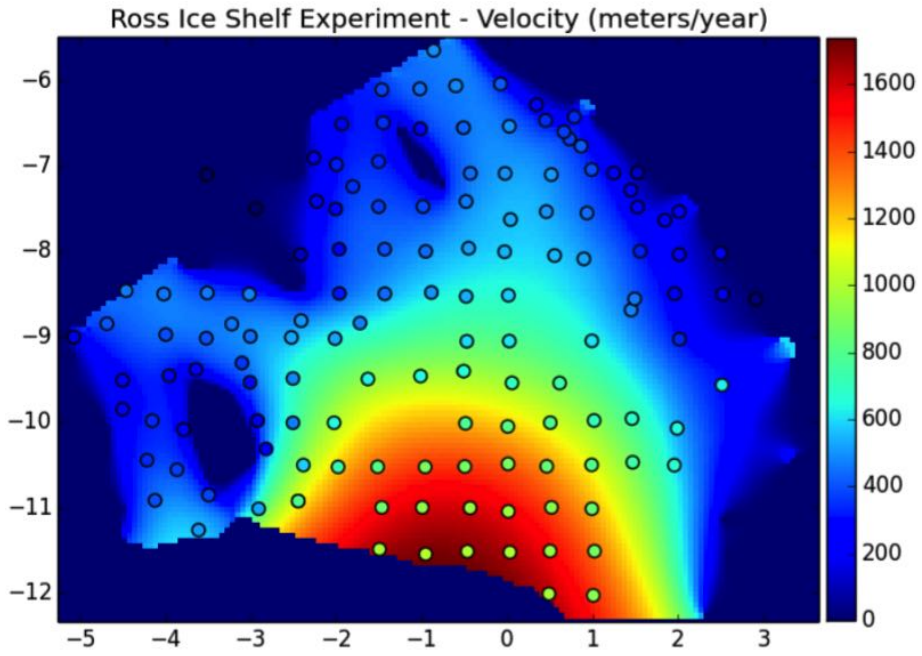
Ross Ice Shelf Experiment - Velocity (meters/year)
−6
−7
−8
−9
−10
−11
−12
−5
−4
−3
−2
−1
0
1
2
3
1600
1400
1200
1000
800
600
400
200
0

(b)

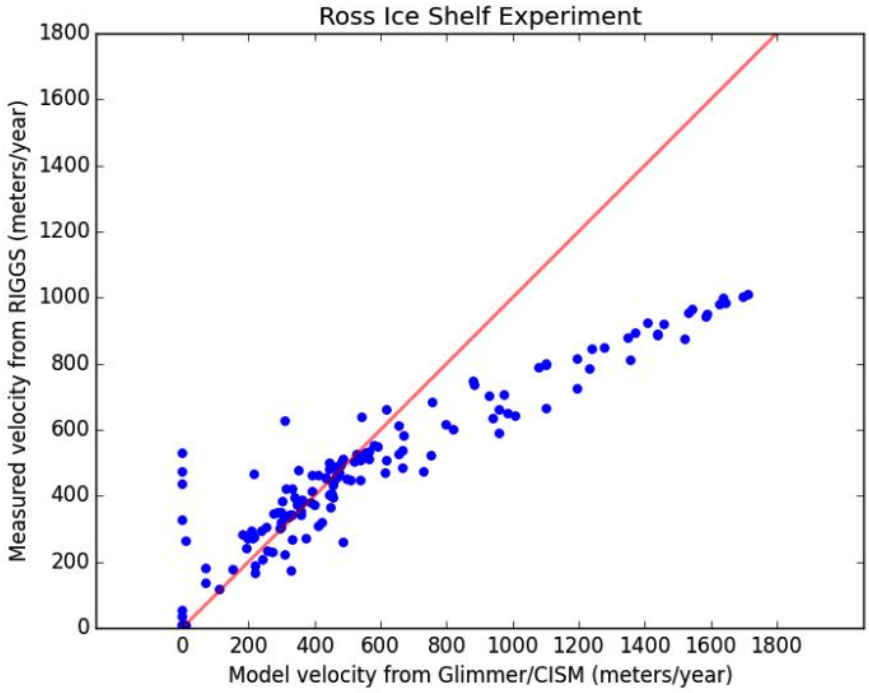
Ross Ice Shelf Experiment
Measured velocity from RIGGS (meters/year)
Model velocity from Glimmer/CISM (meters/year)
0
200
400
600
800
1000
1200
1400
1600
1800

Figure 3.7 : Under constant flow factor, the comparison between Ross Ice Shelf velocity field (a) in map representation (y-axis : distance from South Pole; x-axis: distance from Antemeridian, unit : 100 kilometres) generated by model (in background) and RIGGS measurement (in circle dot); and (b) in graph representation, with the red line indicating prefect match.

It is observed that the modeled velocity matches very well with GPS measurement near inland coasts. However, gradually outward into the main shelf region, the model tends to over-predict the velocity and the discrepancy increases as the domain approaches to the calving front. At this stage, it cannot be concluded whether the flow parameter constant, 4.6×10^{-18} Pa^{-3} yr^{-1}, is a suitable choice, or a good idealized assumption in this case because the problem could lie on the momentum balance approximation. It is necessary to carry out another experiment to examine the performance of SSA.

3.3.2 Temperature-Dependent Flow Law with SSA

Hence, another experiment was devised by replacing the constant flow parameter with a temperature dependent flow parameter as calculated from the formulation of Paterson and Budd (1982), which was previously covered in Chapter 2 as Equation (13). The other parameter settings remain the same. The temperature dependent flow factor was calculated based on the supply of ice surface temperature data and

assumption of uniform initial ice temperature throughout whole ice column. The flow factor over the region is quite inhomogeneous, ranging from 1.9×10^{-18} to 3.7×10^{-18} $Pa^{-3}\,yr^{-1}$ (see Figure 3.8), which is a fraction lower than value used in the idealized experiment (4.6×10^{-18} $Pa^{-3}\,yr^{-1}$).

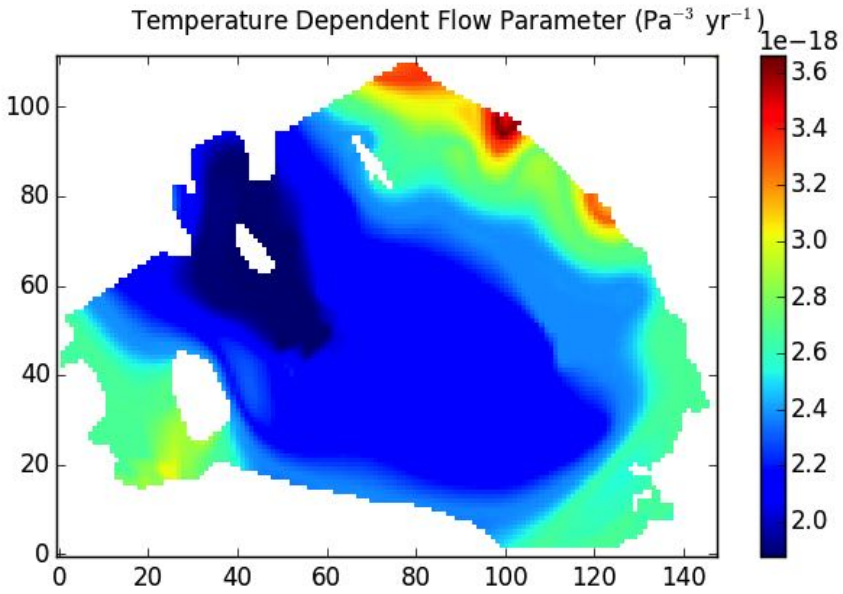

Figure 3.8 : The modeled flow factor *A* in Ross Ice Shelf Experiment under a temperature dependent flow law.

Presented by Figures 3.9 (a) and (b) are the modeling result with temperature dependent flow factor. Figure 3.9 (b) shows a high degree of matching between modeled velocities and measured velocities for most places, albeit a slight tendency of under-prediction. At some inlets to Ross Ice Shelf, modeled velocities tend to be lower than the observations (Figure 3.9 (a)). This could be because the approximation of shallow shelf may not be very appropriate in such stream-shelf transition region. It also suggests

that a uniform constant flow factor is inadequate to reproduce the observed velocity on Ross Ice Shelf.

(a)

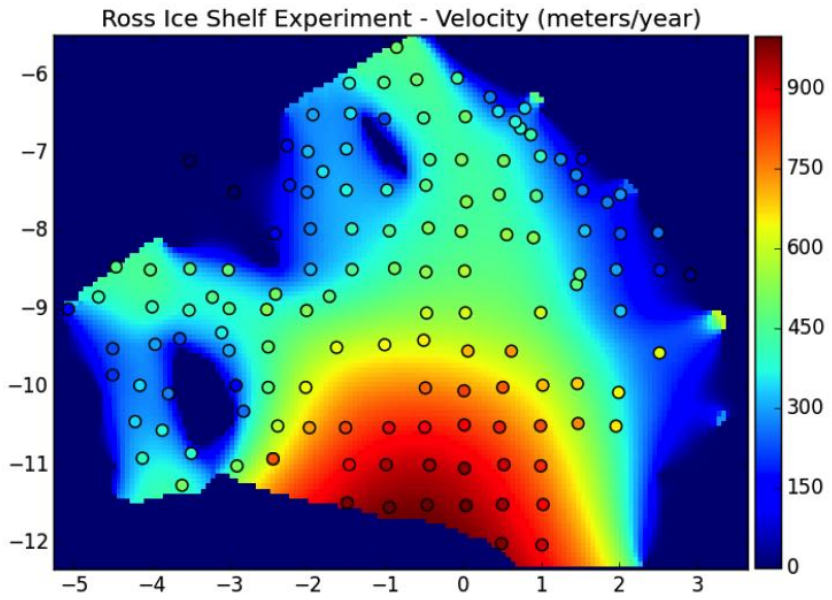

(b)

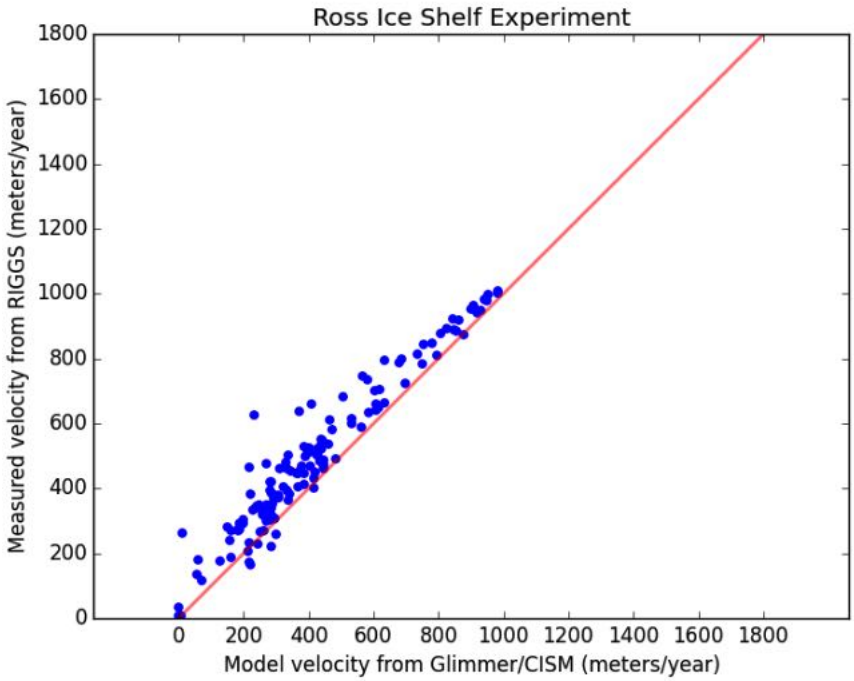

Figure 3.9 : Under temperature dependent flow factor, the comparison between Ross Ice Shelf velocity field (a) in map representation generated by model (in background) and RIGGS measurement (in circle dot); and (b) in graph representation, with the red line indicating prefect match.

3.3.3 Temperature-Dependent Flow Law with BP Higher Order Model

According to the theory of glacial mechanics (as summarized in Chapter 2), SSA should perform well on modeling large ice shelves; however, it is still much of a simplification that neglects several stress components (Chapter 2.3.3). Therefore, the final question is that how different would be the output ice velocities from a BP higher order model compared to an SSA model? Hence, I carried out another experimental run using BP higher model with temperature dependent flow law. From the comparison results shown in Figure 3.10, it is observed that the velocity differences are of magnitude centimetres per year, which are negligible given the absolute ice velocity magnitude is of the order hundreds of metres per year. In addition, computing with BP higher order model takes longer than using the SSA model. Therefore, I conclude that SSA is accurate enough and computationally efficient to be applied than modeling ice shelf flows.

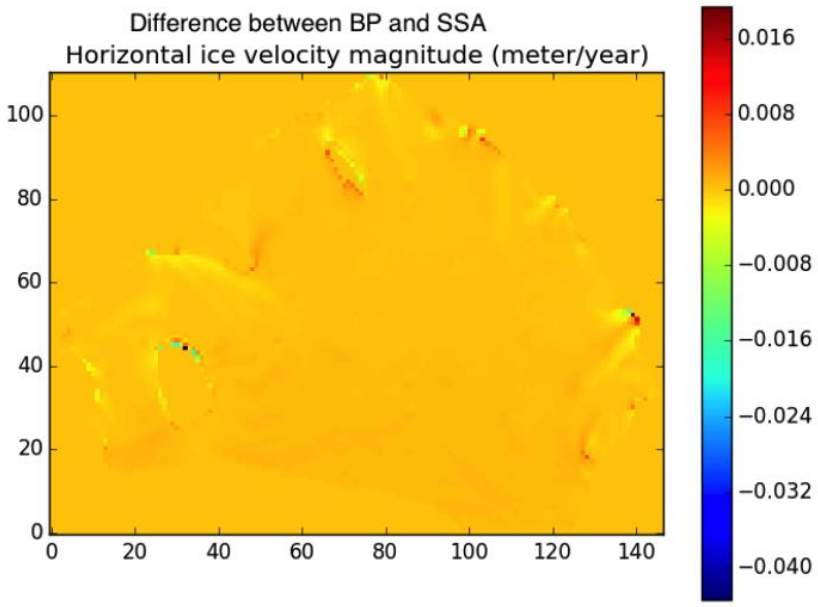

Figure 3.10 : The difference between modeled velocities applying BP higher order model and SSA on Ross Ice Shelf, using temperature dependent flow law.

3.3.4 Summary

It is shown from these numerical experiments that SSA is a feasible approximation to apply on large ice shelves. Applying SSA on ice shelves rather than higher order or even FS models much reduces computation time while not sacrificing accuracy. On the other hand, it could be further supporting that ice viscosity is critical in affecting ice flow. Also, the temperature dependent flow law derived by Paterson and Budd (1982) is shown to improve the agreement between the modeled and observed velocities on Ross Ice Shelf.

Chapter 4

Simulation :

Data & Model Initialization

4.1 Data and Processing

To carry out a simulation study, observation data are important as they provide essential initial and boundary conditions for solving numerical models and as a reference for output validation and comparison. In CISM, data should be provided in finite difference gridding. Information of bedrock topography, ice thickness and an ice mask can define the geometry of a particular ice sheet. These data are therefore considered as essential. Surface velocity data, although not a compulsory information to supply to the model, is very helpful as initial guesses in the modeling.

4.1.1 Surface Velocity

Glacial surface velocity is one of the most important data in this project. It serves as (1) the initial guess in simulation runs to reduce time for model self-adjustment and (2) boundary conditions at the upstream of the glacier systems. The surface velocity data of Upernavik Isstrøm outlet

glaciers in 2010 summer were obtained from National Snow & Ice Data Center (NSIDC) (Joughin et al., 2011). The data were produced based on the technique of radar interferometry with speckle tracking (Joughin, 2002) using images obtained by the TerraSAR-X satellite. The temporal resolution of the velocity dataset was 11 days; and the spatial resolution was 100 metres.

Eventually, same as the resolution of velocity data, the model gridding was taken to be 100 metres. The main advantage is the convenient comparison between model output and observed velocities. A resolution of 100 metres allows one to well resolve the topography of outlet glacier drainage basin. It is also a suitable choice to conduct modeling in transient timescale (refer to the analysis in Chapter 4.2.1) same as surface velocity data. However, the velocity map produced from TerraSAR-X (Figure 4.1 (a)) is not in polar-stereographic rectangular grids due to flying path of satellite. Eventually, the modelled domain in this study was determined by applying spatial interpolation to fill in the missing velocity values after cropping the velocity map into a perfect rectangular domain (Figure 4.1 (b)) , where the origin represents a geographic location, approximately, of 54.48 °W, 72.63 °N.

(a)

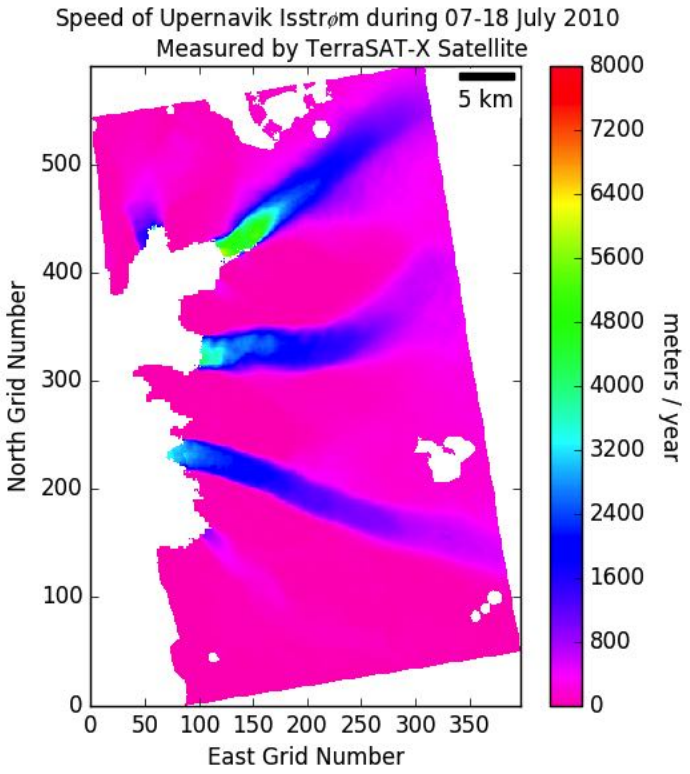
Speed of Upernavik Isstrøm during 07-18 July 2010
Measured by TerraSAT-X Satellite
5 km
North Grid Number
East Grid Number
meters / year
0
50
100
150
200
250
300
350
0
100
200
300
400
500
8000
7200
6400
5600
4800
4000
3200
2400
1600
800
0

(b)

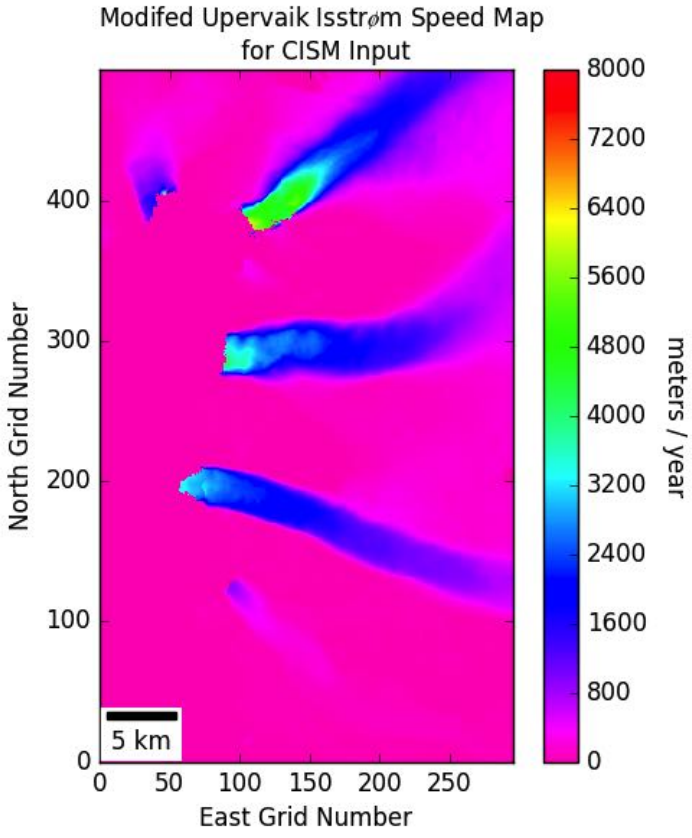
Modifed Upervaik Isstrøm Speed Map
for CISM Input
5 km
North Grid Number
East Grid Number
meters / year
0
50
100
150
200
250
0
100
200
300
400
8000
7200
6400
5600
4800
4000
3200
2400
1600
800
0

Figure 4.1 : (a) Surface velocity magnitude of Upernavik Isstrøm outlet glaciers during 07 – 18 July 2010 from TerraSAR-X satellite images (Joughin et al., 2011); and (b) the cropped and interpolated velocity magnitude map for model simulation input.

4.1.2 Mass Conservation Dataset

Based on conservation of mass, inversion from surface velocity, hydrostatic equilibrium and statistical interpolation, the Mass Conservation Dataset produced by Morlighem et al. (2014) provides a self-consistent and high-resolution (150 metres) dataset, including ice/land/ocean mask, land ice thickness, bed topography and surface elevation over the entire Greenland. To match the resolution of surface velocity map, the dataset was further upscaled into 100 metres by linear interpolation and supplied to the model as essential information.

(a)

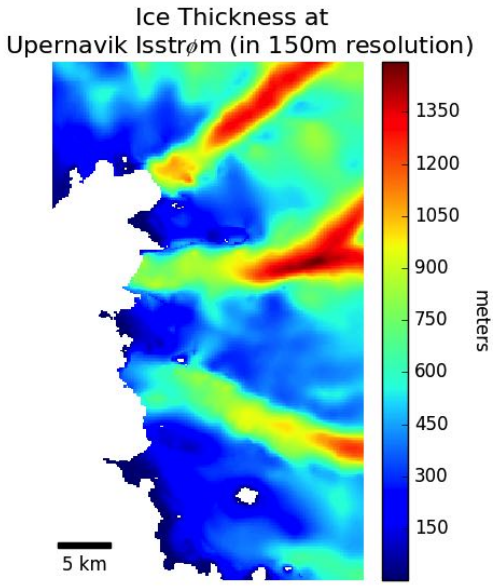

(b)

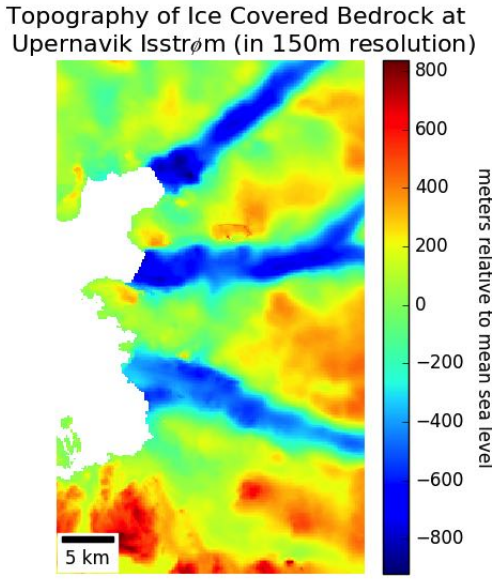

(c)

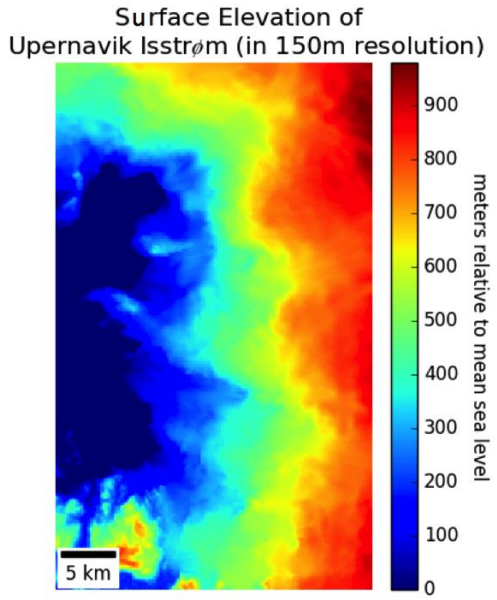

(d)

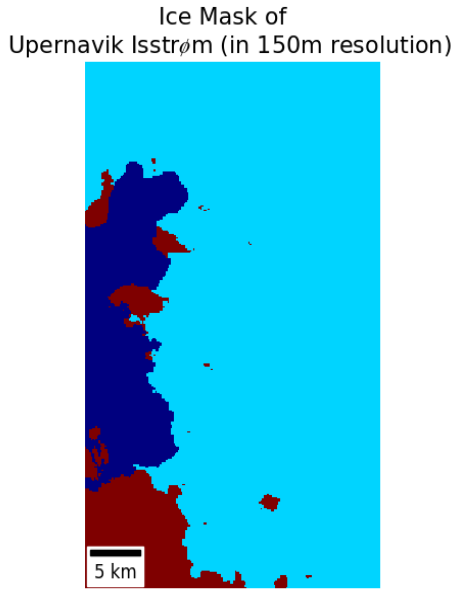

Figure 4.2 : (a) Ice thickness, (b) ice covered and land bedrock topography, (c) surface elevation; and (d) ice mask (land: brown, ice: light blue, ocean: dark blue) of Upernavik Isstrøm based on the Mass Conservation Dataset (Morlighem et al., 2014) in 150-metres resolution.

4.1.3 Bathymetry

The sea floor bathymetry over the model domain was constructed by combining the Mass Conservation Dataset and the global bathymetry dataset produced by Smith and Sandwell (1997). The Mass Conservation Dataset does not provide bedrock topography over non-ice-covered areas. The global topography data, with resolution of global 1-minute grid, were inverted from global gravity data with assumptions of uniform density (Smith and Sandwell, 1997). However, it suffers from particularly large systematic errors as the density of ice is way lower than solid earth. Thus the values presented from global topography dataset have some discrepancies against the high-resolution Mass Conservation Dataset. For simplicity and continuity, the global topography data were calibrated with a constant (using a spot at Glacier 2 outlet as reference) to match the data of Mass Conservation Dataset at outlet Glacier 1.

The adjust bedrock topography over the entire field obtained by this simply fusion method is reasonably consistent in the spatial domain. As shown in Figure 4.3, the sea floor westward the terminus of Glacier 2 deepens, which agrees with the presence of considerable amount of floating ice tongue there. Also, the frontal positions of Glacier 3 and 4 have remained relatively steady and slight afloat. Therefore, the bedrock topography in a short distance away from the terminus of these two glaciers is not likely to have a significant effort on the dynamics.

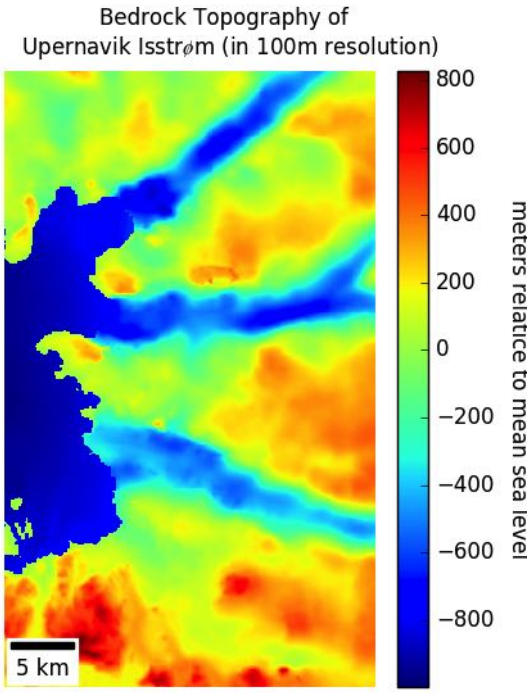

Figure 4.3 : Bedrock topography over model domain after adjusting the seafloor topography data from Smith and Sandwell (1997) to be consistent with the ice bed elevation from the Mass Conservation Dataset.

4.1.4 External Forcing

The effect of precipitation surface melting driven by atmospheric temperature can be collectively described by surface mass balance rate. The output from regional climate model RACMO 2.3 (Noël et al., 2015) was used to supply the data of 2010. In order to investigate the effect of different surface mass balance rates on changes in glacier dynamics, two scenarios have been devised – annual average surface balance rates and summer (July – September) average surface mass balance rates, which has

values of -150 and -1000 water equivalent millimetres/year. CISM takes SMB rates in terms of ice equivalent height per year and therefore adjustment was made according to the density difference, which is then able to compute the respective mass changes at each timestep after multiplying the rate with grid area (10^6 metre^2 in this simulation).

According to the climatic record (1982 – 2012) (http://en.climate-data.org/location/274141/), the average atmospheric temperature of Upernavik is around 5 - 6 °C during peak summer (July and August), and around 1 - 2 °C at beginning (June) and end (September) of summer. For simplicity, 2 °C is taken as the surface air temperature over Upernavik Isstrøm in the simulation study as the abrupt change was observed in July 2010. Ocean water temperature was not considered in this study because currently CISM, as a standalone model, does not include ice-ocean coupling.

4.2 Model Configurations

4.2.1 Gridding and Time Stepping

Following the discussion in section 4.1.1, the domain of surface velocity data in 100-metres resolution was truncated for the convenience of finite difference modeling. It was cropped into a rectangular domain with a reference to a polar stereographic coordinate, centered at the North Pole and using 70 °N, 45 °W as standard parallel and central meridian respectively. The grid dimensions of the final velocity domain are 296 (East-West) by 494 (North-South).

Two sets of finite difference grids were adopted in CISM to improve numerical stability on diffusion equation solving. As illustrated in Figure 4.4, one grid system is a staggered centering of the another. The grid system with larger dimensions, called the standard grid, was for non-diffusive quantities, including ice thickness, bedrock topography, and surface mass balance. The grid system with one unit less in the dimensions, or called centered grid, was for ice velocities and other diffusive quantities.

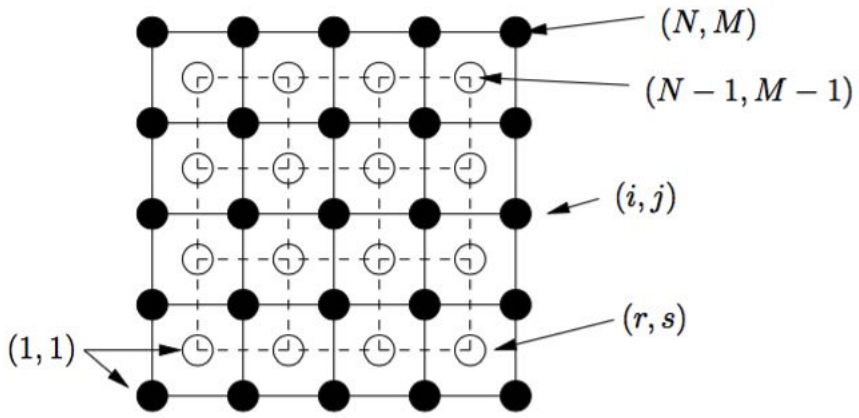

Figure 4.4 : Horizontal grids used in CISM. Solid dots represent one grid system, called the standard grid; hollow dots, which are at center positions of solid dots, represent another grid system (adopted from Price et al., 2015).

20 vertical levels (sigma levels) are designed in irregular distribution, based on Rutt et al. (2009) :

$$\sigma_k = \frac{4}{3}\left[1 - \left(\frac{k-1}{N_\sigma - 1} + 1\right)^{-2}\right] \tag{49}$$

where σ_k is the k-th sigma level (k = 1, 2, … , 20) ;

N_σ = 20, which is the total number of sigma levels.

Vertical grids assigned with this method are closer spaced near the base than at the surface, which allows more concentration of computation effort to characterize the flow variability at the glacial base. Among the 20 sigma levels assigned, 14 levels are located at the lower half of a vertical ice body on each grid point. Compared to evenly-spaced vertical levels, this

irregular gridding is particularly advantageous for this simulation study on transient glacial dynamics as the dynamical characteristics of basal ice can change extensively over the transition zone at outlet glaciers and thus affect surface ice flow.

A high temporal resolution simulation is essential for studying the transient flow properties. CISM uses an explicit method to numerically compute the state of ice system of a future time from the current time. Here we introduce the Courant–Friedrichs–Lewy (CFL) condition (Courant et al., 1928) which states the necessary condition for numerical convergence when solving partial differential equations through finite difference method in explicit scheme :

$$\max \frac{|\boldsymbol{u}|\Delta T}{\Delta x} \leq 1 \quad , \tag{50}$$

where $|\boldsymbol{u}|$is the magnitude of velocity in model domain;

Δx is the spatial resolution in model domain;

ΔT is the time step of simulation respectively,

It suggests that the maximum timestep allowed with 100-metres spatial resolution in our model setup is 5 days. This is a reasonable range for a transient study as it is shorter than the temporal solution of original SAR imageries. However, it was discovered in our test runs with a timestep of 5 days that numerical instabilities arise occasionally when solving

advection equations near ice-ocean boundaries. To cope with this problem, experiments with shorter time steps had been carried out and eventually a 1-day time step has been adopted in all subsequent simulations as it does not cause instabilities at boundaries. This simulation study runs the model for 75 time steps, which roughly correspond to from 18 July 2010 to the remaining of summer around early October 2010.

4.2.2 Model Parameters

A parallel 3D dynamical core implemented in CISM was chosen to solve the glacial mechanical model with BP higher order. Ice temperature was allowed to evolve following the thermodynamics equation. A temperature dependent viscosity scheme was adopted. Supplying the model with a velocity profile would effectively reduce the initial self-adjustment time. However, in reality only surface velocity map is readily available. Hence the initial vertical velocity profile is assumed to follow the following simple shear model :

$$\boldsymbol{v}(\sigma_k) = \boldsymbol{v_{obs}}(\sigma_0)(1-\sigma_k)^{\frac{1}{n}} \quad , \tag{51}$$

where $\boldsymbol{v}(\sigma_k)$ is the velocity at the k-th sigma level;

$\boldsymbol{v_{obs}}(\sigma_0)$ is the observed surface velocity; and

n = 3 is the Glen's exponent introduced in Equation (12).

This velocity profile implies a non-slipping condition at the base of glaciers. The variation of velocity mainly takes place at lower vertical levels, which is controlled by the internal deformation driven movement in that region. This profile assumption is only meant for model initialization. Velocity profiles evolve during the simulation processes.

To reduce complexity, a uniform geothermal heat flux is used across the entire model domain. Isostatic adjustment, which leads to bedrock changes, is not considered because the effects are negligible in transient timescales. Due to deficiency in data constraints on effective pressure in ice, we cannot apply Weertman-style (Equation 33) or cavitation included Columb-style basal friction and sliding laws (Equation 34 and 35), which are more physical and theoretic based. However, we can still apply the simple Columb friction law (Equation 32) with local basal balance consideration and simple shearing assumption, where traction parameter is calculated as the inverse of basal water thickness. Since no physical calving model is included in CISM version 2.0.5, we choose to set the ice loss proportional to frontal thickness and adjust it so that virtually all ice in ice-ocean margin grid are lost in each time step.

4.3 Spinning Up

A spinning up step is carried out before moving to the simulation part in order to reduce the simulation uncertainty due to missing of these

data and model self-adjustment. Even with the supplied of velocity, glacier and bedrock geometry and some environmental forcing data, some essential information is still missing which would cause model output at initial steps unreliable. For instance, ice temperature and basal water content are hardly available. Also, the assumption of non-slipping and simple-shearing based assumption as an initial velocity profile is questionable as water penetration at downstream of outlet glaciers should favour basal sliding. These all have significant impacts on the model result because the calculation of ice flow factors and basal motion heavily depend on them.

The purpose of spin-up is to allow certain highly-varied or uncertain parameters to evolve, with some physical constraints applied, until a statistical equilibrium is reached under the applied forcing. When that steady state is reached, the physical variables are consistent with each other and the system is self-adjusted under the given model framework. In this study with CISM, the spin-up is performed by fixing the ice geometry (i.e., unchanged ice thickness and front position). By assigning an initial ice temperature (constant across the model domain for simplicity), the model evolves under external forcing including surface temperature and geothermal heating. The spin-up process is also expected to generate basal water content. To monitor the progress of spin-up, the magnitude of velocity at Glacier 1 is chosen as the reference. The spin-up step ends if the magnitude of velocity at Glacier 1 begins to show a steady trend.

The remaining problem is: what initial ice temperature should be chosen for a meaningful spin up followed by simulation study? After testing with several initial ice temperatures and comparing the post-spin-up velocity outputs with observations (the latter of which are shown in Figure 4.1), it was found that an initial ice temperature of -3 °C results in the highest agreement between the post-spin-up velocity and observations (see Figure 4.5). Correspondingly, as illustrated in Figure 4.6, the velocity at Glacier 1 changes considerably and eventually becomes relatively steady since 31st model day. Although a mild velocity increment of about 20 metres/year for each model day after the 31st model day is observed, which implies an equilibrium state is not reached, strictly speaking. Yet due to constraint of computation time, it is not possible to run the spin up trials for months or even years long in search of the true equilibrium state. As a result, here it is claimed that spinning up is completed on the 31st model day. The simulation result as of 31st model day was extracted as spin-up outputs, which consist of updated basal water content (see Figure 4.7), update ice temperature profile (see Figure 4.9) and velocity profile (see Figure 4.5 (b) and Figure 4.8 (b)), are used for subsequent simulation study. It is worth mentioning that the absolute velocity magnitudes are not ideal to use for comparison because of systematic uncertainty due to incomplete understanding and complexity of glacier dynamics in its nature. For instance, all of the four test cases show particularly large velocities near the calving front of Glacier 1 compared with low slightly upstream (around 2 kilometres from the front) region. Such contrast in

velocity is not as apparent in InSAR-observed velocity field. This discrepancy is likely due to the inability of CISM to model the motion resistive effect from ice mélange, floating ice tongue and ocean water.

(a)

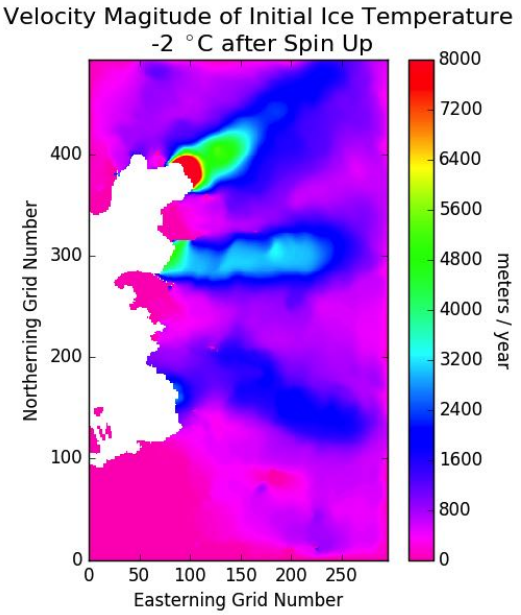

(b)

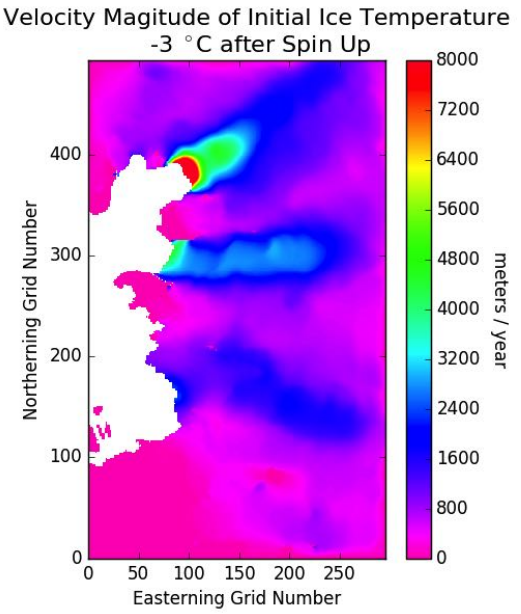

(c)

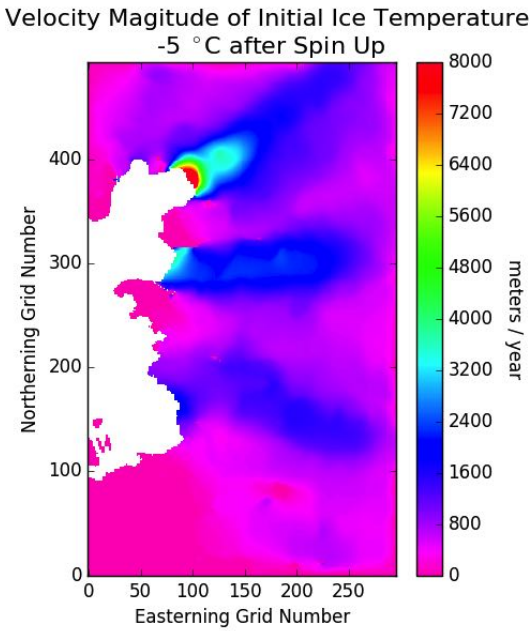

(d)

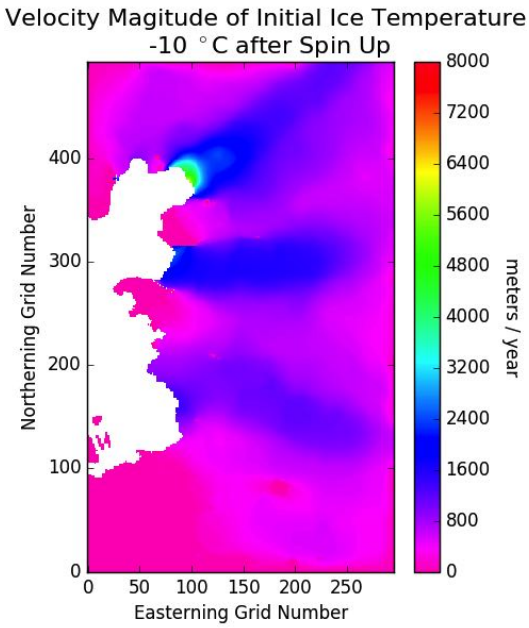

Figure 4.5 : Velocity magnitude output of Upernavik Isstrøm simulation after spin up phase with initial ice temperatures of (a) -2 °C, (b) -3 °C, (c) -5 °C, and (d) -10 °C, respectively.

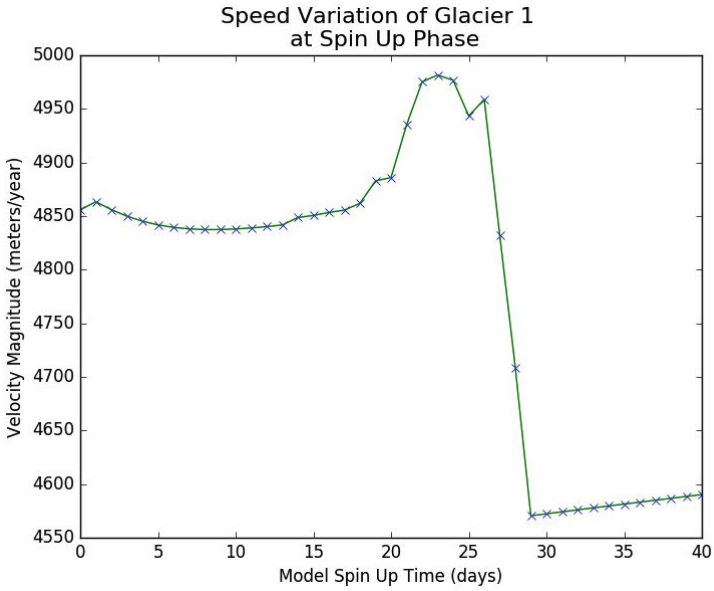

Figure 4.6 : Speed variation at Glacier 1 with an initial ice temperature of -3 °C during the spin up phase, indicating a relative steady state is reached on the 31st model day.

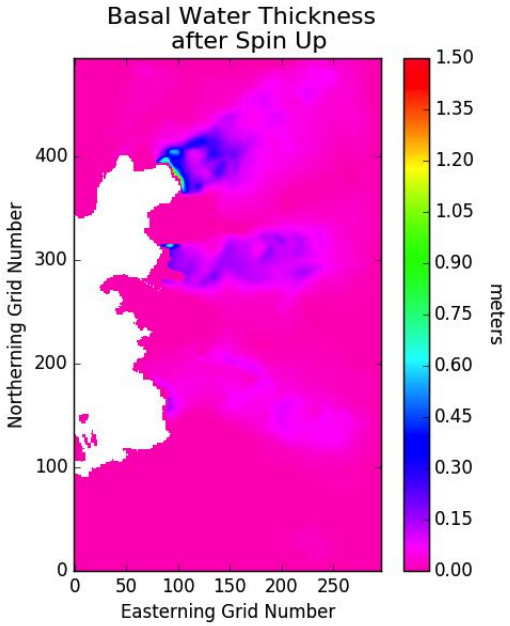

Figure 4.7 : Basal water thickness of Upernavik Isstrøm after spin up phase with initial ice temperatures -3 °C.

(a) (b)

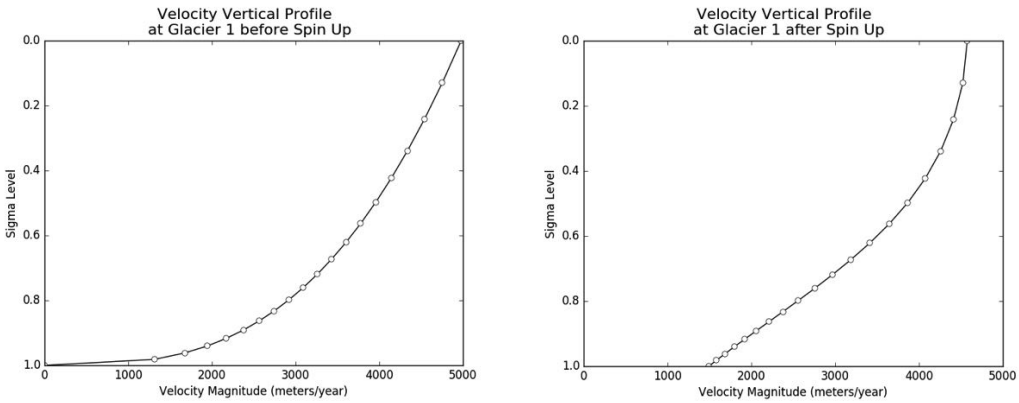

Figure 4.8 : Vertical velocity magnitude profile of Glacier 1 (a) before spin up and; (b) after spin up phase.

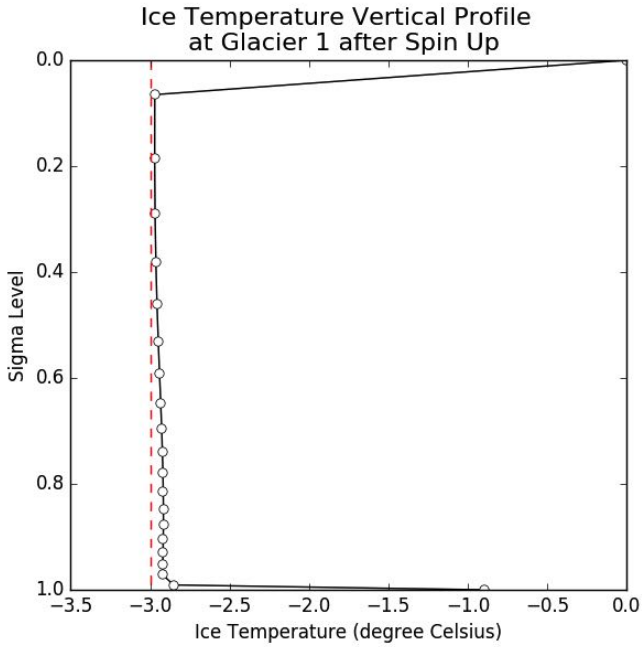

Figure 4.9 : Vertical ice temperature profile of Glacier 1 with initial ice temperature -3 °C before (in red dotted line) and after spin up phase (in solid line).

From the spin-up outputs, it could be seen from Figure 4.7 that approaching downstream of each glacier, the amount of basal water is higher than inland locations. This is because the basal water flows towards downstream following the gradient of bedrock topography and eventually converges and accumulates at tip of glaciers. As the genesis of basal water by pressure melting is largely controlled to local ice thickness, it is therefore noted from the spin-up outputs that a significantly greater amount of basal water is present at the front of Glacier 1, followed by Glacier 2, whereas for Glacier 3 and 4 the extents are tiny. The presence of basal water also modifies the velocity field as it allows basal motion on the original assumed non-slip velocity profile (see Figure 4.8 (a)). It could be seen from Figure 4.8 (b) the vertical velocity profile at Glacier 1 after spinning-up that a substantial magnitude of surface ice motion (around 4600 kilometres per year) is driven by basal sliding (around 1500 kilometres per year). The increment in ice velocity at bottom half is almost linear whereas across the top 30% of ice depth, the flow is almost laminar. The spinned-up velocity profile provides an insight consistent with theory that at the downstream of outlet glaciers, basal sliding is an important contribution to overall ice motion and flow is driven by a combination of vertical shearing and longitudinal straining in this transition zone. And thus a simple shearing ice velocity profile model is unsuitable to apply under these circumstances. The ice temperature profile after spin-up (see Figure 4.9) shows that a significant temperature change takes place only right at the surface and base. In particular, it could be seen that both ice

on surface and at bottom has reached its melting point respectively. This is because 31 days is too short of a timescale for heat from the boundaries to diffuse into ice.

After the spin-up phase, a self-contained system with more realistic ice temperature profile and basal water thickness is obtained. The model output containing these information, together with the existed boundary conditions, are then transferred to the core simulation exercise, which allow ice thickness to evolve against model time (see more in Chapter 5).

Chapter 5

Simulation:

Results & Discussions

Following from model spin up, it is subjected to produce simulations that would allow to investigate how various physical conditions affect dynamic behaviors of Upernavik Isstrøm glaciers. In this study, we examined the impact of ice temperature (Chapter 5.1), surface mass balance rates (Chapter 5.2) and the occurrence of large calving events (Chapter 5.3) on outlet glaciers velocity changes. From the simulation results, velocity fields near the terminus of each of the four glaciers are extracted for analysis and discussion.

We set a control run as a reference to compare and contrast the effects of different parameters on ice dynamics. The control model run is an experiment which follows from the model spin up using initial ice temperature -3 °C, an annual averaged surface mass balance rate (-150 water equivalent milimetres/year) and a default calving rate (at most 100 metres retreat per model day), and continue to adopt so.

5.1 Effect of Ice Temperature

Ice temperature is believed to have a fundamental control over speed of glaciers, as it affects ice viscosity directly. Higher ice temperature is often associated with higher glacier speed as ice viscosity is reduced. The purpose of this numerical simulation experiment, instead, is to investigate whether there is relation between ice temperature and the speed variation at outlet of each glacier in Upernavik Isstrøm.

It was found that for all four outlet glaciers, increasing ice temperature causes not only higher ice velocities, but also larger extent of variation. Figure 5.1 shows the simulated speed variations at outlet of four glaciers at Upernavik Isstrøm across 75 model days , obtained by setting initial ice temperatures as -2 °C, -3 °C, -5 °C, and -10 °C respectively. For example, at Glacier 1, the speed variation extent is around 300 metres/year when the average speed is around 5200 metres/year at initial ice temperature of -2 °C; whereas at initial ice temperature of -5 °C, the extent of variation is only around 200 metres/year on an average speed of 3600 metres/year.

(a)

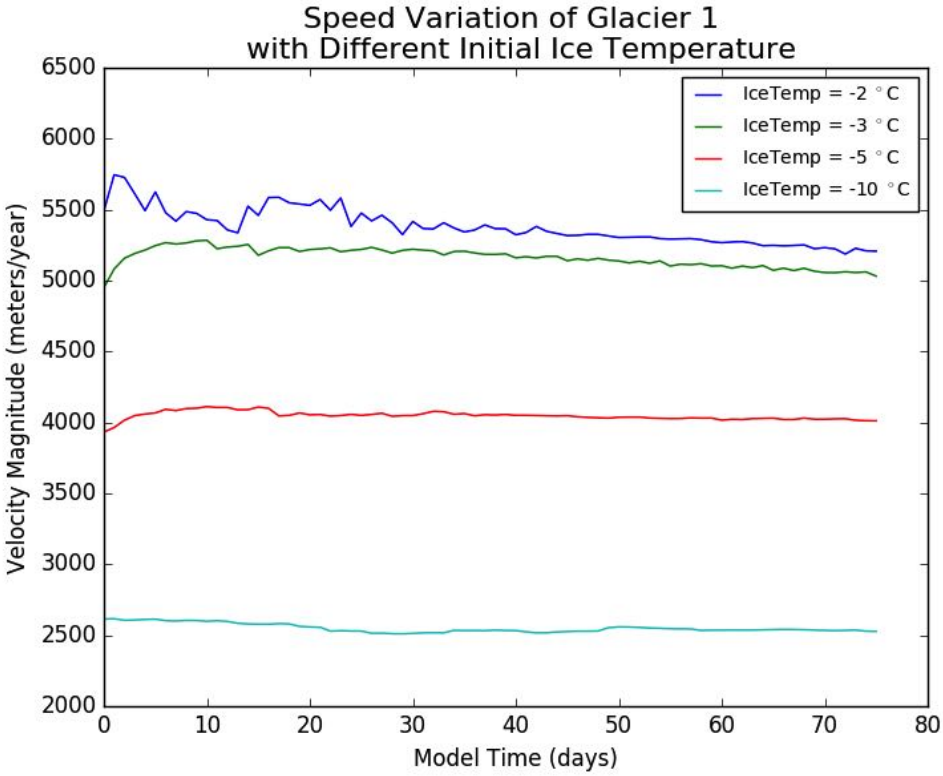
Speed Variation of Glacier 1
with Different Initial Ice Temperature
IceTemp = -2 °C
IceTemp = -3 °C
IceTemp = -5 °C
IceTemp = -10 °C
Velocity Magnitude (meters/year)
Model Time (days)
6500
6000
5500
5000
4500
4000
3500
3000
2500
2000
0
10
20
30
40
50
60
70
80

(b)

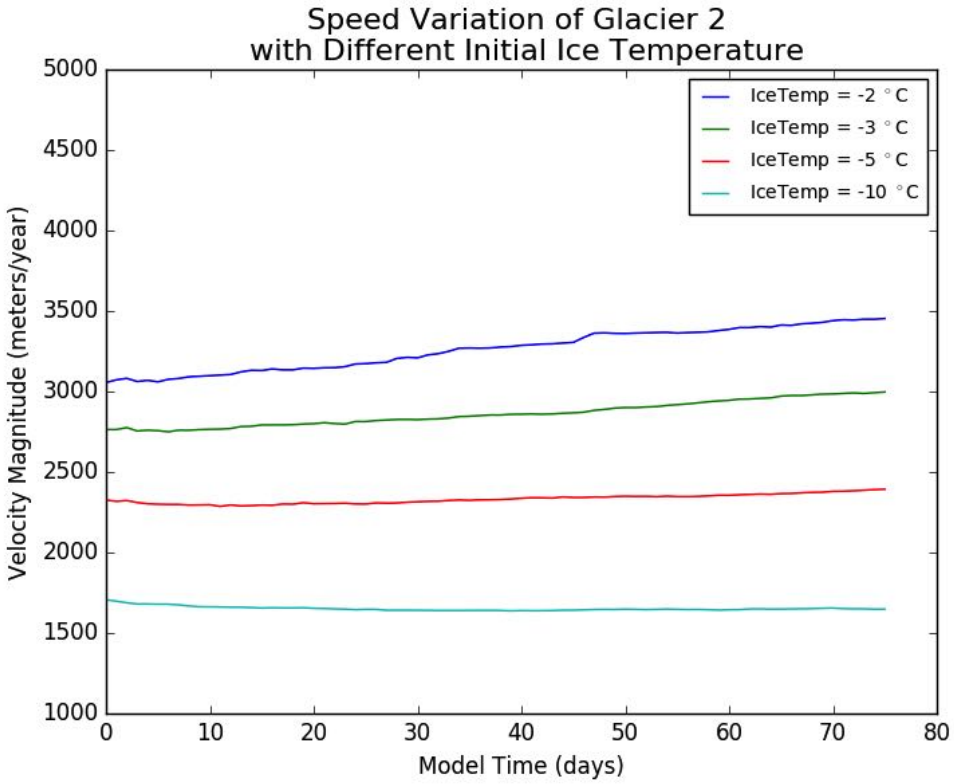
Speed Variation of Glacier 2
with Different Initial Ice Temperature
IceTemp = -2 °C
IceTemp = -3 °C
IceTemp = -5 °C
IceTemp = -10 °C
Velocity Magnitude (meters/year)
Model Time (days)
5000
4500
4000
3500
3000
2500
2000
1500
1000
0
10
20
30
40
50
60
70
80

(c)

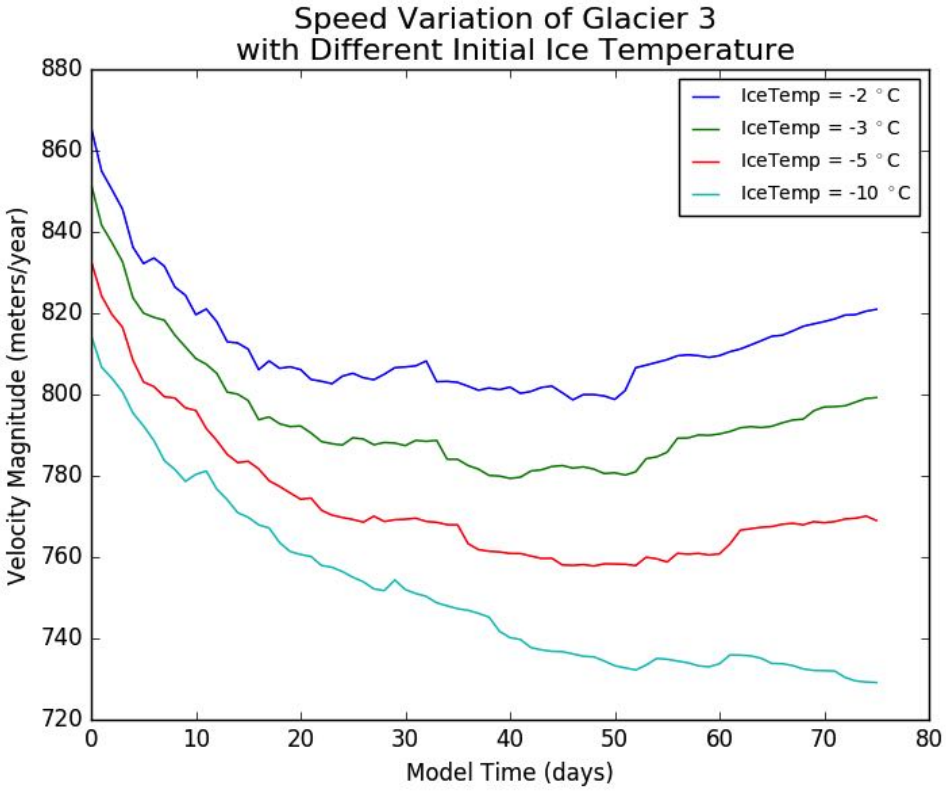
Speed Variation of Glacier 3
with Different Initial Ice Temperature
IceTemp = -2 °C
IceTemp = -3 °C
IceTemp = -5 °C
IceTemp = -10 °C
Velocity Magnitude (meters/year)
Model Time (days)
880
860
840
820
800
780
760
740
720
0
10
20
30
40
50
60
70
80

(d)

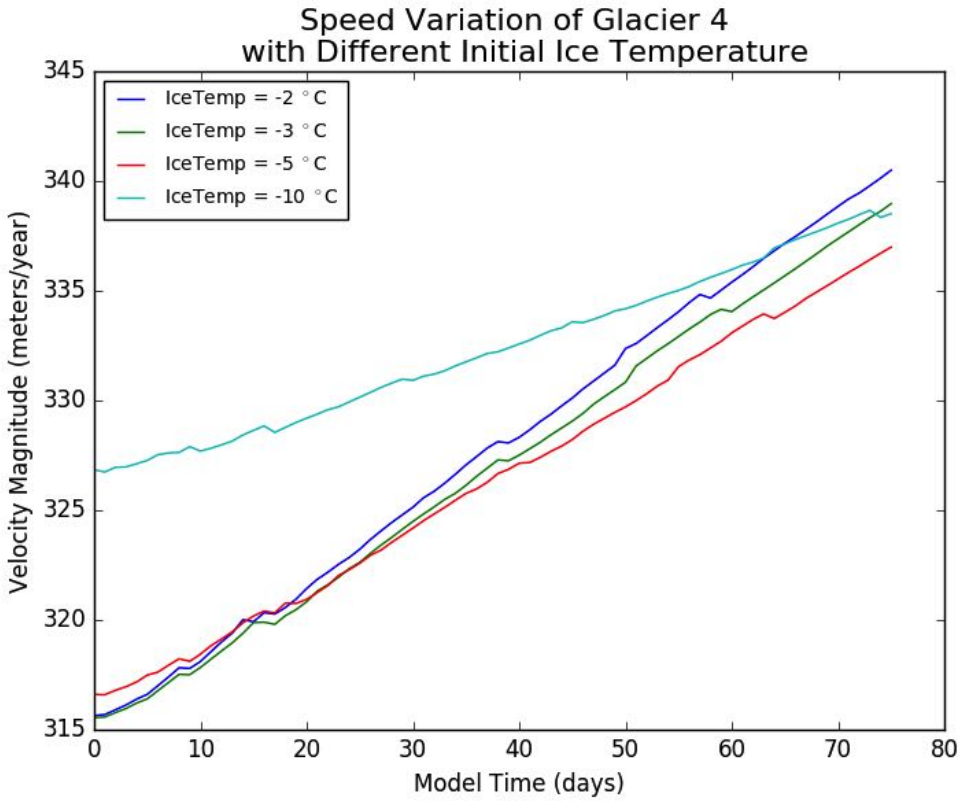
Speed Variation of Glacier 4
with Different Initial Ice Temperature
IceTemp = -2 °C
IceTemp = -3 °C
IceTemp = -5 °C
IceTemp = -10 °C
Velocity Magnitude (meters/year)
Model Time (days)
345
340
335
330
325
320
315
0
10
20
30
40
50
60
70
80

Figure 5.1 : Velocity variations of (a) Glacier 1, (b) Glacier 2, (c) Glacier 3, and (d) Glacier 4 with different initial ice temperatures in model simulation.

This ice-temperature dependency could be a consequence of variation of basal melting. Although under forcing of same magnitude of geothermal heat flux, the scenario with higher ice temperature is more likely to melt at bottom which supplies more basal water, favouring larger extent of basal sliding. On Glacier 1, pressure melting is strong so the basal melting extents under different ice temperatures are similar (Figure 5.2 (a)). But such variation becomes more apparent for thinner glaciers i.e., Glaciers 2–4. It is worth noting that on Glacier 3, the basal water increment rate under -2 °C initial ice temperature is almost twice of -5 °C initial ice; and no basal water could be produced at circumstance of -10°C initial ice temperature. As under all cases of initial ice temperature at Glacier 4, no basal water genesis across time is observed from model simulation (see Figure 5.2 (d)), the small variation of Glacier 4 is thus likely due to that ice viscosity variation under different initial ice temperatures..

(a)

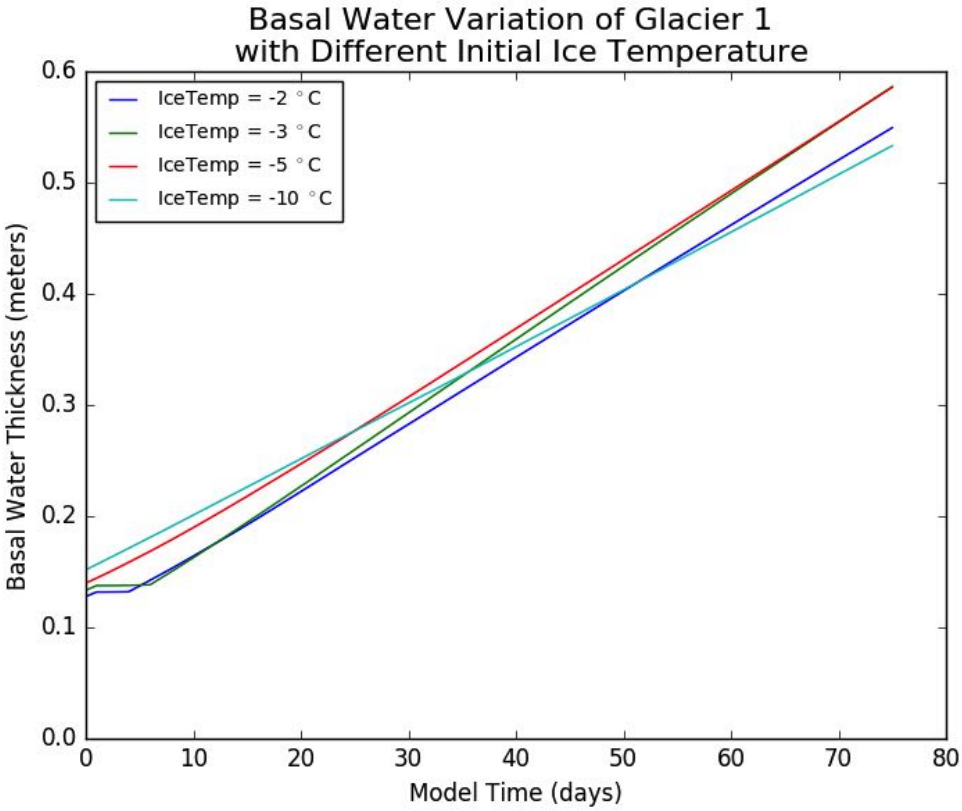
Basal Water Variation of Glacier 1
with Different Initial Ice Temperature
IceTemp = -2 °C
IceTemp = -3 °C
IceTemp = -5 °C
IceTemp = -10 °C
Basal Water Thickness (meters)
Model Time (days)
0.0
0.1
0.2
0.3
0.4
0.5
0.6
0
10
20
30
40
50
60
70
80

(b)

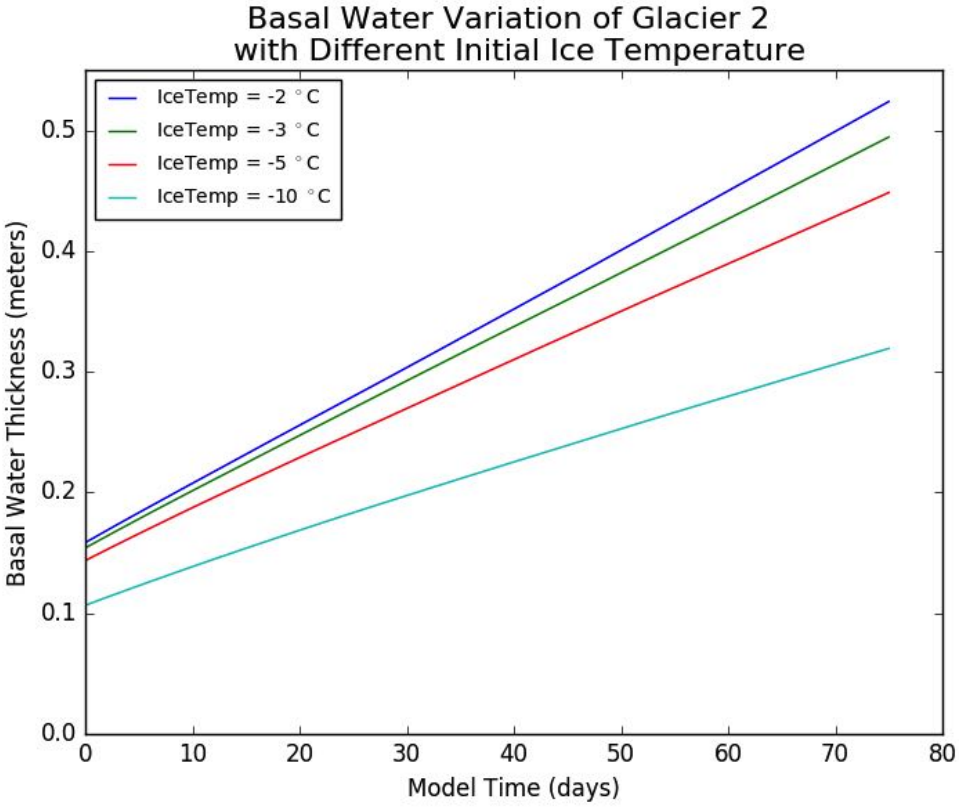
Basal Water Variation of Glacier 2
with Different Initial Ice Temperature
IceTemp = -2 °C
IceTemp = -3 °C
IceTemp = -5 °C
IceTemp = -10 °C
Basal Water Thickness (meters)
Model Time (days)
0.0
0.1
0.2
0.3
0.4
0.5
0
10
20
30
40
50
60
70
80

(c)

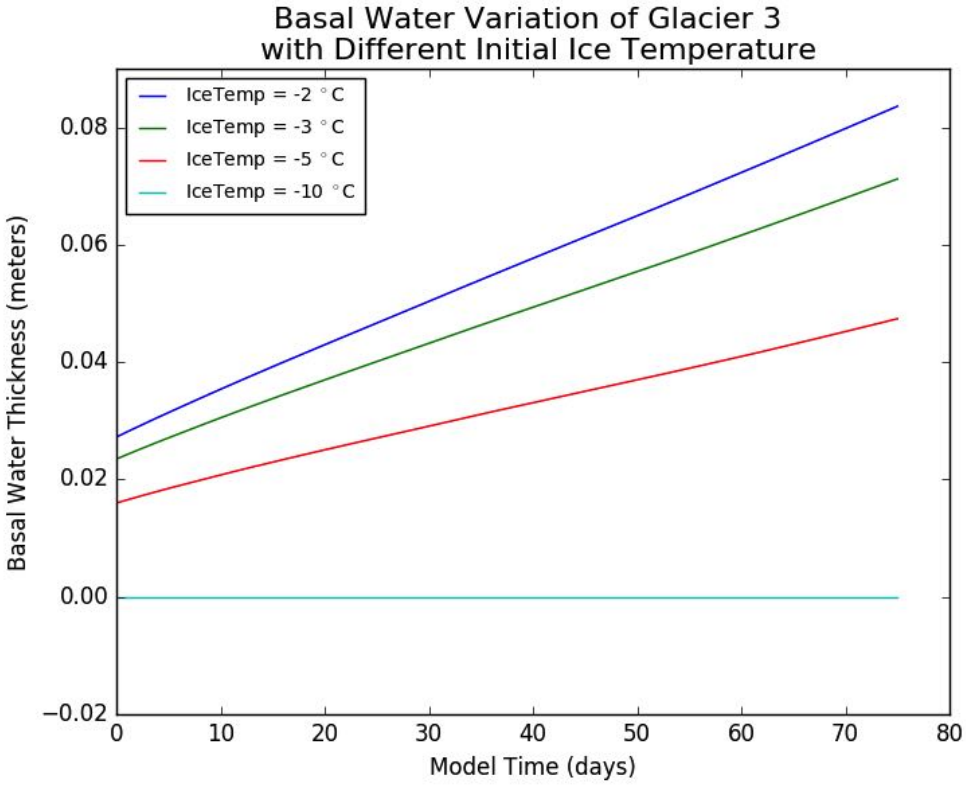
Basal Water Variation of Glacier 3
with Different Initial Ice Temperature
IceTemp = -2 °C
IceTemp = -3 °C
IceTemp = -5 °C
IceTemp = -10 °C
Basal Water Thickness (meters)
0.08
0.06
0.04
0.02
0.00
−0.02
0
10
20
30
40
50
60
70
80
Model Time (days)

(d)

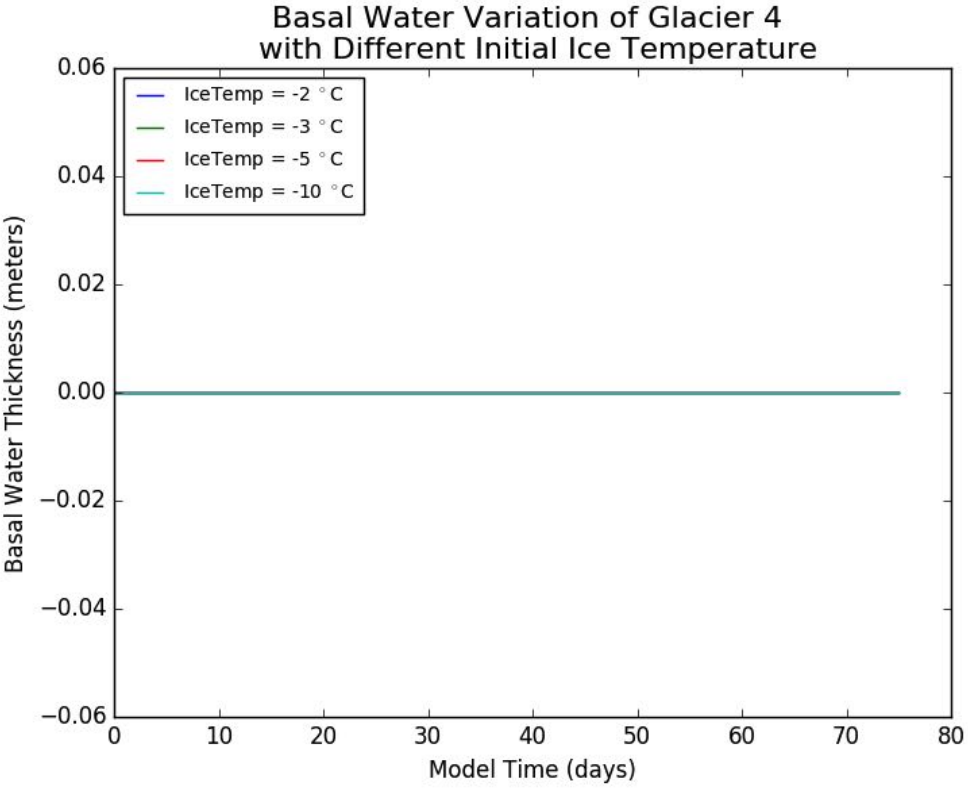
Basal Water Variation of Glacier 4
with Different Initial Ice Temperature
IceTemp = -2 °C
IceTemp = -3 °C
IceTemp = -5 °C
IceTemp = -10 °C
Basal Water Thickness (meters)
0.06
0.04
0.02
0.00
−0.02
−0.04
−0.06
0
10
20
30
40
50
60
70
80
Model Time (days)

Figure 5.2 : Temporal variations of basal water thickness of (a) Glacier 1, (b) Glacier 2, (c) Glacier 3, and (d) Glacier 4 terminus with different initial ice temperatures in model simulation.

Another observation from Figure 5.1 is that both Glacier 1 and Glacier 2 show a general trend of deceleration; and Glacier 3 decelerates at first but accelerates afterward; while Glacier 4 shows a mild acceleration trend. These different behaviors are likely related to different surface gradient changes and ice tongue area changes. The considerably large and growing ice tongues at Glacier 1 serve as strong buffer not only hindering the possibility of large extent of speed-up, but also responsible for gradual slowing down trend across 75 model days under all tested initial ice temperature cases. Contrary to real world observation which suggests Glacier 1 at Upernavik Isstrøm exhibits a calving front retreat trend in summers, the model simulation shows an advance tendency because of model limitation. The current calving scheme in CISM framework can only reduce a constant portion of ice at the margin of floating ice and ocean, which is less than amount of ice contributing from upstream upon a high glacier velocity at Glacier 1. Eventually ice thickness near grounding line and terminus increases, which decreases surface elevation gradient and reduces the tendency of flowing towards downstream. Thus, the consequence of lengthening of ice tongue on Glacier 1 in the model simulation is the provision an enhancing resist on ice motion and more gentle surface gradient, which does not favour speeding up and

reduces the extent of speed fluctuations. This mechanism is not applicable on Glacier 3 or Glacier 4 because they have small and thin ice tongues, which the built-in calving scheme can remove effectively. Despite the fact that Glacier 2 is also a thick glacier with a large portion of ice tongue afloat, it has not shown the gradual deceleration trend as Glacier 1 in model simulation because no decreased in surface elevation is resulted, as the amount of ice calved away is similar to the ice contributed from glacier upstream. Therefore, the surface gradients at these two glaciers could be maintained or even slightly strengthened.

Both the ice area and elevation changes could be seen by comparing the ice thickness maps at the beginning (Figure 5.3 (a)) and ending stage (Figure 5.3 (b)) of model simulation with initial ice temperature -3 °C . The contrast of two figures reveals that terminus position of Glacier 1 has advanced by more than 1 kilometre, in a simulation with CISM built-in calving scheme, whereas other three Glaciers has not shown notable change in respective terminus positions. The relative steady ice front positions observed at Glacier 2, 3 and 4 in simulation of 2010 summer agrees with satellite observation. It suggests that the current CISM calving mode and parameter, which removes floating ice at the ice-ocean margin at every timestep, is applicable on these three glaciers. However, for Glacier 1, the apparent discrepancy of change in frontal position between model simulation and observations suggests a necessity of including or adopting a larger scale calving scheme in order to match up

with observation. Hence, numerical experiments of impact on glacial dynamics upon the occurrence of large calving events are initiated from the terminus position disagreement at Glacier 1 and results are presented in Chapter 5.3.

(a) (b)

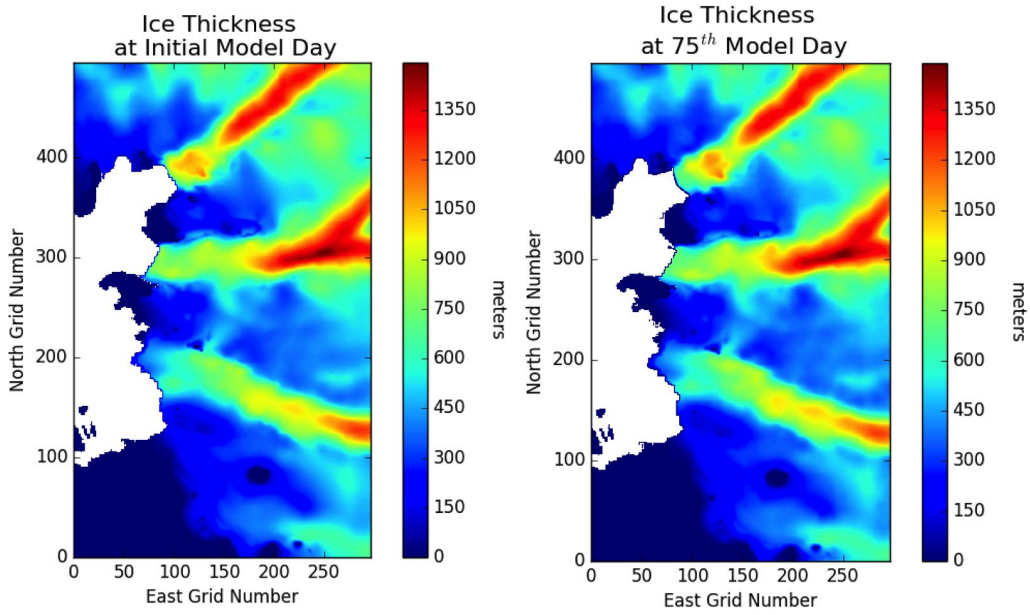

Figure 5.3 : Ice thickness distribution of Upernavik Isstrøm (a) on initial model day and (b) on the 75th model day in simulation with an initial ice temperature of -3 °C.

Nevertheless, the magnitude of ice temperature, is not suggested to be the reason for the abrupt speed-up of Glacier 1 in 2010. This is because model simulation (Figure 5.1) suggests even at high ice temperature, the variation extent is less than 10% of the averaged velocity magnitude. In order to achieve a sudden change in velocity for over 30% in an outlet

glacier, qualitatively it would involve a corresponding temperature increment by at least 2 °C which is unlikely to happen in transient timescale. Hence it is concluded that ice temperature change is not likely to be the cause leading towards a sudden speed-up at Glacier 1.

5.2 Effect of Surface Mass Balance

Following from Chapter 5.1 which investigated the effect of different initial ice temperature with annual averaged SMB value, this section compares the effects on glacier dynamics response under same initial ice temperature but different SMB rates in CISM version 2.0.5. As described in Chapter 4.1.4, annual averaged and summer averaged rates of -150 and -1000 water equivalent millimetres per year are used respectively. As illustrated in Figure 5.4, more negative surface mass balance rate in summer means more ice loss from the surface and thus leads to a higher rate in reduction of ice volume over the model domain. This is usually associated with an increment in velocity, as more negative surface balance implies more surface melting which contributes extra meltwater to base. However, model simulation results, as illustrated in Figure 5.5, suggest that in both scenarios ice velocities at Glacier 1 show a gradual decreasing trend. And the case with summer SMB, Glacier 1 experiences a greater slow down compared to annual SMB case.

The intuition countering results obtained from this experiment is likely due to the deficiency of CISM version 2.0.5 for not handling surface mass balance information well enough. Figure 5.6 shows the basal water content variation in both scenarios. A significantly more negative SMB rate imposed for the summer case has not led to a major difference in basal water increment, compared with the annual SMB case. The possible reason is that as water transport model is a missing piece in this model, meltwater generated from a negative surface mass balance is neither considered to be drained to the base of glacier nor retain inside an ice body. Instead, the effect of changing the surface mass balance rate during simulation is simply to change the local ice thickness – more negative SMB reduces ice thickness to a greater extent, but not contributing to the changing ice dynamics from basal hydrology. Thus, an extra reduction in ice thickness resulting from more negative SMB rate would lead to a decrease in gravitational driving stress acting on ice body, which leads to lower ice velocity. In additional to the model deficiency, the uniform surface mass balance rates prescribed in both cases could also be a cause for the unphysical slow-down trend. In fact, the lower stream of a glacier is expected to experience more negative summer and annual surface mass balance rates compared to upper stream, simply because air temperature normally decreases with increasing altitude. The variation in extent surface mass balance rates over different regions of an outlet glacier also has a role in altering surface elevation gradient and thus the surface velocity.

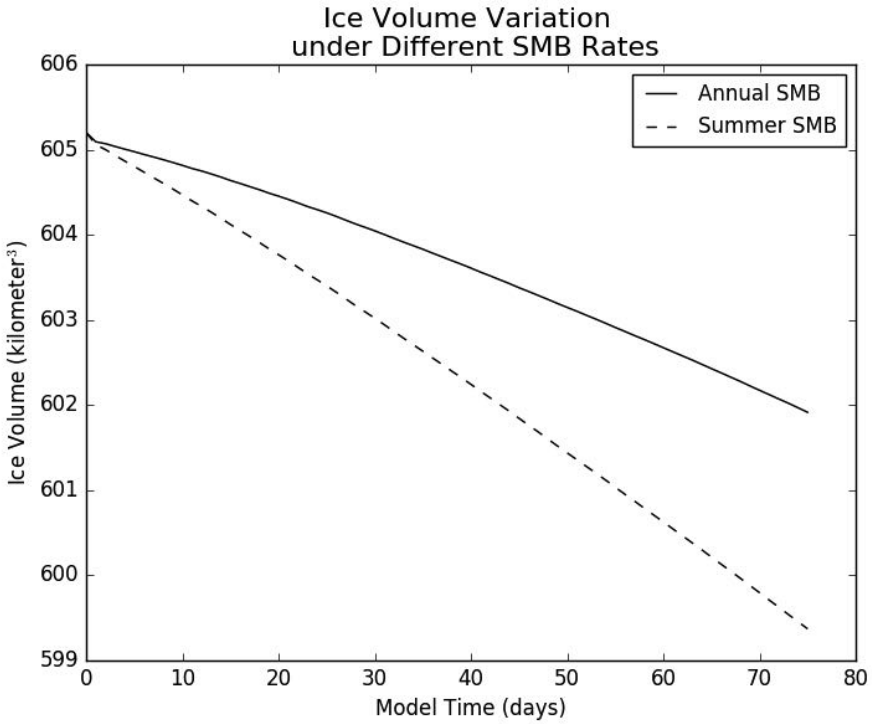

Figure 5.4 : Total ice volume change of four glaciers in Upernavik Isstrøm subjected to annual averaged surface mass balance rate and summer averaged surface mass balance rate in model simulation respectively.

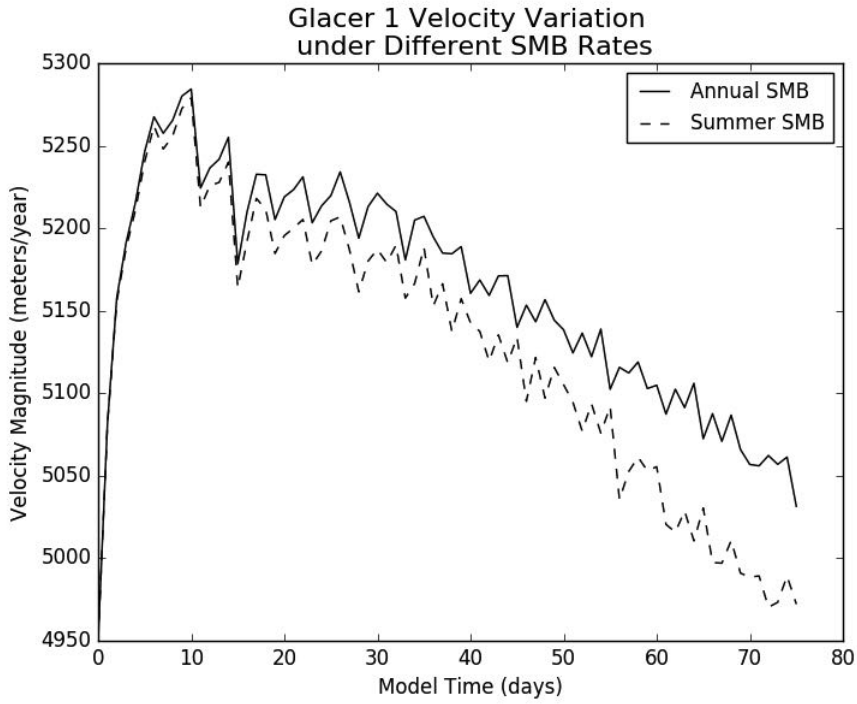

Figure 5.5 : Velocity variation of Glacier 1 subjected to annual-averaged surface mass balance rate and summer-average surface mass balance rate in model simulation, respectively.

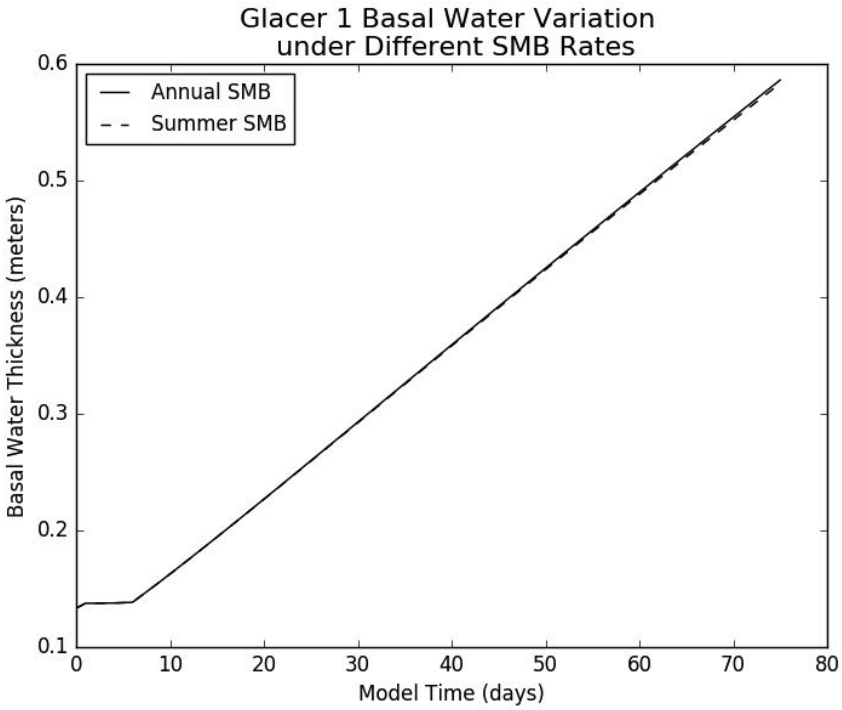

Figure 5.6 : Basal water thickness variation of Glacier 1 subjected to annual averaged surface mass balance rate and summer average surface mass balance rate in model simulation respectively.

Therefore, it is not possible to draw a conclusion whether a change in surface mass balance rates is a potential factor causing the sudden speed-up for Glacier 1. This is because a major deficiency exists in the model which makes the effects and consequences of surface mass balance not treated completely and correctly during the model simulations. It could be seen from this exercise that unphysical results would be produced if

effect of hydrological changes arising from a negative surface mass balance is not taken into consideration.

5.3 Effect of Large-Scale Calving

Events of large-scale calving of floating ice is believed to have potential to induce major change in the dynamics by altering internal ice stress balance. The purpose of simulation experiment in this part is to investigate whether a calving event can lead to a speed-up at Upernavik Isstrøm outlet glaciers, and if so, the sensitivity of the speed-up magnitude on the scale of calving. As CISM version 2.0.5 only supports a heuristic calving scheme, of removing a portion of ice thickness at ice-ocean margin, which could only represent situations of ice tongue thinning and micro-scale calving in a high-resolution simulation. A large piece of calving could only be triggered by an interruption to model outputs at certain timestep and then resuming the model simulation. Based on the previous model simulations, we devised four extents of calving, namely case A, B, C, and D, each differed by a distinct scale, on Glacier 1 and Glacier 2 on the 50th model day, as illustrated in Figure 5.7. This experiment is only carried out on Glacier 1 and Glacier 2 because large-scale calving and thus internal stress changes are only likely to happen on outlet glacier with a substantial amount of floating ice tongue. For instance, on the 50th model day, Glacier 1 and Glacier 2 have around 2.5 kilometres and 3.8 kilometres floating ice tongue, respectively. On Glacier 1, case A corresponds to a 2 kilometres

retreat and is the scenario where ice front is retreated closest to the grounding line; whereas cases B, C, and D represent retreats of around 1.5 kilometre, 1 kilometre, and 0.5 kilometre, respectively. On Glacier 2, cases A, B, C and D represent retreats of 3 kilometres, 2.5 kilometres, 2 kilometres, and 1.5 kilometre, respectively. After we convert the information of calved ice into ocean for each calving case on the 50th model day, the updated model variables are subjected to model self-adjustment at first and run for the remaining 25 model days.

(a) (b)

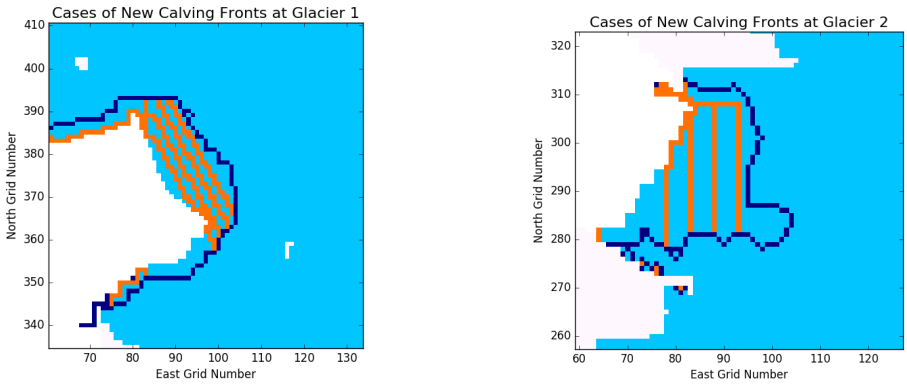

Figure 5.7 : Illustration of modified calving fronts positions of (a) Glacier 1 and (b) Glacier 2 in model domain on the 50th model day, for further simulation experiment. Light blue represents ice cover; white represents ocean and land; dark blue line represents the grounding line; and orange lines represent new front positions after case A, B, C, D calving respectively (ordering from nearest to furthest away from the grounding line).

Model simulations show that both glaciers speed up after all calving scenarios, and higher magnitudes of speed-ups are observed for larger

calving areas. The comparisons are made for immediate speed change after calving and difference in speed trend after different cases of calving, using previous simulation in Chapter 5.1 with built-in simple heuristic calving scheme as reference. Figure 5.8 (a) and (b) show speed variations with different calving cases on the 50th model day at Glacier 1 and Glacier 2, respectively. In cases A and B, Glacier 1 shows an immediately minor speed-up after model self-adjustment at restart stage by and extent of 50 and 30 metres/year respectively, followed by a further gain in speed of 200 and 100 metres/years on the 2 model days. In cases C and D, a minor speed-up of tens of metres/year is observed after 3 model days, but not immediately during the model self-readjustment stage. Despite that Glacier 1's velocities in all cases of large calving are higher than without large calving, they still show a deceleration trend afterwards due to accumulation of floating ice. However, in all cases of large calving, Glacier 2 shows very distinct increases in velocities, followed by a trend of further speeding up. Larger calving areas are associated with larger immediate speed-up and subsequent acceleration. For instance, Glacier 2 in case A shows a speed increase of more than 600 metres/year immediate after restarting the model from the large calving, and a 500 metres/year increment during the next 25 model days. In cases B, C and D, calving produces 300 metres/year, 200 metres/year and 100 metres/year increment upon model restart after calving, and followed by a speed-up of 100 – 300 metres/year.

(a)

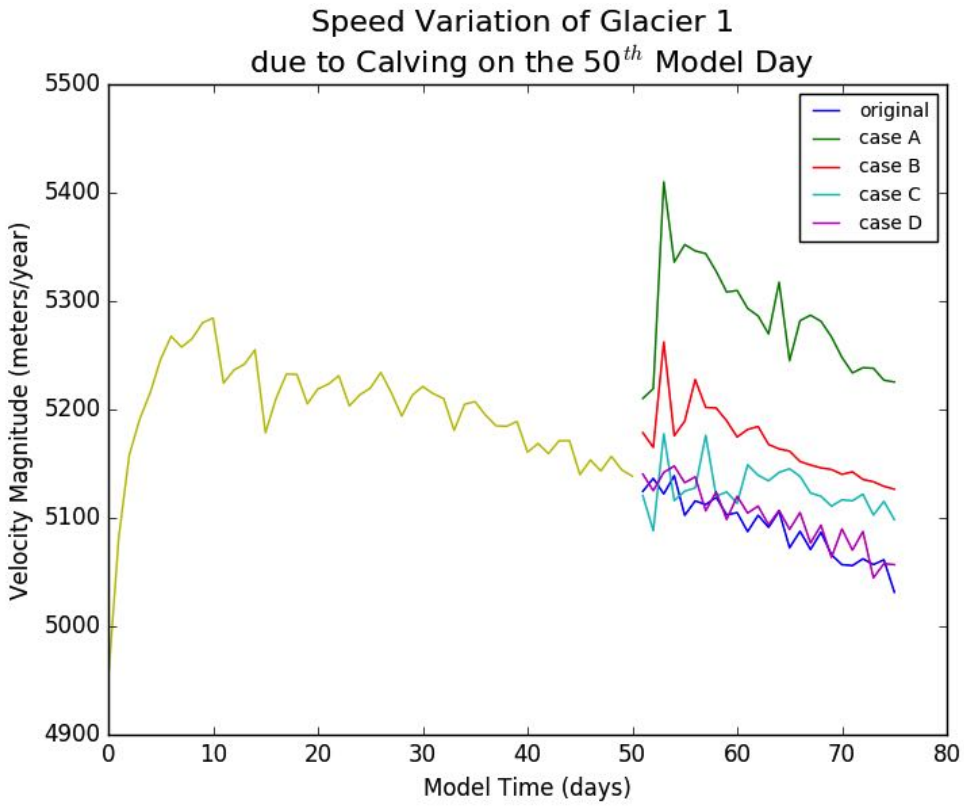
Speed Variation of Glacier 1
due to Calving on the 50th Model Day
original
case A
case B
case C
case D
Velocity Magnitude (meters/year)
Model Time (days)
5500
5400
5300
5200
5100
5000
4900
0
10
20
30
40
50
60
70
80

(b)

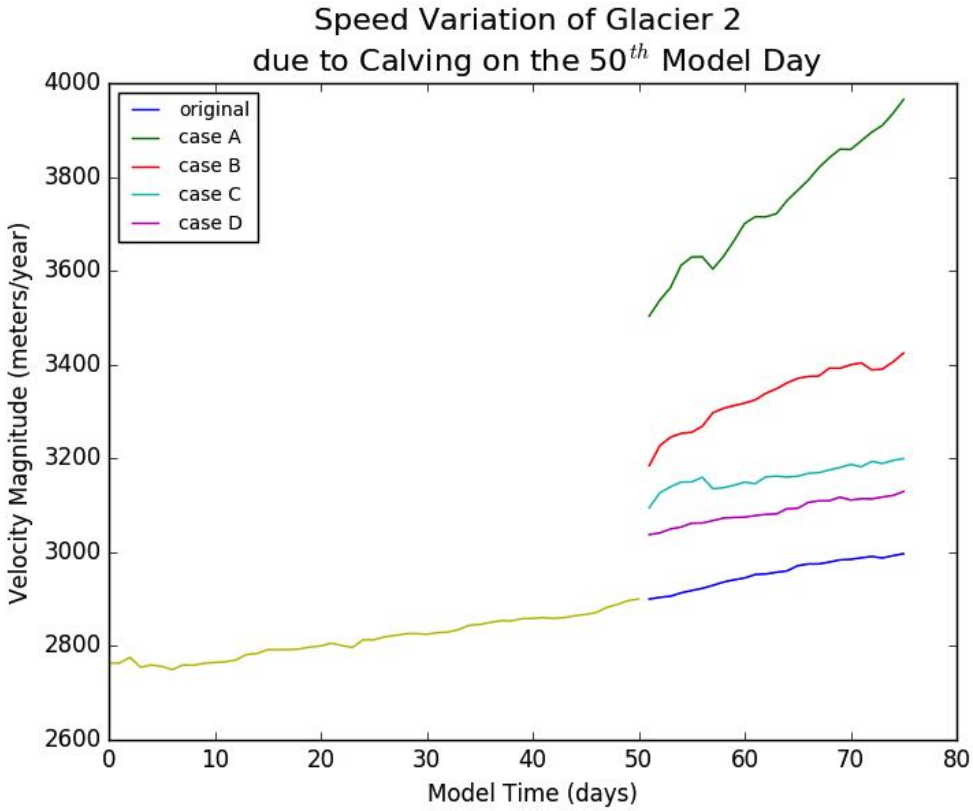
Speed Variation of Glacier 2
due to Calving on the 50th Model Day
original
case A
case B
case C
case D
Velocity Magnitude (meters/year)
Model Time (days)
4000
3800
3600
3400
3200
3000
2800
2600
0
10
20
30
40
50
60
70
80

Figure 5.8 : Comparison of velocity magnitude variation of (a) Glacier 1 and (b) Glacier 2 due to different extents of calving on the 50th model day in model simulation respectively.

Change in effective stress after large calving is responsible for the immediate speed-up in model simulations. Figures 5.9 (a) and (b) show the vertical effective stress of Glacier 1 and Glacier 2, respectively, in original no large calving simulation and after different cases of large calving. Here we investigate stress changes along flowline because only ice calving at front is involved in this experiment. Figure 5.9 (a) shows that stress changes after calving mainly happen near the surface of Glacier 1, whereas there is only tiny effective stress change near the glacial base. Case A shows the greatest magnitude of effective stress increase (~10000 Pascal), followed by case B (~5000 Pascal); yet, cases C and D show little difference in effective stress profile, compared with the stress before these calving cases. This could explain why previously model interpreted case A and B would have the respective increase in velocity magnitude after calving but case C and D seem no particular change. As shown in Figure 5.9 (b), on Glacier 2, the effective stress changes after calving are more homogenous across ice depth that those on Glacier 1. For instance, effective stresses increase by around 30000 Pascals for case A, 20000 Pascals for case B, and around 15000 Pascals for case C and D. These different stress changes result in the distinct velocity increases among cases of different calving

sizes. The difference in fraction of effective stress increment after calving also explains why large-scale calving causes a larger speed-up at Glacier 2 than at Glacier 1, despite related speed-up and large calving is not observed on Glacier 2.

The different changes in effective stress of Glacier 1 and Glacier 2 are likely due to the dynamic characteristics of these two glaciers. Throughout the simulation study, it is found that Glacier 1 initially has a short floating ice tongue. It gets longer substantially (compare Figure 5.3 (a) and (b)) due to ice contribution from fast glacier movement. But Glacier 2 begins with a vast floating ice tongue with a steady frontal position. Neglecting the stress contribution from ocean buoyancy (which is a missing piece in the model), we interpreted that the flow of Glacier 1 is more shearing dominated whereas Glacier 2 is more controlled by horizontal stress under the well-developed floating ice portion. As a result, removing a great amount of floating ice from Glacier 1 is expected to cause slightly greater change to effective stress near the ice surface than at the base (i.e., the most shearing dominating region). In contrast, the longitudinal stress balance at Glacier 2 floating ice would be more strongly affected if the resistive stress decreases over entire column. Since the strength of resistive stress is proportional to floating ice mass and almost homogenous across depths, distinct difference of effective stress increases (uniform vertically) is resulted from different extents of calving. This mechanism explains the large speed variations at Glacier 2 due to calving.

(a)

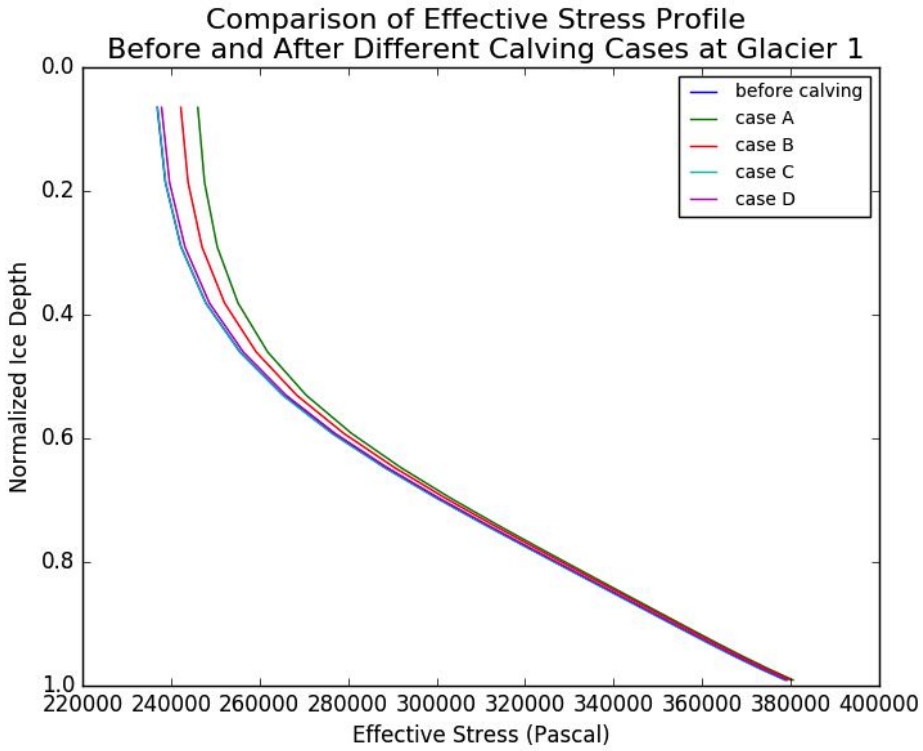
Comparison of Effective Stress Profile
Before and After Different Calving Cases at Glacier 1
before calving
case A
case B
case C
case D
Normalized Ice Depth
0.0
0.2
0.4
0.6
0.8
1.0
220000 240000 260000 280000 300000 320000 340000 360000 380000 400000
Effective Stress (Pascal)

(b)

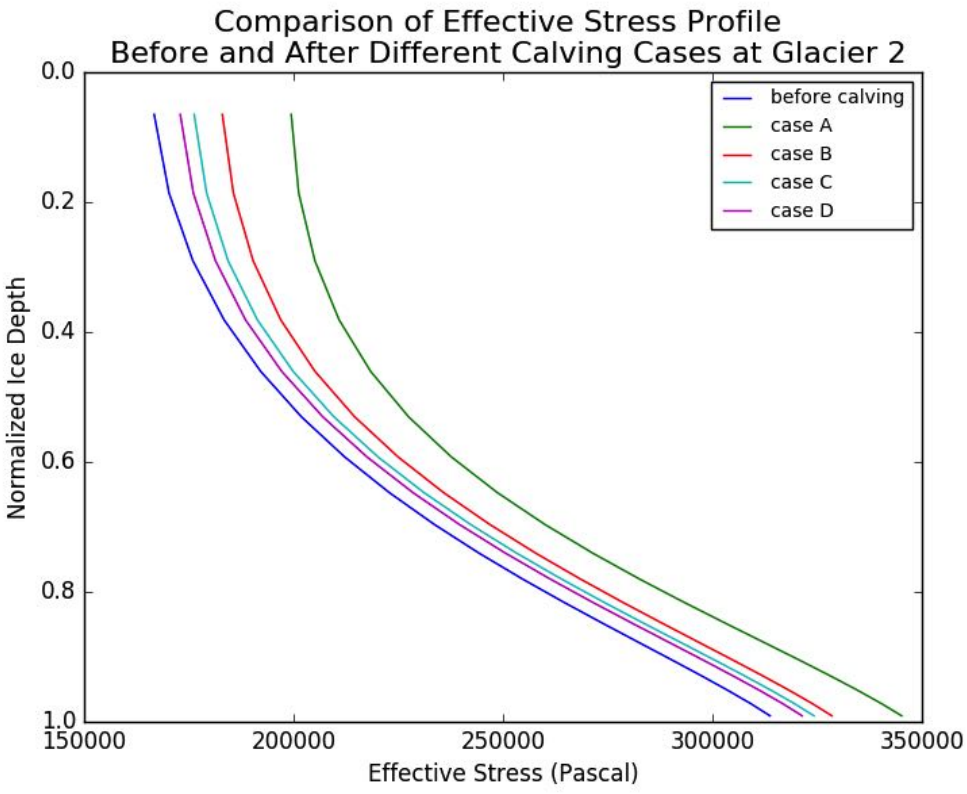
Comparison of Effective Stress Profile
Before and After Different Calving Cases at Glacier 2
before calving
case A
case B
case C
case D
Normalized Ice Depth
0.0
0.2
0.4
0.6
0.8
1.0
150000
200000
250000
300000
350000
Effective Stress (Pascal)

Figure 5.9 : Comparison between effective stress profile at (a) Glacier 1 and (b) Glacier 2 before and after different cases of calving in model simulation.

In summary, model simulation in this exercise suggests that the occurrence of large-scale calving could increase frontal effective stress, leading to a glacial speed and possibly subsequent changes in dynamic behaviours. However, calving involves a complex ice-ocean interaction process from triggering to responding of glacier ice internal stresses, which is not completely covered in CISM version 2.0.5. This exercise cannot determine whether the immediate speed-up shown when restarting the model after calving would be a transient reaction or process with delayed response. The velocity increase on Glacier 1 and Glacier 2 after a user-manipulated large-ice calving is resulted from a change in ice effective stress interpreted by the model due to sudden disappearance of a portion of floating ice from the output of a specific model time. Since the calving is resulted from interruption of model, information of time required to yield the corresponding stress changes is not obtainable. Though it is difficult to understand how many days would it take for a large calving to alter internal stress distribution and thus changes the glacier dynamics behaviour from this method, it still provides an insight that calving events can change ice effective stress glacier and eventually lead to a speed-up.

Chapter 6

Conclusions

6.1 Major Conclusions

This research has examined the effect of ice temperature, surface mass balance and iceberg calving on short-term dynamic changes of outlet glaciers at Upernavik Isstrøm, Greenland, in summer 2010. It is achieved by incorporating satellite observations and model simulations using CISM version 2.0.5. It is concluded from model simulations that large-scale calving could lead to a large magnitude of speed-up of outlet glaciers, while a more negative surface mass balance has not led to a higher velocity. Also, higher ice temperature is found to cause higher speed variations.

Model simulations suggest that large-scale calving could lead to the abrupt speed-up of Glacier 1 in Upernavik Isstrøm in the summer of 2010. Model simulations also suggest that large-scale calving can lead to an increase in glacier frontal speed as the effective resistive stress is greatly reduced. It is also found that the magnitude of velocity increase is proportional to the size of calved ice. Yet, it is uncertain how fast the change in speed would occur after calving as a physical-based calving process has not been comprehensively included in CISM.

On the other hand, although a more negative surface mass balance is often associated with increased ice velocity, this phenomenon is not captured in model simulations of this study. Instead, our simulations suggested a lower glacier speed under forcing summer-averaged surface mass balance, which is more negative, compared to annual-averaged surface mass balance. This is due to the incomplete consideration of meltwater production brought about by a negative surface mass balance and its consequential interaction with the glacier body. This discrepancy has highlighted the importance of surface melting contributed hydrological impact, including change in basal water content and effective water pressure, on understanding short-term glacier dynamics.

Finally, it is found that ice temperature is an important control speed variation of outlet glaciers of Upernavik Isstrøm, on cases without large calving. The effect is more significant on large glaciers (Glacier 1 and Glacier 2). Ice temperature affects the ice flow by its fundamental control over ice viscosity, and speed variation from variability of sliding due to differences in basal water production.

6.2 Lessons Learnt in This Study

This work has illustrated the application of the numerical ice sheet model in studying, in fine detail, the dynamics of individual outlet glaciers by conducting high spatiotemporal simulations. It has also examined the advantages and limitations of CISM as the tool for carrying out regional tidewater glacier dynamics modeling at this resolution. Through this study, I have learned (1) how the movement and physical changes of outlet glaciers are brought about by the ice body itself and the external environment; (2) the development and history of the theory and computation work on ice sheet modeling, related observation techniques, and climatic studies; and (3) experience in using computer modeling as well as analyzing the outputs.

6.3 Future Directions

Even though this study has demonstrated that large-scale calving can result in outlet glacier speed increase by model simulation of CISM as a standalone model, there remains plenty of room for further work on understanding this phenomenon in detail. For instance, it would be important and interesting to investigate (1) the relation between ice tongue stability and oceanic thermal and dynamic condition; (2) the detailed calving process and the stress response, from triggering of

factures, to crevasses growth and eventually detachment; and (3) the super- and sub-glacier hydrological processes.

The next version of CISM will implement damaged-based calving scheme and support coupling with ocean and atmosphere models. Scheduled for public release late 2016, it is optimistic that a variety of numerical modeling research topics will then become possible. These computing tools would be helpful in deepening our understanding of ice sheets and glaciers, and their interactions with the warming atmosphere and ocean.

Appendix

Notes on CISM Configuration

This appendix presents a brief summary of selection of model parameters used in this study for a high-resolution coastal-region simulation with CISM version 2.0.5. The default of model parameters in CISM is targeted and suitable for ice sheet simulation in kilometers resolution. However, in this study, a high-resolution regional simulation of ice dynamics is desired. Numerical instability is likely since the coastal region of Upernavik Isstrøm involves complex geometry and some of the numerical schemes adopted in CISM are sensitive to geometric changes. Therefore, specific sets of model configuration and parameters are chosen and tested, which have proven to allow the model to run and complete the simulations we described in Chapter 5. A sample for model configurations and parameters adopted in model simulation of this study is shown in Figure B.1, which has been used for producing simulation results in Chapter 5.1 and 5.2 after spin up phase. Readers are encouraged to refer to CISM version 2.0.5 User Manual (Chapter 7.3: Model Configuration) for better understanding of the settings.

Spatial derivatives in CISM are computed by central gradient by default, which requires quantities from neighbouring grids. Yet, numerical

ambiguity would raise in central gradient method when one of the neighbouring grid is not ice-covered. CISM is thus set to compute spatial derivatives with upstream gradient, with considering only ice-cover grids cells. Despite that the incremental remapping scheme is the most accurate method available in CISM version 2.0.5 to model mass transport, it is unable to function stably especially at ice-ocean margin because ice front position frequently migrates due to calving. Therefore, instead, we use a first-order upwind scheme to compute ice thickness evolution. We choose these configurations with higher numerical tolerance, which however, give an accuracy of one order than what would be obtained using the default setting on spatial derivatives and thickness evolution computation method. Nonetheless, these are also safe and accurate numerical schemes considering that the dynamical core of CISM solves for momentum balance and diffusion equations through fixed point iteration with a very low error tolerance.

Calving as a major way outlet glaciers lose ice into ocean is taken into account by setting the ice-ocean margin cell to lose a fraction of ice at every timestep (heuristic calving scheme as described in Chapter 5). The parameter corresponds to the faction of ice remained is tunable. Strictly speaking, this parameter of any value other than 0 should imply an ice tongue thinning scenario instead of calving. However, this parameter cannot be set to 0 in this simulation because numerical instability also happens at locations where ice is completely grounded while in contact

with ocean. At Upernavik Isstrøm, most of coastline has only little amount of floating ice which would be calved entirely soon in model simulation and reaches a condition for this numerical problem to occur. Hence, a tiny value, 0.01, is used instead of 0 for this parameter to overcome numerical problems.

```
[Upernavik-Isstrøm-Experiment]

[grid]
upn = 20                          # 20 vertical grids
ewn = 297                         # 297 east grids
nsn = 495                         # 495 north grids
dew = 100                         # 100m east grid spacing
dns = 100                         # 100m north grid spacing
sigma = 0                         # Glimmer sigma-coordinate

[time]
tstart = 0.
tend = 0.06849315                 # simulation duration = 75 days
dt = 0.002739726                  # timestep = 1 day
dt_diag = 0.002739726             # display Glacier 1 velocity and temperature at every timestep
idiag = 115
jdiag = 387

[options]
dycore = 2                        # parallel, 3D, first-order accuracy dynamic core
evolution = 4                     # first-order upwind scheme for thickness evolution
temperature = 1                   # prognostic temperature calculation
temp_init = 2                     # linearly interpolated initial ice temperature
flow_law = 2                      # temperature dependent flow factor
basal_water = 1                   # local basal water balance
basal_mass_balance = 1            # include basal melt rate
slip_coeff = 4                    # basal melt rate dependent slipping
marine_margin = 2                 # lose ice at ocean margin
gthf = 0                          # uniform geothermal heat flux
isostasy = 0                      # no isostatic adjustment

[ho_options]
which_ho_nonlinear = 0            # Picard iteration for solving nonlinearity
which_ho_sparse = 3               # Chronopoulos-Gear algorithm for sparse linear system
which_ho_efvs = 2                 # effective visosity computed from effective strain rate
which_ho_disp = 1                 # temperature dissipation under first-order dynamics
which_ho_babc = 3                 # basal traction linearly inverse to basal water thickness
which_ho_resid = 3                # L2-norm for system residual
which_ho_approx = 2               # Blatter-Pattyn higher-order approximation
which_ho_precond = 2              # shallow ice preconditioner
which_ho_gradient = 1             # computing spatial gradient by upstream gradient
which_ho_gradient_margin = 2      # compute spatial gradient on ice covered cells only
glissade_maxiter = 500            # max. 500 iterations

[parameters]
log_level = 6                     # log file store most detail available
ice_limit = 1.0                   # min. ice thickness for dynamics
ice_limit_temp = 1.0              # min. ice thickness for temperature
marine_limit = -1000.0            # assume no ice when water depth < -1000m
calving_fraction = 0.01           # fraction of floating ice remained after calving
geothermal = -0.05                # geothermal heat flux (W/m^2)
```

Figure A.1 : One example of CISM version 2.0.5 model configuration applied in simulating high-resolution regional Upernavik Isstrøm transient glacier dynamics.

Bibliography

[1] Aschwanden, A., Bueler, E., Khroulev, C., Blatter, H., 2012. An enthalpy formulation for glaciers and ice sheets. *Journal of Glaciology*, 58 (209) pp. 441–457.

[2] Benn, D.I., Warren, C.R. and Mottram, R.H., 2007. Calving processes and the dynamics of calving glaciers. *Earth-Science Reviews*, *82*(3), pp.143-179.

[3] Bevan, S.L., Luckman, A., Khan, S.A. and Murray, T., 2015. Seasonal dynamic thinning at Helheim Glacier. *Earth and Planetary Science Letters*, *415*, pp.47-53.

[4] Bindschadler, R., 1983. The importance of pressurized subglacial water in separation and sliding at the glacier bed. *Journal of Glaciology*, *29*(101), pp.3-19.

[5] Bindschadler, R.A., Nowicki, S., Abe-Ouchi, A., Aschwanden, A., Choi, H., Fastook, J., Granzow, G., Greve, R., Gutowski, G., Herzfeld, U. and Jackson, C., 2013. Ice-sheet model sensitivities to environmental forcing and their use in projecting future sea level (the SeaRISE project). *Journal of Glaciology*, *59*(214), pp.195-224.

[6] Blatter, H., 1995. Velocity and stress fields in grounded glaciers: a simple algorithm for including deviatoric stress gradients. *Journal of Glaciology*, *41*(138), pp.333-344.

[7] Box, G.E. and Draper, N.R., 1987. *Empirical model-building and response surfaces* (Vol. 424). New York: Wiley.

[8] Box, J.E., Yang, L., Bromwich, D.H. and Bai, L.S., 2009. Greenland Ice Sheet Surface Air Temperature Variability: 1840-2007*. *Journal of Climate*, *22*(14), pp.4029-4049.

[9] Budd, W.F. and Jacka, T.H., 1989. A review of ice rheology for ice sheet modelling. *Cold Regions Science and Technology*, *16*(2), pp.107-144.

[10] Bueler, E. and Brown, J., 2009. Shallow shelf approximation as a "sliding law" in a thermomechanically coupled ice sheet model. *Journal of Geophysical Research: Earth Surface*, *114*(F3).

[11] Church, J.A., P.U. Clark, A. Cazenave, J.M. Gregory, S. Jevrejeva, A. Levermann, M.A. Merri eld, G.A. Milne, R.S. Nerem, P.D. Nunn, A.J. Payne, W.T. Pfeffer, D. Stammer and A.S. Unnikrishnan, 2013: Sea Level Change. In: *Climate Change 2013: The Physical Science Basis. Contribution of Working Group I to the Fifth Assessment Report of the Intergovernmental Panel on Climate Change* [Stocker, T.F., D. Qin, G.-K. Plattner, M. Tignor, S.K. Allen, J. Boschung, A. Nauels, Y. Xia, V. Bex and P.M. Midgley (eds.)]. Cambridge University Press, Cambridge, United Kingdom and New York, NY, USA.

[12] Clarke, G.K., 1996. Lumped-element analysis of subglacial hydraulic circuits. *Journal of Geophysical Research: Solid Earth*, *101*(B8), pp.17547-17559.

[13] Courant, R., Friedrichs, K. and Lewy, H., 1967. On the partial difference equations of mathematical physics. *IBM journal*, *11*(2), pp.215-234.

[14] Cuffey, K.M. and Paterson, W.S.B., 2010. *The physics of glaciers*. Academic Press.

[15] Davies, J.H. and Davies, D.R., 2010. Earth's surface heat flux. *Solid Earth*, *1*(1), p.5.

[16] Enderlin, E.M., Howat, I.M. and Vieli, A., 2013. High sensitivity of tidewater outlet glacier dynamics to shape. *The Cryosphere*, *7*(3), pp.1007-1015.

[17] Enderlin, E.M., Howat, I.M., Jeong, S., Noh, M.J., Angelen, J.H. and Broeke, M.R., 2014. An improved mass budget for the Greenland ice sheet. *Geophysical Research Letters*, *41*(3), pp.866-872.

[18] Feistel, R. and Wagner, W., 2006. A new equation of state for H_2O ice Ih. *Journal of Physical and Chemical Reference Data*, *35*(2), pp.1021-1047.

[19] Fox Maule, C., Purucker, M.E., Olsen, N. and Mosegaard, K., 2005. Heat flux in Antarctica revealed from satellite magnetic data, *Science*, 309, 464-467.

[20] Gagliardini, O., Zwinger, T., Gillet-Chaulet, F., Durand, G., Favier, L., De Fleurian, B., Greve, R., Malinen, M., Martín, C., Råback, P. and Ruokolainen, J., 2013. Capabilities and performance of Elmer/Ice, a new-generation ice sheet model. *Geoscientific Model Development*, *6*(4), pp.1299-1318.

[21] Gardner, A.S., Moholdt, G., Cogley, J.G., Wouters, B., Arendt, A.A., Wahr, J., Berthier, E., Hock, R., Pfeffer, W.T., Kaser, G. & Ligtenberg, S.R., 2013. A reconciled estimate of glacier contributions to sea level rise: 2003 to 2009. *Science*, *340*(6134), 852-857.

[22] Glen, J.W., 1952. Experiments on the deformation of ice. *Journal of Glaciology*, *2*, pp.111-114.

[23] Glen, J.W., 1955, March. The creep of polycrystalline ice. In *Proceedings of the Royal Society of London A: Mathematical, Physical and Engineering Sciences* (Vol. 228, No. 1175, pp. 519-538). The Royal Society.

[24] Gomez, N., Mitrovica, J.X., Huybers, P. and Clark, P.U., 2010. Sea level as a stabilizing factor for marine-ice-sheet grounding lines. *Nature Geoscience*, *3*(12), pp.850-853.

[25] Greve, R. and Blatter, H., 2009. *Dynamics of ice sheets and glaciers*. Springer Science & Business Media.

[26] Halfar, P., 1983. On the dynamics of the ice sheets 2. *Journal of Geophysical Research: Oceans*, *88*(C10), pp.6043-6051.

[27] Hindmarsh, R.C.A., 2004. A numerical comparison of approximations to the Stokes equations used in ice sheet and glacier modeling. *Journal of Geophysical Research: Earth Surface*, *109*(F1).

[28] Holland, D.M. and Jenkins, A., 1999. Modeling thermodynamic ice-ocean interactions at the base of an ice shelf. *Journal of Physical Oceanography*, *29*(8), pp.1787-1800.

[29] Holland, D.M., Thomas, R.H., De Young, B., Ribergaard, M.H. and Lyberth, B., 2008. Acceleration of Jakobshavn Isbrae triggered by warm subsurface ocean waters. *Nature Geoscience*, *1*(10), pp.659-664.

[30] Holton, J.R. and Hakim, G.J., 2012. *An introduction to dynamic meteorology* (Vol. 88). Academic press.

[31] Howat, I.M., Joughin, I. and Scambos, T.A., 2007. Rapid changes in ice discharge from Greenland outlet glaciers. *Science*, *315*(5818), pp.1559-1561.

[32] Howat, I.M., Joughin, I., Fahnestock, M., Smith, B.E. and Scambos, T.A., 2008. Synchronous retreat and acceleration of southeast Greenland outlet glaciers 2000–06: Ice dynamics and coupling to climate. *Journal of Glaciology*, *54*(187), pp.646-660.

[33] Hughes, T.J., Liu, W.K. and Zimmermann, T.K., 1981. Lagrangian-Eulerian finite element formulation for incompressible viscous flows. *Computer Methods in Applied Mechanics and Engineering*, *29*(3), pp.329-349.

[34] Hutter, K., 1983. *Theoretical glaciology: material science of ice and the mechanics of glaciers and ice sheets* (Vol. 1). Springer.

[35] Huybrechts, P., Payne, T. and EISMINT, I., 1996. The EISMINT benchmarks for testing ice-sheet models. *Annals of Glaciology*, *23*, pp.1-12.

[36] Joughin, I., 2002. Ice-sheet velocity mapping: a combined interferometric and speckle-tracking approach. *Annals of Glaciology*, *34*(1), pp.195-201.

[37] Joughin, I., Das, S.B., King, M.A., Smith, B.E., Howat, I.M. and Moon, T., 2008. Seasonal speedup along the western flank of the Greenland Ice Sheet. *Science*, *320*(5877), pp.781-783.

[38] Joughin, I., Smith, B. E., Shean, D. E. and Floricioiu, D., 2014. Brief communication: Further summer speedup of Jakobshavn Isbræ. *The Cryosphere*, *8*(1), 209-214.

[39] Joughin, I., Howat, I., Smith, B. and Scambos, T., 2011, updated 2016. *MEaSUREs Greenland Ice Velocity: Selected Glacier Site Velocity Maps from InSAR, Version 1*. [Wcoast-72.90N]. Boulder, Colorado USA. NASA National Snow and Ice Data Center Distributed Active Archive Center. doi: http://dx.doi.org/10.5067/MEASURES/CRYOSPHERE/nsidc-0481.001. [03 Aug 2015].

[40] Khan, S.A., Kjaer, K.H., Korsgaard, N.J., Wahr, J., Joughin, I.R., Timm, L.H., Bamber, J.L., Broeke, M.R., Stearns, L.A., Hamilton, G.S. and Csatho, B.M., 2013. Recurring dynamically induced thinning during 1985 to 2010 on Upernavik Isstrøm, West Greenland. *Journal of Geophysical Research: Earth Surface*, *118*(1), pp.111-121.

[41] Khan, S. A., Kjær, K. H., Bevis, M., Bamber, J. L., Wahr, J., Kjeldsen, K. K., Bjørk A.A., Korsgaard, N.J., Stearns, L.A., Van den Broeke, M.R., Liu, L., Larsen, N.K. and Muresan, I.S., 2014. Sustained mass loss of the northeast Greenland ice sheet triggered by regional warming. *Nature Climate Change*, *4*(4), 292-299.

[42] Krug, J., J. Weiss, O. Gagliardini and G. Durand, 2014. Combining damage and fracture mechanics to model calving, *The Cryosphere*, 8, 2101-2117, doi:10.5194/tc-8-2101-2014.

[43] Lambeck, K. and Nakiboglu, S.M., 1980. Seamount loading and stress in the ocean lithosphere. *Journal of Geophysical Research: Solid Earth*, *85*(B11), pp.6403-6418.

[44] Larour, E., Seroussi, H., Morlighem, M. and Rignot, E., 2012. Continental scale, high order, high spatial resolution, ice sheet modeling using the Ice Sheet System Model (ISSM). *Journal of Geophysical Research: Earth Surface*, *117*(F1).

[45] Larour, E., Utke, J., Csatho, B., Schenk, A., Seroussi, H., Morlighem, M., Rignot, E., Schlegel, N., and Khazendar, A., 2014. Inferred basal friction and surface mass balance of the Northeast Greenland Ice Stream using data assimilation of ICESat (Ice Cloud and land Elevation Satellite) surface altimetry and ISSM (Ice Sheet System Model), *The Cryosphere*, 8, 2335-2351, doi:10.5194/tc-8-2335-2014.

[46] Larsen, S.H., Khan, S.A., Ahlstrøm, A.P., Hvidberg, C.S., Willis, M.J., and Andersen, S.B., 2016. Increased mass loss and asynchronousbehavior of marine-terminating outlet glaciers at Upernavik Isstrøm, NW Greenland, *Journal of Geophysical Research: Earth Surface*, 121, doi:10.1002/2015JF003507

[47] Lipscomb, W.H. and Hunke, E.C., 2004. Modeling sea ice transport using incremental remapping. *Monthly weather review*, *132*(6), pp.1341-1354.

[48] Lipscomb, W.H., Fyke, J.G., Vizcaíno, M., Sacks, W.J., Wolfe, J., Vertenstein, M., Craig, A., Kluzek, E. and Lawrence, D.M., 2013. Implementation and initial evaluation of the glimmer community ice sheet model in the community earth system model. *Journal of Climate*, *26*(19), pp.7352-7371.

[49] Lüthi, M.P., Ryser, C., Andrews, L.C., Catania, G.A., Funk, M., Hawley, R.L., Hoffman, M.J. and Neumann, T.A., 2015. Heat sources within the Greenland Ice Sheet: dissipation, temperate paleo-firn and cryo-hydrologic warming. *The Cryosphere*, *9*(1), pp.245-253.

[50] Martin, P.J. and Sanderson, T.J.O., 1980. Morphology and dynamics of ice rises. *Journal of Glaciology*, *25*, pp.33-45.

[51] MacAyeal, D.R., 1989. Large-scale ice flow over a viscous basal sediment: Theory and application to ice stream B, Antarctica. *Journal of Geophysical Research: Solid Earth*, *94*(B4), pp.4071-4087.

[52] MacAyeal, D.R., Rommelaer, V., Huybrechts, P., Hulbe, C.L., Determann, J., and Ritz, C., 1996. An ice-shelf model test based on the Ross Ice Shelf, Antarctica. Annals of Glaciology, 23:46–51.

[53] Moon, T. and Joughin, I., 2008. Changes in ice front position on Greenland's outlet glaciers from 1992 to 2007. *Journal of Geophysical Research: Earth Surface*, *113*(F2).

[54] Morlighem, M., Rignot, E., Mouginot, J., Seroussi, S., and Larour, E., 2014. Deeply incised submarine glacial valleys beneath the Greenland Ice Sheet. *Nature Geoscience*, 7, 418–422, doi:10.1038/ngeo2167

[55] Morlighem, M., Bondzio, J., Seroussi, H., Rignot, E., Larour, E., Humbert, A., and Rebuffi, S., 2016. Modeling of Store Gletscher's calving dynamics, West Greenland, in response to ocean thermal forcing, *Geophysical Research Letters*, 43, doi:10.1002/2016GL067695.

[56] Murray, T., Scharrer, K., James, T.D., Dye, S.R., Hanna, E., Booth, A.D., Selems, N., Luckman, A., Hughes, A.L.C., Cook, S. and Hybrechts, P., 2010. Ocean regulation hypothesis for glacier dynamics in southeast Greenland and implications ice sheet mass change. *Journal of Geophysical Research*, 115(F03026).

[57] Nettles, M., Larsen, T.B., Elósegui, P., Hamilton, G.S., Stearns, L.A., Ahlstrøm, A.P., Davis, J.L., Andersen, M.L., de Juan, J., Khan, S.A. and Stenseng, L., 2008. Step-wise changes in glacier flow speed coincide with calving and glacial earthquakes at Helheim Glacier, Greenland. *Geophysical Research Letters*, *35*(24).

[58] Nick, F.N., Vieli, A., Howat, I. and Joughin, I., 2009. Large-scale changes in Greenland outlet glacier dynamics triggered at the terminus. *Nature Geoscience*, 2:110–114

[59] Nick, F.N., van der Veen, C.J., Vieli, A. and Benn, D.I., 2010. Aphysically based calving model applied to marine outlet glaciers and implications for their dynamics. *Journal of Glaciology*, 56(199):781–794

[60] Nick, F.M., Vieli, A., Andersen, M.L., Joughin, I., Payne, A., Edwards, T.L., Pattyn, F. and van de Wal, R.S., 2013. Future sea-level rise from Greenland/'s main outlet glaciers in a warming climate. *Nature*, *497*(7448), pp.235-238.

[61] Nielsen, K., Khan, S.A., Spada, G., Wahr, J., Bevis, M., Liu, L. and Dam, T., 2013. Vertical and horizontal surface displacements near Jakobshavn Isbræ driven by melt-induced and dynamic ice loss. *Journal of Geophysical Research: Solid Earth*, *118*(4), pp.1837-1844.

[62] Noël, B., van de Berg, W.J., van Meijgaard, E., Kuipers Munneke, P., van de Wal, R.S.W. and van den Broeke, M.R., 2015, Summer snowfall on the Greenland Ice Sheet: a study with the updated regional climate model RACMO2.3. *The Cryosphere Discussions* 9(1):1177–1208. doi: 10.5194/tcd-9-1177-2015

[63] Nye, J.F., 1953, October. The flow law of ice from measurements in glacier tunnels, laboratory experiments and the Jungfraufirn borehole experiment. In *Proceedings of the Royal Society of London A: Mathematical, Physical and Engineering Sciences* (Vol. 219, No. 1139, pp. 477-489). The Royal Society.

[64] Nye, J.F., 1976. Water flow in glaciers: jökulhlaups, tunnels and veins. *Journal of Glaciology*, *17*, pp.181-207.

[65] Osher, S., and Sethian J.A., 1988. Fronts propagating with curvature-dependent speed: algorithms based on Hamilton-Jacobi formulations. *Journal of Computational Physics* 79.1: 12-49.

[66] Paterson, W.S.B. and Budd, W.F., 1982. Flow parameters for ice sheet modeling. *Cold Region Science and Technology*, 6(2):175–177.

[67] Pattyn, F., 2003. A new three-dimensional higher-order thermomechanical ice sheet model: Basic sensitivity, ice stream development, and ice flow across subglacial lakes. *Journal of Geophysical Research: Solid Earth*, *108*(B8).

[68] Pattyn, F., Perichon, L., Aschwanden, A., Breuer, B., De Smedt, B., Gagliardini, O., Gudmundsson, G.H., Hindmarsh, R., Hubbard, A., Johnson, J.V. and Kleiner, T., 2008. Benchmark experiments for higher-order and full Stokes ice sheet models (ISMIP-HOM). *The Cryosphere Discussions*, *2*(1), pp.111-151.

[69] Pattyn, F., Schoof, C., Perichon, L., Hindmarsh, R.C.A., Bueler, E., Fleurian, B.D., Durand, G., Gagliardini, O., Gladstone, R., Goldberg, D. and Gudmundsson, G.H., 2012. Results of the marine ice sheet model intercomparison project, MISMIP. *The Cryosphere*, *6*(3), pp.573-588.

[70] Petrunin, A. G., Rogozhina, I., Vaughan, A. P. M., Kukkonen, I. T., Kaban, M. K., Koulakov, I., and Thomas, M., 2013. Heat flux variations beneath central Greenland's ice due to anomalously thin lithosphere. *Nature Geoscience*, *6*(9), 746-750.

[71] Poinar, K., I. Joughin, S. B. Das, M. D. Behn, J. T. M. Lenaerts, and M. R. van den Broeke, 2015. Limits to future expansion of surface-melt-enhanced ice flow into the interior of western Greenland, *Geophysical Research Letters*, 42, 1800–1807.

[72] Price, S., Lipscomb, W., Hoffman, M., Hagdorn, M., Rutt, I., Payne, T. and Hebeler, F., 2015. *CISM 2.0.5 Documentation*. http://oceans11.lanl.gov/cism/index.html .

[73] Pritchard, H.D., Arthern, R.J., Vaughan, D.G. and Edwards, L.A., 2009. Extensive dynamic thinning on the margins of the Greenland and Antarctic ice sheets. *Nature*, *461*(7266), pp.971-975.

[74] Radić, V. and Hock, R., 2013. Glaciers in the Earth's hydrological cycle: assessments of glacier mass and runoff changes on global and regional scales. In *The Earth's Hydrological Cycle* (pp. 813-837). Springer Netherlands.

[75] Rignot, E., Box, J.E., Burgess, E. & Hanna, E., 2008. Mass balance of the Greenland ice sheet from 1958 to 2007. *Geophysical Research Letters*, *35*(20).

[76] Rignot, E., Koppes, M. and Velicogna, I., 2010. Rapid submarine melting of the calving faces of West Greenland glaciers. *Nature Geoscience*, *3*(3), pp.187-191.

[77] Rignot, E., Velicogna, I., Van den Broeke, M.R., Monaghan, A. and Lenaerts, J.T.M., 2011. Acceleration of the contribution of the Greenland and Antarctic ice sheets to sea level rise. *Geophysical Research Letters*, *38(5)*, p.L05503.

[78] Röthlisberger, H., 1972. Water pressure in intra- and subglacial channels. *Journal of Glaciology*, Vol. 11, No. 62, p. 177-203.

[79] Rutt, I.C., Hagdorn, M., Hulton, N.R.J. and Payne, A.J., 2009. The Glimmer community ice sheet model. *Journal of Geophysical Research: Earth Surface*, *114*(F2).

[80] Seddik H., R. Greve, T. Zwinger, F. Gillet-Chaulet and O. Gagliardini, 2012. Simulations of the Greenland ice sheet 100 years into the future with the full Stokes model Elmer/Ice, *Journal of Glaciology*, 58(209), 427-440.

[81] Seroussi, H., Morlighem, M., Larour, E., Rignot, E. and Khazendar, A., 2014. Hydrostatic grounding line parameterization in ice sheet models, *The Cryosphere*, 8, 2075-2087, doi:10.5194/tc-8-2075-2014.

[82] Solomon, S. ed., 2007. *Climate change 2007-the physical science basis: Working group I contribution to the fourth assessment report of the IPCC* (Vol. 4). Cambridge University Press.

[83] Schoof, C., 2005, March. The effect of cavitation on glacier sliding. In *Proceedings of the Royal Society of London A: Mathematical, Physical and Engineering Sciences* (Vol. 461, No. 2055, pp. 609-627). The Royal Society.

[84] Schoof, C., 2006. A variational approach to ice stream flow. *Journal of Fluid Mechanics*, *556*, pp.227-251.

[85] Schoof, C., 2007. Ice sheet grounding line dynamics: Steady states, stability, and hysteresis, *Journal of Geophysical Research*, 112, F03S28.

[86] Schoof, C., 2010. Ice-sheet acceleration driven by melt supply variability. *Nature*, *468*(7325), pp.803-806.

[87] Schoof, C. and Hewitt, I., 2013. Ice-sheet dynamics. *Annual Review of Fluid Mechanics*, *45*, pp.217-239.

[88] Smith, W. H. F., and Sandwell, D.T., 1997. Global seafloor topography from satellite altimetry and ship depth soundings, *Science*, v. 277, p. 1957-1962.

[89] Stokes, G.G..,1845. On the theories of internal friction of fluids in motion, *Transactions of the Cambridge Philosophical Society*, 8, 287–305.

[90] Sundal, A.V., Shepherd, A., Nienow, P., Hanna, E., Palmer, S. and Huybrechts, P., 2011. Melt-induced speed-up of Greenland ice sheet offset by efficient subglacial drainage. *Nature*, *469*(7331), pp.521-524.

[91] Thomas, R.H., D.R. MacAyeal, D.H. Eilers, and D.R. Gaylord, 1984. Glaciological Studies on the Ross Ice Shelf, Antarctica, 1972-1978. The Ross Ice Shelf: Glaciology and Geophysics Antarctic Research Series, Volume 42, Paper 2, 21-53.

[92] Todd, J. and Christoffersen, P.: Are seasonal calving dynamics forced by buttressing from ice mélange or undercutting by melting? Outcomes from full-Stokes simulations of Store Glacier, West Greenland, *The Cryosphere*, 8, 2353-2365, doi:10.5194/tc-8-2353-2014, 2014.

[93] Van der Veen, C.J., 2013. *Fundamentals of glacier dynamics*. CRC Press.

[94] Van Der Veen, C.J. and Whillans, I.M., 1989. Force budget: I. Theory and numerical methods. *Journal of Glaciology*, *35*(119), pp.53-60.

[95] Vaughan, D.G., J.C. Comiso, I. Allison, J. Carrasco, G. Kaser, R. Kwok, P. Mote, T. Murray, F. Paul, J. Ren, E. Rignot, O. Solomina, K. Steffen and T. Zhang, 2013: Observations: Cryosphere. In: *Climate Change 2013: The Physical Sci- ence Basis. Contribution of Working Group I to the Fifth Assessment Report of the Intergovernmental Panel on Climate Change* [Stocker, T.F., D. Qin, G.-K. Plattner, M. Tignor, S.K. Allen, J. Boschung, A. Nauels, Y. Xia, V. Bex and P.M. Midgley (eds.)]. Cambridge University Press, Cambridge, United Kingdom and New York, NY, USA.

[96] Vieli, A. and Nick, F.M., 2011. Understanding and modelling rapid dynamic changes of tidewater outlet glaciers: issues and implications. *Surveys in Geophysics*, *32*(4-5), pp.437-458.

[97] Weertman, J., 1964. The theory of glacier sliding. *Journal of Glaciology, 5(39):* 287-303.

[98] Weertman, J., 1973. Creep of ice. *Physics and chemistry of ice*, pp.320-337.

[99] Weertman, J., 1974. Stability of the junction of an ice sheet and an ice shelf. *Journal of Glaciology*, *13*, pp.3-11.

[100] Werder, M.A., Hewitt, I.J., Schoof, C.G. and Flowers, G.E., 2013. Modeling channelized and distributed subglacial drainage in two dimensions. *Journal of Geophysical Research: Earth Surface*, *118*(4), pp.2140-2158.

[101] Winkelmann, R., Martin, M.A., Haseloff, M., Albrecht, T., Bueler, E., Khroulev, C. and Levermann, A., 2011. The Potsdam parallel ice sheet model (PISM-PIK)–Part 1: Model description. *The Cryosphere*, *5*(3), pp.715-726.

[102] Zwally, H.J., Abdalati, W., Herring, T., Larson, K., Saba, J. and Steffen, K., 2002. Surface melt- induced acceleration of Greenland ice-sheet flow. *Science* 297, 218–222.

Glossary

°C : degree Celsius

2D : two-dimensional

3D : three-dimensional

ALE : Arbitrary Lagrangian-Eulerian

BP : Blatter-Pattyn

CESM : Community Earth System Model

CFL : Courant–Friedrichs–Lewy

CISM : Community Ice Sheet Model

CSC : Center for Scientific Computing

DEM : digital elevation model

EGCC : Eastern Greenland Costal Current

FS : full Stokes

GIA : Glacial Isostatic Adjustment

GPS : Global Positioning System

InSAR : Interferometry Synthetic Aperture Radar

IPCC : Intergovernmental Panel on Climate Change

ISSM : Ice Sheet System Model

JPL : Jet Propulsion Laboratory

NCAR : National Center for Atmospheric Research

L1L2 : one-layer longitudinal stress scheme using $\dot{\epsilon}_{xx}$ at surface computed by solving elliptical equations with a vertical correction of τ_{xx}'

LGM : Last Glacial Maximum

N-channel : Nye-channel

NSIDC : National Snow & Ice Data Center

O-H : Oxygen-Hydrogen

PIK : Potsdam Institute for Climate Impact Research

PISM : Parallel Ice Sheet Model

R-channel : Röthlisberger-channel

RACMO : Regional Atmospheric Climate Model

RIGGS : Tabular Velocity Data for the Ross Ice Shelf

SAR : Synthetic Aperture Radar

SIA : Shallow Ice Approximation

SMB : Surface Mass Balance

SSA : Shallow Shelf Approximation

UAF : University of Alaska at Fairbanks

UCL : University of California, Irvine

UCSD : University of California, San Diego